Eduardo Albuquerque Hartmann

The Phenomenon of multiple stellar population in Galactic globular clusters through multi-band photometry and *Gaia*

Porto Alegre, Brasil

Março de 2023

Eduardo Albuquerque Hartmann

The Phenomenon of multiple stellar population in Galactic globular clusters through multi-band photometry and *Gaia*

Dissertação submetida ao Programa de Pós Graduação em Física do Instituto de Física da UFRGS, como quesito parcial para obtenção do título de Mestre em Física, com ênfase em Astronomia.

Universidade Federal do Rio Grande do Sul – UFRGS

Instituto de Física

Programa de Pós-Graduação

Supervisor: Charles José Bonatto

Co-supervisor: Ana Leonor Chies Santiago Santos

Porto Alegre, Brasil

Março de 2023

To those that keep the flame alive — be cinder when the world is ash.

Acknowledgements

Este trabalho, assim como todos aqueles feitos pelas mãos humanas, é um fruto coletivo. Sem o apoio de muitas pessoas ele não seria possível, aqui está o agradecimento a algumas delas:

Aos meus orientadores, Ana e Charles, que me apoiam, aconselham e empurram nessa caminhada desde o 4^o semestre da gradução. Obrigado não somente por apontarem o caminho, mas participarem da jornada em cada curva e pedra, vocês foram fundamentais para que eu chegasse aqui.

Aos meus pais, Janete e Paulo, palavras falham ao descrever o amor que tenho por vocês. Obrigado por serem a base sobre a qual me apoio, por serem exemplo de amor, carinho, justiça e ética. Obrigado por me encorajarem nessa aventura que é tentar ser um cientista no Brasil e além. A minha irmã Gabriela, minha melhor amiga, que invade meu quarto quando bem entende para discutir bobagens. Ter você no meu dia-a-dia torna a vida mais leve.

Ao meu companheiro de viagem, Victor. Ainda temos muitos lugares para conhecer. Bruno, Felipe, Gui, Julio, Lucas e Victor, as coincidências da vida nos levaram a estudar juntos, mas foi as bobagens que fizemos juntos que nos uniram como amigos.

Às pessoas que contribuiram com este trabalho. A Javier Alonso e Rafael de Souza da Silva, que fizeram importantes contribuições. The Liverpool group and specially Cris and Nate. Ao grupo do S-PLUS, Claudia, Fábio, Roderik, Felipe, Hélio, Thais, e outros.

À Bernardete, minha tia querida, que sempre foi muito preocupada, mas nunca esqueceu de levar um docinho e adora sair para jantar. Fernanda e Sandro, dinda e dindo, vocês foram um pilar fundamental da minha vida e hoje são pais maravilhosos para a Alexia. A minha família, que aumenta a cada dia e é muito grande para que eu nomeie a todos aqui.

João, Nicholas, Cris, Mônica e Henrique, obrigado por dividirem os pesos da vida academica comigo, e por fazer isso sempre comendo.

À todas as pessoas que encontrei por aí, fui mais feliz por cruzar com vocês. Ao meu grande professor de piano, Alexandre Alles, em 30 anos eu toco como você. As pessoas que encontrei na academia, Carlos, Augusto, Vitor, Rodrigo, Gabriel, Otávio, Catarina, William. To Kam, Alex and Sam, we still have a trail in the canadian wilderness to hike and a pint to have together. Aos profesores que tive, do primário a pós-graduação, o conhecimento não é nada se não for partilhado. Obrigado a uns por me inspirarem e educarem, e a outros por me ensinarem como não ser.

À UFRGS, que foi minha casa nesses últimos 7 anos e que me mostrou o que é uma Universidade de excelência. Aos orgãos de fomento a pesquisa CAPES e CNPq, que lutam diariamente para que a pesquisa e pós graduação do Brasil exista e seja da mais alta qualidade.

Um agradecimento também a todos os profissionais anônimos que fazem as engrenagens do mundo girar, da auxiliar de limpeza ao cobrador do ônibus.

Agradeço aos membros da banca por aceitarem o convite de ler este trabalho e pelos comentários que enriqueceram este manuscrito.

Um agradecimento final ao acaso. Sobre os acontecimentos da vida, ao que me parece, não possuo nenhum controle. Me resta utilizar aquilo que me foi dado, um corpo e uma mente, da melhor forma que posso.

The gods had condemned Sisyphus to ceaselessly rolling a rock to the top of a mountain, whence the stone would fall back of its own weight. They had thought with some reason that there is no more dreadful punishment than futile and hopeless labour.

[...]

I leave Sisyphus at the foot of the mountain! One always finds one's burden again. But Sisyphus teaches the higher fidelity that negates the gods and raises rocks. He too concludes that all is well. This universe henceforth without a master seems to him neither sterile nor futile. Each atom of that stone, each mineral flake of that night-filled mountain, in itself forms a world. ***The struggle itself toward the heights is enough to fill a man's heart. One must imagine Sisyphus happy.***

- The Myth of Sisyphus, Albert Camus.

Abstract

The phenomenon of Multiple Stellar Populations (MSPs) is present in all well studied massive Globular Clusters (GCs) of the Milky Way Galaxy. Both spectroscopic and photometric studies have established that these objects had a more complex formation history than previously thought. Measurements of the abundance of light elements (e.g. Na, O, C, N) show a star-to-star variation. This presents itself in colour magnitude diagrams as splits primarily in the Red Giant Branch (RGB) of clusters when appropriate filters are used. In this work we have used the multi-band survey *Southern Photometric Local Universe Survey* (S-PLUS) to study MSPs in four GCs, namely NGC 104, NGC 288, NGC 3201 and NGC 7089. S-PLUS consists of 12 filters spanning a range from 3485 Å(u) to 9114 Å(z), with seven narrow bands and five broad bands. We have performed PSF photometry in the images gathered by the survey and selected likely cluster members using proper motion information from the *Gaia* survey. We calibrated the data using a comparative method taking advantage of the presence of a GC in the field and corrected NGC 3201, a cluster displaying large extinction, by differential reddening. We identified the presence of MSPs in the rectified RGB, constructed six colour combinations and used the K-means algorithm to separate the populations. We characterised the populations as Na-rich and Na-poor using abundance data from the literature. We have also traced the radial profiles of the MSPs. In NGC 288 and NGC 7089 the second population is more centrally concentrated while for NGC 3201 the opposite trend is true. Current MSPs formation theories suggest a higher concentration of the second population. NGC 104 does not show a significant difference in the populations. Furthermore, we have analysed the proper motion of the populations in the four studied clusters. By separating the movement of the stars within the cluster in their radial and tangential components and using a Heteroscedastic Gaussian Regression to trace the velocity dispersion profiles along the radial direction. Significant differences are found in three of the clusters, namely NGC 104, NGC 288 and NGC 7089, while NGC 3201 has very similar profiles between populations.

Key words: Surveys — globular clusters: individual: (NGC 104) (NGC 288) (NGC 3201) (NGC 7089)

Resumo

O fenômeno de Múltiplas Populações Estelares (MPEs) está presente em todos os Aglomerados Globulares (AGs) massivos bem estudados da Via Láctea. Tanto estudos espectroscópicos quanto fotométricos já estabeleceram que estes objetos possuem um histórico de formação mais complexo do que se imaginava. Medições da abundância de elementos leves (como por exemplo Na, C, O, N) mostram uma variação de estrela para estrela. Isto se reflete em sequências distintas principalmente no Ramo das Gigantes Vermelhas (RGV) quando filtros apropriados são utilizados para construir diagramas cor-magnitude. Neste trabalho utilizamos o levantamento de dados de multi-banda *Southern Photometric Local Universe Survey* (S-PLUS) para estudar as MPEs em quatro aglomerados: NGC 104, NGC 288, NGC 3201 e NGC 7089. O S-PLUS consiste de 12 filtros que alcançam de 3485 Å(u) até 9114 Å(z), com sete bandas estreitas e cinco largas. Fotometria por PSF foi feita nas imagens coletadas pelo S-PLUS e os prováveis membros dos aglomerados foram selecionados utilizando informações de movimento próprio do levantamento de dados *Gaia*. Os dados foram calibrados através de um método comparativo se aproveitando do fato de um aglomerado globular estar no campo observado e NGC 3201, um aglomerado com avermelhamento diferencial significativo, foi corrigido por avermelhamento diferencial. A presença de MPEs foi identificada no RGV retificado, seis combinações de cores foram construídas e o algoritmo *K-means* foi utilizado para separar as populações. Essas foram caracterizadas como Na-ricas e Na-pobres usando dados de abundância da literatura. Os perfis radiais das EMPs foram traçados. Em NGC 288 e NGC 7089 a segunda população está mais concentrada enquanto que em NGC 3201 o contrário é verdadeiro. As atuais teorias de formação de MPEs sugerem uma concentração maior da segunda população. O aglomerado NGC 104 não mostra uma diferença significativa entre as populações. Além disso, analisamos o movimento próprio das populações nos quatro aglomerados. Separando o movimento das estrelas no aglomerado nas suas componentes radial e tangencial e usando uma Regressão Gaussiana Heteroscedástica para traçar os perfis de dispersão de velocidade ao longo da direção radial. Diferenças significativas foram encontradas em três dos aglomerados: NGC 104, NGC 288 e NGC 7089, enquanto que NGC 3201 possui perfis similares entre as duas populações.

Palavras-chave: levantamentos de dados — aglomerados globulares: individual: (NGC 104) (NGC 288) (NGC 3201) (NGC 7089)

Comunicado de Imprensa

Aglomerados Globulares são objetos compostos de centenas a milhares de estrelas que orbitam nossa Galáxia, a Via Láctea. Na nossa Galáxia conhecemos em torno de 150 deles, outras galáxias maiores podem possuir milhares destes objetos. A maioria dos aglomerados globulares é muito velho, tendo se formado junto ou logo após a formação da Galáxia, quase 12 bilhões de anos atrás. Até a década de 80 a ideia corrente era de que a formação dos aglomerados ocorria a partir do colapso de uma grande nuvem de gás e poeira. A nuvem era perturbada e caia sobre si mesma, fragmentando-se em nuvens menores que se contraiam formando estrelas em seus interiores. Esse conjunto de estrelas é o que formaria um aglomerado globular, com todas elas possuindo características similares, como por exemplo a quantidade de metais leves.

Porém, estudos recentes e mais precisos dessas características levantaram dúvidas sobre a veracidade dessa teoria de formação. Foram encontradas variações significativas na quantidade de alguns metais leves em estrelas de um mesmo aglomerado. Com o passar dos anos, e principalmente após os anos 2000, essas anomalias foram encontradas em quase todos os aglomerados estudados. Um conjunto de estrelas com características similares é chamado de população estelar, então o fenômeno em que diferentes conjuntos de estrelas do mesmo aglomerado possuiam características distintas ficou conhecido Múltiplas Populações Estelares em Aglomerados Globulares. Ainda não se sabe como foi que estas populações se formaram no início da vida dos aglomerados e várias teorias já foram propostas, porém nenhuma foi capaz de explicar todas as características observadas nestes objetos.

É na busca de respostas para esse questionamentos que continuamos a estudar as múltiplas populações utilizando observações feitas pelo levantamento de dados S-PLUS (Southern Photometric Local Universe Survey — Levantamento de Dados Fotométrico do Universo Local Sul, em tradução livre). Este é um projeto liderado por pesquisadores brasileiros, e que conta com colaboradores do mundo todo, que está observando quase um quarto do céu noturno em doze bandas (faixas específicas do espectro eletromagnético). A Figura 1 mostra um mapa do céu onde as regiões que estão sendo observadas pelo S-PLUS estão em azul e todos os aglomerados conhecidos da Via Láctea estão identificados por estrelas roxas. Os aglomerados observados neste trabalho estão em destaque.

Para nossos propósitos utilizamos combinações destas bandas para separar as populações presentes em quatro aglomerados (NGC 104, NGC 288, NGC 3201 e NGC 7089). Utilizamos dados da literatura da quantidade de sódio em algumas estrelas de três dos aglomerados

para corroborar nossa separação e traçamos o perfil radial cumulativo de cada uma delas. A Figura 2 mostra estes perfis, onde em azul é a primeira população (mais pobre em metais leves) e em vermelho a segunda população (com quantidades anômalas de metais). A ideia por trás de fazer este perfil é que, dependendo do local de formação da segunda população dentro do aglomerado, ela pode apresentar um perfil diferente da primeira. Assim, podemos apontar para um cenário de formação destas múltiplas populações mais provável, dentro dos já propostos. A segunda população aparece mais concentrada nas regiões internas nos aglomerados NGC 288 e NGC 7089, ao contrário do que ocorre em NGC 3201. Também utilizamos informações sobre o movimento das estrelas dentro do aglomerado, feitas pelo levantamento *Gaia*, para estudar a dispersão de velocidades das populações.

Ainda há muito o que ser descoberto sobre esses objetos e é fundamental para a astronomia entender todos os processos que ocorrem durante a formação das estrelas em aglomerados. Afinal, são elas que produzem a maior parte da luz que vemos no céu a noite e compreender o seu processo de formação nos levará a conhecer muito mais sobre todos os fenômenos físicos que acontecem no Universo.

Palavras-chave: levantamentos de dados — aglomerados globulares: individual: (NGC 104) (NGC 288) (NGC 3201) (NGC 7089)

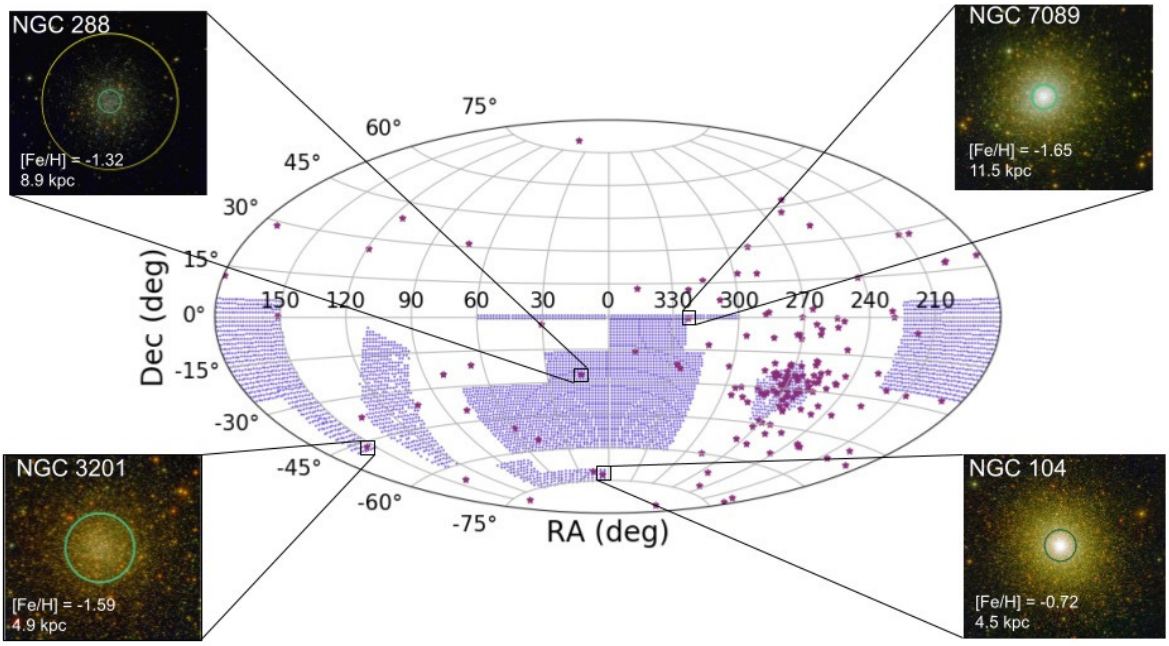

Figura 1

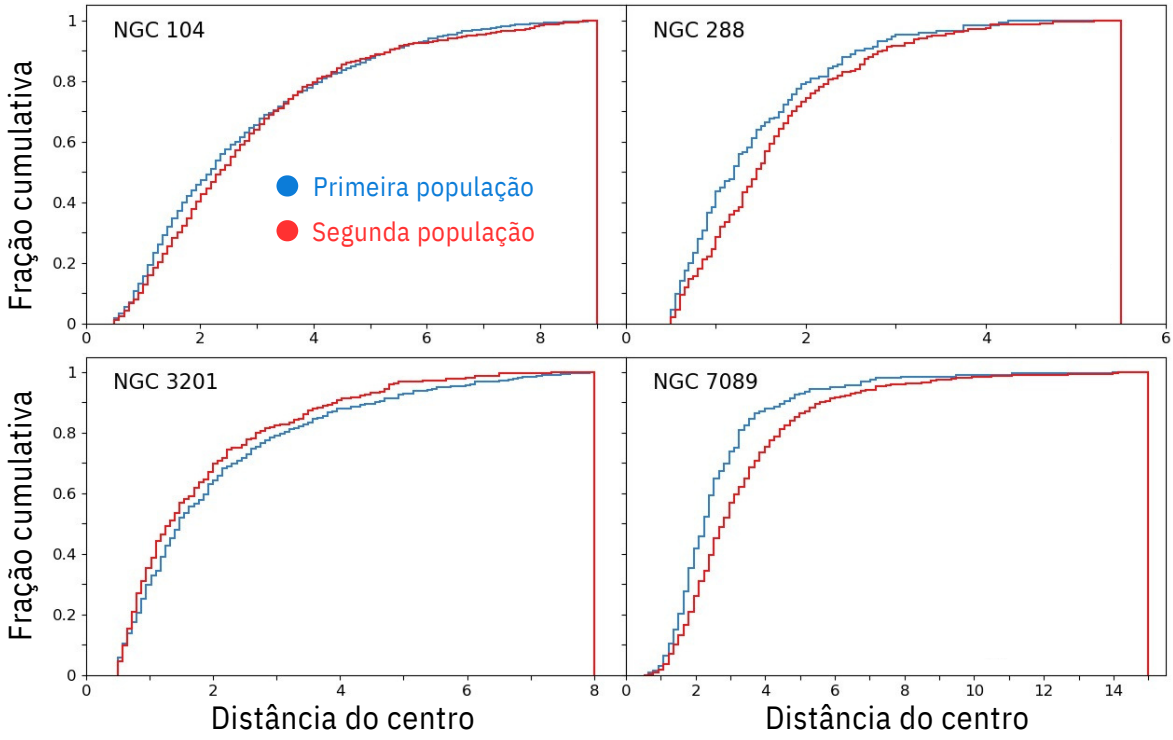

Figura 2

List of Figures

List of Tables

List of abbreviations and acronyms

MS	Main Sequence
AGB	Asymptotic Giant Branch
CMD	Colour Magnitude Diagram
MSTO	Mains Sequence Turn Off
SGB	Sub Giant Branch
RGB	Red Giant Branch
HB	Horizontal Branch
WD	White Dwarf
OC	Open Cluster
GC	Globular Cluster
YMC	Young Massive Cluster
GMC	Giant Molecular Cloud
MSP	Multiple Stellar Populations
MW	Milky Way
ChM	Chromosome Map
FG	First Generation
SG	Second Generation
IMF	Initial Mass Function
FRMS	Fast Rotating Massive Star
SMS	Super Massive Star
ICM	Intra-Cluster Medium
VMS	Very Massive Star
S-PLUS	Southern Photometric Local Universe Survey

J-PLUS	Javalambre Photometric Local Universe Survey
FWHM	Full Width Half Maximum
IRAF	Image Reduction and Analyses Facility
PSF	Point Spread Function
HST	Hubble Space Telescope
FoV	Field of View

Contents

1 Introduction

1.1 The life of a star as seen in a Colour Magnitude Diagram[1]

Stars can be considered the primary building blocks in Astronomy in general and galaxies in particular. They are the main source of the light we observe in the Universe today, at least in the visible, near-infrared and ultraviolet parts of the spectrum. Understanding their birth and evolution is of paramount importance to Astronomy, especially to any study involving galaxies and its components, such as Globular Clusters. One of the tools used to investigate stellar evolution is the Colour Magnitude Diagram (CMD), the observational counterpart of the Hertzprung-Russel diagram (Hertzsprung, 1911; Russell, 1914), where luminosity and surface temperature (or colour) are compared. In the CMD at least two magnitudes are used to construct a colour that is plotted against a magnitude. Thus in the y-axis we can see the brightness and in the x-axis we have a proxy for the temperature of the star. Figure 1 is a schematic view of a CMD of NGC 7089 showing the main stages of the life cycle of a number of stars. It was constructed using publicly available data from the *Hubble Space Telescope* (HST) UV Globular Cluster Survey (HUGS) (Piotto et al., 2015) and colour coded according to the major phases of stellar evolution.

A star is a rough spheroidal gas structure that is in a constant battle between the gravitational force, due to the star's mass, and the mechanical and radiation pressures coming from the nuclear reactions in its interior. Its formation, the collapse and coalescence of the molecular cloud that gives origin to a star is a complex process and some of it will be explored in section 1.3. For now, we begin the analyses of the evolution of a star once it has enough pressure and temperature (a few million degrees) for sustainable nuclear reactions to occur in its central parts[2]. This is when it enters the Main Sequence (MS), shown in green in Fig. 1. An important parameter, arguably the most important when it comes to stellar evolution, is the mass of the star: stars form with masses between $\sim$0.08 $M_\odot$[3] and a few hundred solar masses. Objects with masses lower than $\sim$0.08 $M_\odot$ do not have enough internal pressure to achieve fusion in their cores and are called brown dwarfs; on the other end, there are two limits for how massive a star can be: the accretion limit and the Eddington limit. During the accretion process it is expected that when reaching masses of 120-150 $M_\odot$ the temperature of the star is high enough to drive away any orbiting material, thus the name accretion limit. Although more massive stars have

[1] This section was based on the following books: "Stellar Evolution and Nucleosynthesis", Ryan e Norton (2010) and "Stellar Structure and Evolution", Kippenhahn, Weigert e Weiss (2013)

[2] The presence of an interacting companion can drastically change the evolution of a star. Here we detail the simpler case of an isolated evolution.

[3] the mass of the Sun is used as the standard unit and is equivalent to 1.99×10^{30} kg

been found they are expected to be the results of mergers of close binary systems and to be very unstable, having a life time of only a few million years. The Eddington limit arises due to the fact that as the mass of the star increases, i.e. its gravitational potential, the fusion reaction rate in the core also increases but not in the same proportion. At a certain point the radiation pressure is higher than the gravitational one destabilising the star. This results in an upper limit that is dependent on other factors such as the metal contents of the star.

The metallicity of an object is defined as the proportion of materials composed of elements other than Hydrogen and Helium. Although a formal calculation should involve every element, it is hardly practical. Thus a proxy is used, usually Iron. The metallicity of the star is an important factor in its evolution, having a significant effect in the energy transfer inside the star. Now, the life of the star in the MS is relatively calm, it will transform Hydrogen into Helium via two main processes: the proton-proton chain and the carbon-nitrogen-oxygen (CNO) cycle. The process that dominates the generation of energy will depend, again, on the mass of the object. For $M_\star \lesssim 1.5\,M_\odot$ the proton-proton is the dominant process and this region is called the Lower Main Sequence. For $M_\star \gtrsim 1.5\,M_\odot$ the CNO cycle takes over in the Upper Main Sequence. The time that a star remains in the MS is dependent on how fast it burns the H present in its core. For low mass objects this could be hundreds of billions of years, while super massive objects last only for a few million years. During this time the position of the star in the CMD will not change significantly, that is until it runs out of fuel and passes to the next stages of evolution.

Stars with masses close to $0.6\,M_\odot$ are not capable of burning Helium once the Hydrogen is depleted in the core, thus they will go through a phase of H shell burning where energy is generated via Hydrogen fusion in a shell around the core, causing the star to expand into a red giant and occupying a place in the Red Giant Branch (RGB, shown in red in Fig. 1) but never reaching the tip of the Asymptotic Giant Branch (AGB, shown in orange in Fig. 1). Eventually they shed their outer layers and end their lives as Helium white dwarfs.

For stars with masses similar to the Sun the process is more interesting. Once the Hydrogen is exhausted in the nucleus they will pass through two stages: one where the core is inert and H is burned in a shell around it and a period where He and H are burned in shells inside one another around a inert core of carbon. In this two phases the star inhabits, respectively, the RGB and the AGB and between them it burns Helium in its core while in the Horizontal Branch (shown in blue in Fig. 1). First, as soon as H is exhausted in the core the star leaves the MS in a point called the Main Sequence Turn Off (MSTO) and begins burning Hydrogen in a shell around the core. This deposits more He in the core increasing its mass in a process that can take from a few million years to a couple billion. Here the star is in the Sub Giant Branch (sGB, shown in orange in Fig. 1)

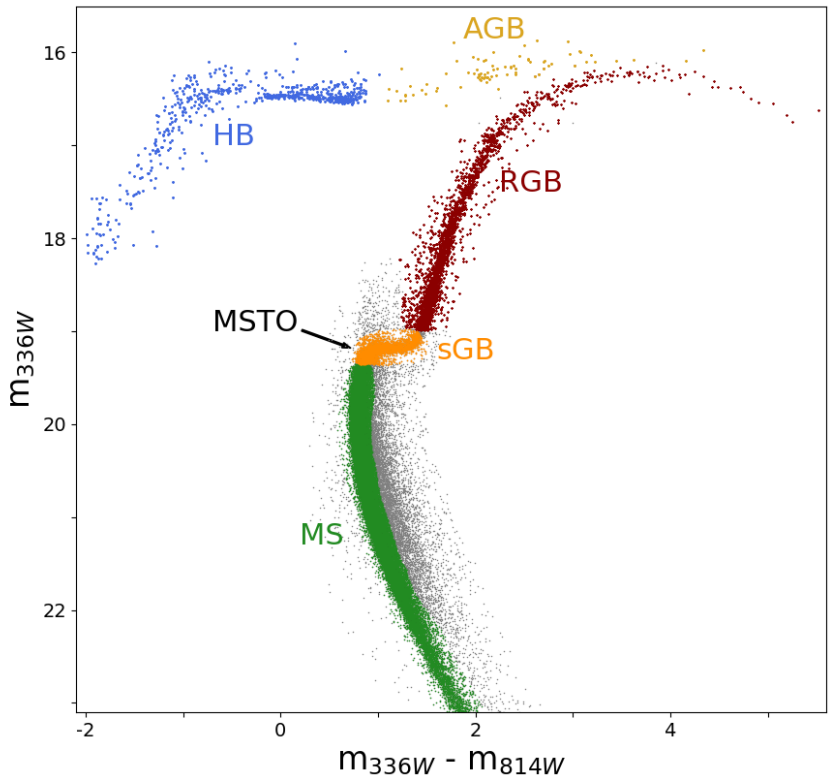

Figure 1 – A colour magnitude diagram of NGC 7089 constructed using HST magnitudes. The main features are colour coded in the following manner: Main Sequence — green, Sub Giant Branch — orange, Red Giant Branch — red, Horizontal Branch — blue, Asymptotic Giant Branch — yellow.

phase, with time either the core will become degenerate (for star with similar mass to the Sun) or the outer layers will cool becoming more opaque (in more massive stars). Both cases lead to an increase in the temperature of the H burning shell and an expansion of the star, leading it into the RGB. During the RGB (shown in red in Fig. 1) this process is exacerbated with the increase of the core mass and eventually it ignites the Helium burning in the core, moving the star to the HB. In stars with masses between 0.6-2 $M_{\odot}$ it occurs the Helium flash at the start of core He burning, where an enormous quantity of energy is generated in a very short time. However, the energy is used to expand the initially degenerate core, not having a visible effect on the outside of the star. As the core expands the outer H burning shells loose energy causing the star to shrink and increase the surface temperature. Higher mass stars can move along the HB to hotter temperatures becoming unstable with pulses, the so called RR Lyrae variables, while others can get even hotter forming a tail in the HB. This causes the HB to have very different morphologies in different clusters depending on metallicity, age and helium content. He burning generates Carbon and Oxygen in the central region. Once a core of carbon/oxygen is formed the

star continues to burn both H and He in shells around it and moves into the AGB phase (shown in yellow in Fig. 1), the He formed in this process can fall into the nucleus and cause instabilities. They are called thermal pulses and appear at the end of the AGB. Ultimately, this process ceases and the star sheds its outer layers forming a planetary nebula with a White Dwarf (WD) in its centre. The WD is nothing more than the cooling core composed of carbon/oxygen of the original star, sometimes with a thin atmosphere.

Stars with masses above $\sim 8\,M_\odot$ have a different evolution than low and intermediate mass stars. When H is depleted in the core it already has enough temperature to start the He fusion via the alpha process generating carbon and oxygen. These objects have enough mass that the fusion processes in the nucleus will only stop once the star produces Fe. The reason for this is that all previous elements produce a surplus of energy when formed. However to make iron the star has to spend more energy than it generates to counter balance gravity. This will lead to its final destruction in a violent event called a supernovae. But before that the star will develop a onion-like structure with shells burning higher atomic number elements from the outside in. Hydrogen burning surrounding He burning, that in turn surrounds a C burning shell and so on. Neon is followed by oxygen, silicon and a final core of iron. The silicon fusion in the core is an incredibly fast process, lasting approximately a day and dooming the star. After the supernovae event what is left is either a neutron star or a black hole, depending on the initial mass. It is during this process that elements heavier than iron are produced (although some heavier than iron elements can also be produced in lower mass red giants) via the capture of neutrons and are subsequently expelled into the inter-stellar medium. What is left can be a neutron star, where during the collapse the electrons are captured by the nuclear protons and, without the repellent force of the electron cloud, form a very compact ball that resists further collapse via the Pauli exclusion principle. If the stellar mass left at the end of its life is big enough (around $\sim 3\,M_\odot$), given that the star looses some mass in various points of its evolution, the neutron degeneracy pressure is not enough to sustain the remaining core causing it to collapse into a black hole.

This is a general overview of the evolution of a star seen in a colour magnitude diagram, a standard tool in the field of globular clusters. In the following sections we will explore what are star clusters, how they form and the challenge that is understanding how multiple populations are present in these objects.

1.2 Star Clusters

Typically, we consider that our Galaxy is made of three constituents: the stars, the interstellar medium (composed of atomic and molecular gas together with dust) and dark matter. Considering that the Milky Way is a spiral galaxy we can separate its stars

into three grand structures: the disk, which can be further split into the thin and thick disks; the bulge, a compact structure in the centre of the Galaxy; and the halo, a low density region that surrounds the disk and bulge. However, when looking at the stars we see that they are organised in smaller structures: the star clusters. They can be divided into two categories: Globular Clusters (GCs) and Open Clusters (OCs). Broadly speaking, in the Milky Way OCs tend to be young ($\lesssim 6\,\mathrm{Gyr}$), loosely bound collections of stars with masses $\lesssim 5,000\,\mathrm{M}_\odot$, while GCs are older (>6 Gyr), more massive ($\gtrsim 10^4\,\mathrm{M}_\odot$, Kharchenko et al. (2013)) and present a spheroidal distribution of its members. The boundary between OCs and GCs is not very precise, and becomes even fuzzier when one includes Young Massive Clusters (YMCs), faint fuzzies (see e.g. Chies-Santos et al. (2013)) and diffuse stellar clusters (Peng et al., 2006) from other galaxies.

We will explore in more detail the current theories of star formation, their triumphs and short comings in section 1.3, but a brief summary is as follows: Giant Molecular Clouds (GMCs) with hundreds of thousands of solar masses of gas composed primarily by Hydrogen and Helium, with trace amounts of heavier elements, are mainly governed by their own gravitation and internal pressure remaining in equilibrium for long periods of time. However, clouds that are in unstable equilibrium may collapse upon themselves when affected by some mechanical perturbation, primarily by external forces such as the explosion of a relatively nearby supernova or tidal interactions with other GMCs or other galactic substructures. During the collapse, the cloud fragments into smaller pieces in a hierarchical process forming smaller clumps of a few solar masses. These clumps then collapse even further forming stars. Although all the details of this process — basically known as the Jeans instability theory — are not yet fully understood, one thing is clear: stars do not form alone.

At first glance a star cluster seems very straightforward to define —a collection of stars gravitationally bound (Portegies Zwart; McMillan; Gieles, 2010)— it is in the edge cases that one finds difficulties and a need for a more precise definition. Lada e Lada (2003) defined a cluster as a collection of bound stars with a high enough density ($\gtrsim 1\,\mathrm{M}_\odot\,\mathrm{pc}^{-3}$) as to be stable against tidal disruption and avoid N-body evaporation for at least 100 Myr. Another way is to look at them as overdensities of stars when compared to the local neighbourhood (Krumholz; McKee; Bland-Hawthorn, 2019). These definitions are more significant when dealing with open clusters, where the number of objects is small and they often have substructures. When studying globular clusters, these definitions hardly disagree given that such objects are very dense and old.

The study of star clusters allows us to probe a variety of processes that are of paramount importance to all areas of Astrophysics. From the complex processes involved in the formation of the stars such as the role of turbulence, gravitation and magnetic fields to the formation of clumps and the Initial Mass Function can be understood by

studying such objects and their progenitor clouds (McKee; Ostriker, 2007). Stellar winds, supernovae and stellar evolution can also be studied in these objects, as they provide a large number of stars and a wide range of important parameters such as mass, age and metallicity. The dynamical and kinematic evolution of these objects is also of particular interest for astronomers, as it pertains to the long term evolution of galaxies. Given the large number of stars and their close proximity in GCs, a number of dynamical phenomenon are present in these objects. Two body relaxation, mass segregation, the collapse of the core, evaporation and tidal disruption are examples of this (Vesperini, 2010).

Globular Clusters were the prime example of a Simple Stellar Population, thought to form from the collapse of a GMC, all of the stars would be expected to share the same chemical composition, only varying in their initial mass. Nonetheless, in the early 70's the first cracks in this idea began to show. Spectroscopic studies found some variation in light elements between stars in the same cluster. Further studies expanded this (see Smith (1987) and Gratton, Sneden e Carretta (2004) for earlier reviews on the topic), and today it is accepted that all old and massive Globular clusters have at least two distinct stellar populations. This is the main focus of this work. However, before we expand on this, a brief explanation of the formation of star clusters is given in the next section.

1.3 Star Cluster Formation[4]

Stars and, consequently, clusters of stars are formed inside of Giant Molecular Clouds, which are composed primarily of molecular Hydrogen. The exact process by which these GMCs contract, fragment and form stars is very complex and it is still not fully understood. One of the most developed scenarios, and the one described here, is the Global Hierarchical Collapse (Vázquez-Semadeni et al., 2019). Since clouds exhibit hierarchical structures with denser regions of clumps and filaments formed by cold molecular gas, they achieve the Jeans mass necessary for collapse rather easily. The Jeans mass (M_J) is the critical mass above which the internal gas pressure cannot maintain the cloud in hydrostatic equilibrium (Jeans unstable) and it collapses under its own gravity. Simulations show that the cloud accretes gas from the surrounding medium and that this process generates supersonic turbulence and instability causing a global gravitational contraction.

Given that the turbulence causes density fluctuations with nonlinear amplitudes and the amorphous and filamentary shape of the cloud, the collapse is far from presenting a uniform spherical profile. In a turbulent system, the density fluctuations have a smaller free-fall time compared to the cloud, thus sub-regions collapse faster than the cloud, fragmenting the entire structure in a series of collapses within collapses. The formation of

[4]This section was based on the following book and reviews: "Star Clusters", Archinal e Hynes (2003); "Star Clusters Across Cosmic Time", Krumholz, McKee e Bland-Hawthorn (2019); "The Physics of Star Cluster Formation and Evolution", Krause et al. (2020).

filaments in GMCs can be attributed to the fact that in a pressureless collapse anisotropic structures tend to contract along their shortest dimension, forming sheets and subsequent filaments that act as 'matter rivers', dragging material from large scales to smaller ones. The points where filaments meet are expected to be the preferential location for star formation and indeed this is supported by observations and self-consistent simulations (Lada; Alves; Lada, 1999; McKee; Ostriker, 2007).

The fragmentation and collapse of the sub-regions in a cloud have to stop when clumps have stellar masses. This happens because during the nearly isothermal phase they release their gravitational potential energy as radiation. However, with the increase in density the opacity also rises until the energy transfer becomes inefficient. The result is that the process becomes adiabatic and, consequently, the fragments begin to heat and increase the internal pressure. At this point further fragmentation stops and the clumps coalesce into rotating spheres of gas that undergo Hydrogen fusion in their nucleus that we call stars. During these phase and up to the initial life of the star it can accrete matter from the surrounding environment (this is a major component in some scenarios of multiple stellar populations formation). The exact models for how such a process occurs are still a source of debate. At this point it is expected that the gas that hasn't been consumed by the stars in their formation is expelled from the cluster by stellar feedback.

From this point on, the cluster evolves mainly dynamically. During the initial $\sim 1\,\mathrm{Gyr}$ the main mechanism of cluster dissolution are tidal 'shocks' due to galactic substructures. Some simulations show that in environments similar to the early Galaxy assembly, i.e. gas-rich, the initial GC population of the Milky Way could be decimated, with only a reduced number surviving till the current epoch (Elmegreen; Hunter, 2010; Kruijssen; Dale; Longmore, 2015). In the long term two-body relaxation becomes a major factor in the dynamical evolution of GCs and has been shown to eventually dissolve all clusters independent of a Galactic tidal field.

Two-body relaxation is the process by which two stars suffer a close encounter and exchange energy. In GCs this will tend to disperse the kinetic energy equally among the stars. One of the main consequences of this is that higher mass objects will have smaller velocities and sink into the cluster potential while lower mass stars will move to larger orbits, eventually escaping the cluster entirely. This also leads to what is refereed as core collapse. This happens when the density in the cluster centre is so high that the surface brightness in the region forms a power law cusp. Now, due to the high density in the collapsed core, tight binary systems are likely to form which when interacting with other stars inject energy into the system leading to a re-expansion of the cluster. The average time for the core collapsing process in MW GCs is of the order of $10^8\,\mathrm{yr}$, much smaller than their lifetimes, thus it is expected that some clusters have already experienced this at least once.

This presents a general picture of how star clusters form, however many aspects are yet to be fully understood. The levels of turbulence observed in GMCs, the role of magnetic fields in clouds and how they are dispersed in the star formation process, the role protostellar feedback plays in disrupting the formation of more massive stars, among other problems (see McKee e Ostriker (2007) for a review). Besides these, the presence of Multiple Stellar Populations (MSPs) in Galactic globular clusters is also a challenge to our understanding of star formation. The observational evidences for MSPs will be explored in section 1.4 and the proposed scenarios for their formation is expanded in section 1.5.

1.4 Observational Evidences of Multiple Stellar Populations

Multiple Stellar Populations are defined as star-to-star chemical abundance variations which do not arise from the normal process of stellar evolution. In Galactic GCs these variations are usually limited to light elements such as He, C, N, O, Na and Al (some anomalous GCs also present spreads in Fe, e.g. Ω Cen (Johnson; Pilachowski, 2010)). In the literature, stars with enhanced He, Na and N and depleted in O and C are usually called 'second generation' or 'second population', while the ones with a similar composition to field stars (at the same metallicity) are dubbed 'first generation' or 'first population'. For this work we use the terms first and second populations (or the shorter 1P and 2P), because the term 'generation' implies a stricter connection and 'parentage' between them. While this is present in some formation scenarios, it has not been firmly established yet in the literature. Such variations in light element abundances produce complex CMDs, particularly as multiple stellar sequences from the MS to the tip of the RGB. This means that it is possible to study this phenomenon using both of the major tools in Astronomy: spectroscopy and photometry. In the next sections the evidences for the presence of multiple populations will be explored, first in the realm of abundance measurements and second in photometric studies.

1.4.1 Light Element Abundance Variations

Evidence for anomalies in the abundance of light elements were first discovered in the early 70s by Osborn (1971), where RGB stars with the same magnitude showed varying strengths in the CH, CN and NH molecular bands. An important finding from this study was that the CN and CH are found to have a negative correlation, thus as stars increase their Nitrogen content they are depleted in Carbon. This was confirmed by later investigations and the C-N correlation was found in almost all well studied GCs (Sneden et al., 1992; Carretta et al., 2009). Further studies have shown that other light elements also present anomalous behaviours, in particular Na, O, Mg and Al. Evolutionary mixing due to the CNO-cycle was raised as a possible explanation of the origin of MSPs (Denisenkov; Denisenkova, 1990), though the presence of anomalies in MS and MSTO stars as well

as the variations in heavier elements has discarded this possibility (Cannon et al., 1998; Gratton; Sneden; Carretta, 2004).

While these correlations are present in virtually all old and massive GCs, the exact shape of the correlation varies greatly between the clusters. In clusters, such as NGC 6397, a rather narrow distribution in the Na-O correlation is apparent, while others present a broader arrangement (see Fig. 8 of Carretta et al. (2009)). Another important feature in the correlations is that some clusters present a more clumpy distribution while others appear smoother. This may be due to intrinsic properties of the origins of these anomalies. However, studies with smaller uncertainties are needed to substantiate these differences.

Another important element to consider is Helium (it's mass fraction is denoted by Y). While direct observations of the lines produces by He are challenging (requiring stars with surface temperatures between ∼8,500 K and ∼11,500 K) some measurements have been made in HB stars and show a typical spread of $\Delta Y = 0.02 - 0.050$ (Mucciarelli et al., 2014). The abundance of He can be inferred by assuming (based on simulations) that the photometric spread in specific colours is due mainly to He. By comparing stellar evolutionary tracks with different He content it is possible to constraint the variations in abundance between the populations. This has been done to a number of GCs (Lagioia et al., 2018; Marino et al., 2019) and the maximum internal ΔY found ranges from ∼0.01 to 0.18. Another important finding is that Helium correlates with the cluster mass, which can be a constraint on formation scenarios (Milone et al., 2015a).

Lithium is a rather fragile element, it can be easily destroyed during the p-capture process in temperatures above ∼2,500 K. It has been found to vary between the populations and presents a negative correlation with Na (Pasquini et al., 2005; D'Orazi et al., 2015). On the other hand, some studies have found no significant variation in the abundance of this element (Mucciarelli et al., 2011).

1.4.2 The Use of Colours in MSPs Studies

While spectroscopic studies can give us a lot of insight into the chemical properties of cluster stars they are limited to a small number of objects (usually less than 200 stars per cluster). In this aspect, photometric studies provide a clear advantage: they are capable of observing thousands of stars simultaneously from the crowded cluster interior to the sparse outskirts. Using photometry we can also better estimate the ratio of first to second population in clusters as well as their radial distributions. When constructing CMDs with specific filter combinations splits can be seen from the MS all the way to the tip of the RGB. This is due to the aforementioned fact that the populations have different chemical compositions. Filters focusing in regions where relevant molecular features are more prevalent can detect magnitude variations. Figure 2 is a reproduction of Fig. 1 from Milone et al. (2015b) showing a CMD of NGC 2808 made using HST filters where multiple

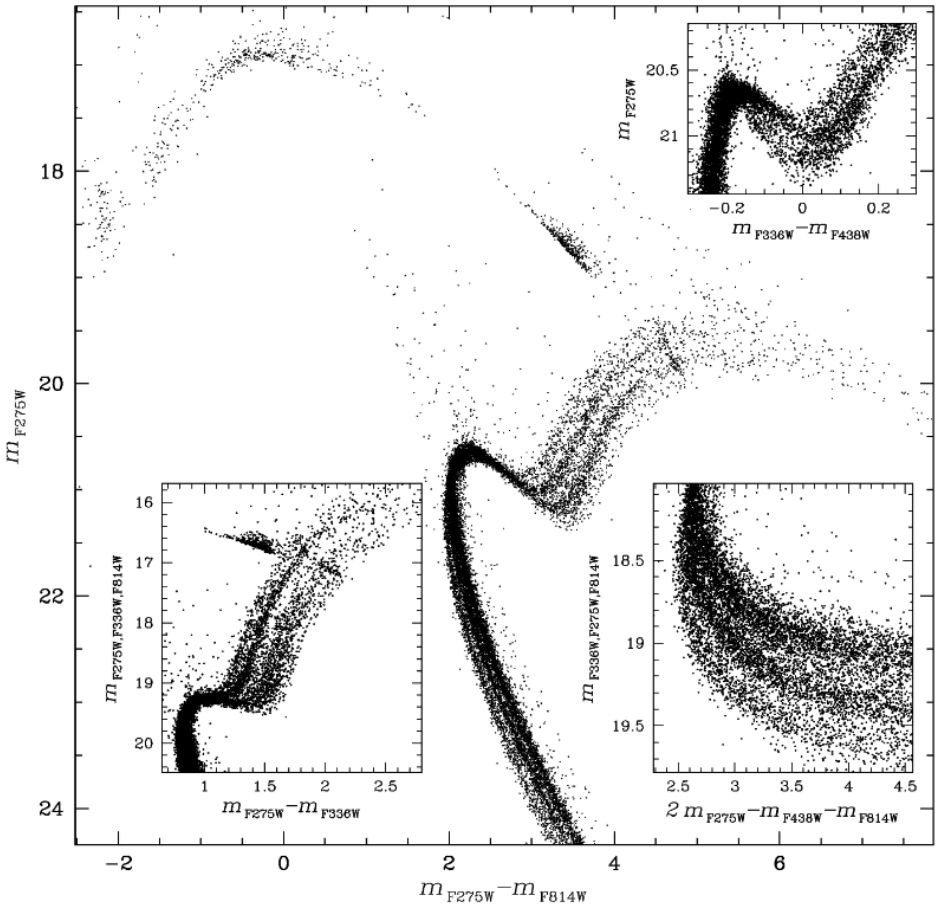

Figure 2 – Reproduction of Fig. 1 from Milone et al. (2015b). A CMD constructed using HST colours of NGC 2808.

sequences are clear in the RGB. The insets focusing in the MS, SGB and RGB and using different colour combinations highlight the clear splits attributed to MSPs.

The *HST UV Legacy Survey of Galactic Globular Clusters* (Piotto et al. (2015) and following papers) coordinated by G. Piotto has been a major tool in understanding the phenomenon of MSPs. Fifty six GCs have been observed in five HST filters allowing a homogeneous study of these clusters. In Milone et al. (2015a) they introduced the *chromosome map* (ChM) which has been paramount in the study of MSPs. The ChM is obtained by plotting $\Delta^N_{F275W,F336W,F438W}$ vs $\Delta^N_{F275W,F814W}$. These are two colour differentials constructed in the following manner: two fiducial lines (blue and red) are defined along the RGB by determining the 5% and 95% percentile of stars per magnitude bin in the F814W vs (F275W - F336W) - (F336W - F438W) and F814W vs (F275W - F814W) CMDs, then each star's Δ is calculated according to the formula:

$$\Delta^N_X = \frac{X - X_{bluefiducial}}{X_{redfiducial} - X_{bluefiducial}} - 1. \tag{1.1}$$

Here, X, $X_{bluefiducial}$ and $X_{redfiducial}$ refers to the colour value of the star, the blue

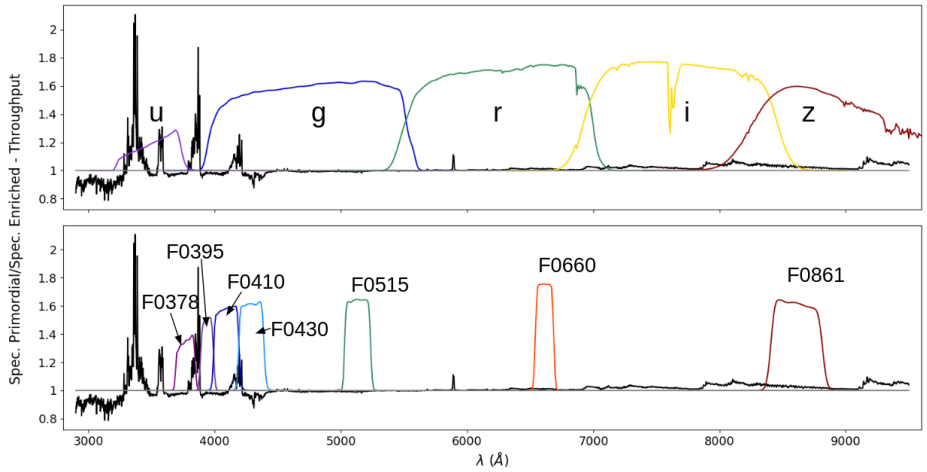

Figure 3 – Ratio between the spectra of first generation and second generation stars, overplotted are the S-PLUS filters.

and red fiducial lines, respectively. Essentially this verticalizes the RGB. By plotting one Δ against another the ChM is created. Using this technique Milone et al. (2015a) found three main stellar populations in NGC 7089, which are corroborated by spectroscopy, and further separated into seven components. One important aspect of looking at the clusters through the ChM is that some show a simple and clear separation between the populations while others display a complex ChM with additional structures. This has lead to the creation of two categories: Type I (simpler) and Type II (complex) clusters (Milone et al., 2017). Some trends have been found in type II clusters, e.g. younger clusters tend to be more metal-rich and further away from the Galactic centre, they also tend to be, on average, more massive and have a more eccentric orbit in comparison to Type I clusters (Simioni; Aparicio; Piotto, 2020).

The filter combinations that provide the best separations between populations, i.e. that show spreads in CMDs, usually combine filters with wavelengths between $2500 \leqslant \lambda \leqslant 4500$ Å. This is due to the fact that important absorption features of the molecules NH and CN are located in this region. Vinicius Branco (*private communications*) used synthetic models to generate two populations of stars with different chemical characteristics, one simulating the primordial composition of the first population of NGC 104 and another with enhanced Na and a decrease in O and C, the second population. In Fig. 3 we show the ratio between both spectra (after being convolved with a Gaussian filter) together with S-PLUS filters. It is clear the importance of the blue part of the spectrum, while the redder section shows little to no difference.

1.4.3 MSPs in Extragalactic GCs

Multiple stellar populations are not a Milky Way exclusive phenomenon, abundance variations have been found in clusters belonging to the Magellanic Clouds and the Fornax

dwarf spheroidal (Larsen et al., 2014) and hints of MSPs due to extended horizontal branches in M87, M31 and M81 (Sohn et al., 2006; Mayya et al., 2013; Peacock et al., 2017). Mucciarelli et al. (2009) found abundance variations of N, Mg, Na and Al in three GCs belonging to the Large Magellanic Cloud (LMC). Lindsay 1, in the Small Magellanic Cloud (SMC), also presents star-to-star chemical inhomogeneity associated with MSPs (Hollyhead et al., 2017). All of this seems to indicate that MSPs are a ubiquitous phenomenon of all old and massive GCs, thus being a fundamental aspect of their formation process.

1.4.4 Global Properties and Known Correlations

Although the exact characteristics of MSPs vary a lot by cluster some general trends are present. One of the main characteristics that arise from the most popular formation scenarios is that 2P stars form in the more central regions of the cluster and thus should be more prevalent there, at least for some time. To asses this in current GCs we can construct radial distributions. In general, the 2P is found to be more centrally concentrated, especially in the inner most region of GCs (Lardo et al., 2011; Simioni et al., 2016). However, there seems to be some exceptions to this, where 1P is more concentrated (e.g. in M 15, Larsen et al. (2015)) and where there is no difference between them (Dalessandro et al., 2014). The ratios of 1P/2P are also an important factor. In general the 2P seems to make up the majority of objects in clusters. However this characteristic appears to be tied to cluster mass, with more massive clusters having a higher fraction of 2P (Milone et al., 2017). Another factor seems to be age, where nearly all clusters older than $\sim$2 Gyr present MSPs, where the youngest cluster showing multiple populations is NGC 1978, at the 2 Gyr mark (Martocchia et al., 2018).

1.5 MSPs formation Scenarios

Initially, the Evolutionary Hypothesis was suggested as an explanation of the anomalous abundance patterns. It consists in the idea that the light-element variations are the result of mixing processes happening in RGB stars. In this scenario convection events would drag processed material from the interior, polluting the atmosphere of the star and leading to anomalous abundance patterns. However, this can be ruled out for a number of reasons, mainly because abundance variations have been found in non-evolved MS stars (Hesser, 1978; Cannon et al., 1998). Another point is the presence of abundance patterns in elements such as Na, Al and Mg, which are not capable of being produced by the small mass stars in present day RGBs (Prantzos; Charbonnel; Iliadis, 2007). This points to an outside source of processed material. For this some possible polluters have been proposed and we analyse their merits and short comings in the following sections.

The proposed formation scenarios can be broadly divided into two categories with the main one being called the Multi-Generations, which proposes that star formation occurred in more than one episode in relatively quick succession[5]. Between each formation episode the intra cluster medium would be polluted by the more massive stars of the previous generation. Possible sources for the polluting material are Asymptotic Giant Branch stars, Interacting Binaries or Super Massive stars. The second type of formation scenario is called Coeval, in which both populations are formed at the same time and the anomalous populations are formed due to abnormalities in the accretion process.

1.5.1 The AGB scenario

Perhaps the most popular scenario was proposed in Cottrell e Da Costa (1981). The initial idea states that a massive molecular cloud collapses and forms the first generation of stars with a single age and abundance pattern. Enough time passes so that feedback of massive stars and supernovae clear away the remaining gas. This prevents Fe spreads that aren't observed in GCs (although some clusters have them, e.g. ω Cen). When stars from the FG pass through the AGB phase, processed material from the core that has been dragged to the surface by convection is expelled into the intra cluster medium (ICM) by low velocity winds. This material is diluted with inflowing pristine gas and falls to the cluster centre. Once the density is high enough a new star formation episode occurs forming the second generation (SG).

The inflow of gas with a chemical composition similar to the FG is important to tackle the problem of the Na-O inverse correlation. AGB yield models are not capable of reproducing the Na-enrichment and O-depletion observed in most clusters (although there is still some debate about this, e.g. Doherty et al. (2014)), thus requiring the dilution of the material with pristine gas. One issue with this model, and many others, is the Mass Budget problem: considering the Initial Mass Function (IMF)[6] of the FG, only a small fraction will be in the mass range of stars that can produce the polluting material. This suggests that the SG would represent only a small percentage of cluster members, in direct contradiction with observed data where the fraction of SG stars f_{SG} is in the range of $0.4 - 0.8$. One possible solution for this is that clusters have lost a large fraction of FG to the field, up to 95% in some cases, and retain most of SG stars.

1.5.2 Fast Rotating Massive Stars

Another possible source for processed material are Massive Stars. In their cores they undergo hot hydrogen burning, forming the necessary materials for enrichment. Since

[5] In this section we will use the terms first and second generations (FG and SG, respectively) when talking about the Multi-Generations scenarios for obvious reasons.

[6] The IMF describes the relative number of stars as a function of their initial mass that form in a single formation episode

the material is produced in the centre of the star and normally they are not entirely convective, another mechanism needs to bring this material to the surface so it can be expelled by winds. If the star is rotating very fast this induces internal mixing which can cause the star to be almost fully mixed. This scenario, developed by Decressin et al. (2007) and Decressin, Charbonnel e Meynet (2007), is very similar to the AGB one, but happens in a much faster time scale (typically of $10 - 20\,\mathrm{Myr}$) and suffers from the same dilution and mass budget problems. However, since the cluster has not had time to expel the leftover gas from the formation of the FG. The dilution can occur without the need for gas accretion into the cluster. Another challenge to this scenario is that Fast Rotating Massive Stars (FRMS) do not reach temperatures high enough to activate the Al-Mg chain, thus they do not reproduce the Mg spreads present in some clusters.

1.5.3 Super-Massive Stars

First proposed by Denissenkov e Hartwick (2014), this scenario envisions the pollution of the gas that would form the SG to come from Super-Massive Stars (SMS, $> 10^3\,\mathrm{M}_\odot$). The SMS could form by the merger of massive stars which sink into cluster centre due to dynamical friction. Such objects would be convective and could achieve temperatures high enough to produce the abundance patterns of SG stars. Since their luminosity could exceed the Eddington limit, a large amount of material would be expelled trough radiation driven winds and, mixing with pristine material, form the SG.

Gieles et al. (2018) also envisioned the pollution of the ICM by the product of mergers, however they proposed the formation of a single Very Massive Star (VMS) in the cluster centre. The gas accretion in the early stages of GC formation would cause an adiabatic contraction and increase the number of collisions in the core, forming the VMS. The VMS would periodically expel enriched material due to instabilities, but could be rejuvenated by further accretion events guaranteeing a sufficient output to form the SG.

1.5.4 Interacting Binaries and Stellar Mergers

de Mink et al. (2009) proposed that massive binary stars close enough to have a significant interaction can shed most of their envelope to the intra cluster medium. This material would have the necessary abundance pattern and low enough velocity that it can remain in the GC gravitational potential well to form the SG. Since the exact yields of this scenario depends on various parameters such as the interaction time, the total mass and mass ratio of the stars, this allows for the large variation observed from cluster to cluster.

Given that early GCs were binary rich environments, Wang et al. (2020) showed trough N-body modelling that a large percentage of massive stars ($> 30\mathrm{M}_\odot$) can merge in the initial $5\,\mathrm{Myr}$ of the cluster life. This mergers are the source of FRMS and SMS. Thus

in this scenario material ejected during the merger process is mixed with ejecta from the merger products to form the SG. This aims to combine more than one source of polluting material which can introduce into the model an important observational feature of MSPs: the variety and uniqueness of each GC.

1.5.5 Early Disk Accretion

All the models analysed here so far invoked multiple episodes of star formation. The scenario envisioned by Bastian et al. (2013) is the first where this is not required. The authors suggest that processed material (be it by SMS, FRMS or interacting binaries) concentrated in the more central regions of the cluster is swept into protoplanetary disks surrounding low-mass stars, eventually being accreted by the star. This scenario was motivated by observations of YMCs, and while it is consistent with observations of such objects it has many problems when considering Galactic GCs. One such problem is that while the disk can accrete material from the ICM it has very low angular momentum, which causes the disk to fall into the star and disappear, resulting in very small abundance spreads.

1.5.6 Extended cluster formation

One aspect to consider is the environment in the early epochs of the Universe, namely high density, turbulence and pressure. First proposed by Prantzos e Charbonnel (2006) and further expanded by Elmegreen (2017) this scenario envisions the formation of a FG in the dense central regions of a GMC. The more massive stars have their envelopes stripped by interactions in the high stellar environment. This material is mixed with pristine gas forming the SG. Here it is expected that a significant fraction of FG is lost to the field, while the SG numbers remain relatively intact. One problem with this model is that since the SG start formation very early on, the FG massive stars did not have enough time to produce large quantities of He, which would make it very difficult to produce the He spreads seen in some clusters.

1.5.7 Failed Clumps Model

Parmentier e Pasquali (2022) investigated the importance of failed cores in the formation of stellar clusters and proposed a model for the formation of MSPs. Failed cores are denser regions inside the molecular cloud that despite having enough mass where their own gravity becomes more relevant than the surrounding medium do not collapse to form a star. After a brief period the core re-expands and disperses the material into the intra-cluster cloud, refuelling the gas reservoir and, once enough cores fail, reigniting

star formation. This would lead to multiple generations of stars[7] depending on parameters such as the core formation efficiency per free-fall time ($\epsilon_{\rm ff,co}$), the fraction of the mass in cores that returns to the clump gas (f_{return}) and associated time-span. For MSPs to appear in this model a source of polluting material needs to be present. The authors propose that in clusters with high enough mass the SMS scenario can be triggered. One of the major advantages is that the formation of multiple generations and populations are decoupled, which can —at least qualitatively— explain the variety of MSPs we observe. Further development of this scenario is still needed.

1.6 Studying Multiple Populations with the Multi-band Survey S-PLUS and *Gaia*

It is in this context that four Galactic globular clusters were chosen to be the object of a multi-band photometric study. To do this we used the observations made by the T80-South telescope, part of the *Southern Photometric Local Universe Survey*, of clusters NGC 104, NGC 288, NGC 3201 and NGC 7089 in 12 bands. Our intention was to verify the power of the S-PLUS filter system in separating the MSPs in these clusters. We also intended to use the wide Field-of-View of S-PLUS (that could encompass the entire cluster in a single pointing) to study how the MSPs vary as we move out of the cluster. To do this, we first applied PSF photometry in these images and derived the zero points using a differential method. We also used proper motion data from the *Gaia* survey in order to establish a clean sample of cluster stars, eliminating the majority of contaminants. With this we selected six filter combinations and used the same method for Δ construction applied in the making of the *Chromosome map* to create a six dimensional space where a K-means algorithm was used to separate the populations in each GC. We used Na abundance data from the literature, available for stars of three of our observed clusters, to corroborate our separation and traced the radial profiles of both populations in each cluster. Chapter 2 details the data reduction, photometry, calibration, correction by differential reddening in NGC 3201, the selection using *Gaia* and the K-means algorithm. An analyses of the recent relevant literature about each cluster is also present in Chapter 2. Chapter 3 contains the article that was published in the *Monthly Notices of the Royal Astronomical Society* in 2022 as a result of this work, in it is the analyses of the data as well as the conclusions.

[7] Here a *generation of stars* refers to the objects formed in an episode of star formation, independent of their chemical composition, while the term *population* is used to refer to stars with similar chemical composition.

1.7 *Gaia* proper motions

A natural line of inquiry following the work on MSPs photometrically and considering the availability of *Gaia* proper motion information (and their limited use in the previous work) is to study the kinematics of the populations. As stated before, different formation scenarios present varying birthplaces inside of the cluster. For example, in the most common scenario where a 2P is formed in the denser regions of the cluster centre, it tends to migrate outwards and disperse into the 1G via two-body relaxation (Tiongco; Vesperini; Varri, 2019). What is important to note here is that the current kinematics of the populations can provide hints to the initial state of the system, i.e. the exact processes involved in the formation of these stars influence how they behave in the cluster even billions of years later, as shown by multiple N-body simulations (Dalessandro et al., 2019; Tiongco; Vesperini; Varri, 2019; Richer et al., 2013; Hénault-Brunet et al., 2015). Naturally, any current simulation is incapable of describing a specific GC system in its entirety. However, they can be used to draw general trends and, by comparing simulations with the current state of GCs, some idea of their initial configuration can be gleaned. This is a rather daunting task, but increment progress is still progress.

In view of this, we took advantage of the availability of proper motion data from the *Gaia* survey and the separation done in the previous paper to study the kinematics of MSPs in the four selected GCs. Chapter 4 contains a review of the relevant literature, a delineation of the methods used and, since this is still a work in progress, observations on the current results and comparisons to the relevant literature.

2 Data and Methods

2.1 The S-PLUS

Beginning in the early 2000s Astronomy saw a large shift in its observational strategies. Before, individual observations of one or a hand full of objects was the norm in almost any field, however the turn of the millennium brought a new era in Astronomy: the large surveys. The *Sloan Digital Sky Survey* (Abazajian; Adelman-McCarthy; Agüeros, 2003) is one such program that observed a large portion of the northern hemisphere's sky in five broad bands and includes comprehensive spectroscopical observations of stars, galaxies and quasars. More recently, the *Gaia* mission (Gaia Collaboration et al., 2016) used a space telescope to measure the precise position of billions of objects in all the sky. With repeated observations the *Gaia* collaboration has been able to obtain very accurate information of the proper motions of millions of Galactic stars (Gaia Collaboration et al., 2021). Such large scale projects are leading into what has been dubbed the *big data* era of Astronomy, where statistical methods are paramount to select and understand these large data sets.

The *Southern Photometric Local Universe Survey* (S-PLUS, Mendes de Oliveira et al. (2019)) is a Brazilian lead photometric survey that is observing over 9000 deg^2 of the southern sky in 12 filters. A 0.8 m aperture robotic telescope named T80s and located in the Cerro Tololo Interamerican Observatory (CTIO), Chile, is being used for this task. The telescope is armed with four broad (*g, r, i* and *z*), two intermediate (*u* and J0861) and six narrow-band (J0378, J0395, J0410, J0430, J0515 and J0660) filters. Table 1 shows

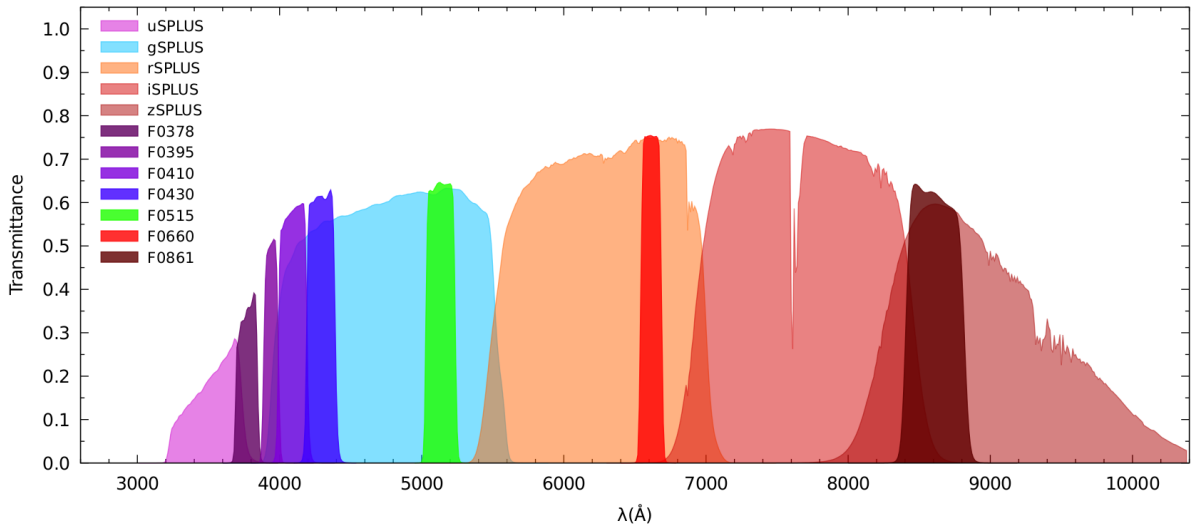

Figure 4 – Filter curves of the S-PLUS bands, courtesy of William Schoenell.

the general characteristics of the filters and their transmission curves are shown in Figure 4. The S-PLUS bands are a subset of the Javalambre filter system and have been chosen because they are focused on important galactic and stellar features. This allows for good stellar classification, especially for metal poor stars, and redshift estimation of nearby galaxies.

Table 1 – Information on the S-PLUS filter system. Filter name, the central wavelength, the FWHM of the transmission curve depicted in figure 4, key spectral feature.

Filter name	λ_{eff} (nm)	$\Delta\lambda$ (nm)	comment
u	357.4	33.0	Jalambre u
F0378	377.1	15.1	[OII]
F0395	394.1	10.3	Ca H+K
F0410	409.4	20.1	Hdelta
F0430	429.2	20.0	G-band
g	475.6	153.6	SDSS-like g
F0515	513.3	20.7	Mgb triplet
r	626.0	146.2	SDSS-like r
F0660	661.4	14.7	H alpha
i	769.2	150.4	SDSS-like i
F0861	861.1	40.8	Ca triplet
z	878.3	107.2	SDSS-like z

The S-PLUS is a great tool for the purposes of studying MSPs. The spectral differences between populations in a GC are mainly relevant in the bluer end of the spectrum, which is captured by filters such as *u*, J0378 and J0395. In combination with the redder filters, they provide a reliable way to separate these populations. Another important characteristic of S-PLUS that is of great importance in this study is its large Field-of-View (FoV), with a CCD comprised of 9232×9216 pixels and a FoV of $1.4 \times 1.4\,\mathrm{deg}^2$, resulting in a plate scale of $0.55\,\mathrm{arcsec\ pixel}^{-1}$. This allows us to observe even close by GCs up to many times their half-light radius ($\mathrm{r_h}$) with a single pointing. This is important when we consider some proposed formation scenarios in which the second population is formed in the cluster centre and migrates outward. Dynamical studies have shown that, if this is the case, radial differences can still be found in some clusters depending on many factors. In particular, cluster mass and ratio of 1P to 2P. Studies of MSPs that encompass the outskirts of GCs are rare in the literature, with the majority of them focusing in the inner regions of these objects.

The S-PLUS is a twin system of the *Javalambre Photometric Local Universe Survey* (J-PLUS, Cenarro, Moles e Cristóbal-Hornillos (2019)) using an identical telescope, camera and filter system. In the science verification phase of the project Drs. Ana Chies-Santos and Charles Bonatto obtained photometric images of M15 in all 12 bands. In the article Bonatto et al. (2019) they explored the capacities of the J-PLUS/S-PLUS colours in

Table 2 – Characteristics of the studied GCs, heliocentric distance, metallicity, interstellar reddening, half-mass radius and tidal radius. All information from Harris (1996), 2010 version.

Name	Distance (kpc)	[Fe/H]	E(B-V) (mag)	r_h (arcmin)	r_t (arcmin)
NGC 104 (47 Tuc)	4.5	-0.72	0.04	3.17	42.86
NGC 288	8.9	-1.32	0.03	2.23	12.94
NGC 3201	4.9	-1.59	0.24	3.1	28.45
NGC 7089 (M 2)	11.5	-1.65	0.06	1.06	21.45

separating MPs present in the metal-poor ([Fe/H] ≈ -2.3) cluster M15. They found that CMDs constructed using a combination of red and blue filters, e.g. (u - z) and (J0378 - J0861), showed a split attributed to MSPs in the upper RGB and AGB sequences.

2.2 The Targets

To select the targets for this study first we started with the entire sample of 56 Galactic Globular Clusters that were within the S-PLUS footprint, with many of them being from the Galactic bulge. The first, and most obvious criteria, was that the clusters had to have already been observed and the images reduced by the S-PLUS pipeline. Because of the size of the telescope we had to limit our study to more massive and close by clusters. For this we considered objects that were closer than 12 kpc from the Sun, a total of 36 GCs. Another important criteria is the interstellar extinction. Also called reddening, extinction is the process by which the light emitted by an astronomical source is scattered, absorbed and re-emitted in a different wavelength by intervening gas and dust. This process preferentially absorbs light from the bluer end of the spectrum and re-emits as infrared radiation, causing the objects to appear redder than in reality. Combining the fact that emissions of old stars are weaker in the blue and that the blue filters have a lower throughput, if a cluster has a high reddening the number of observable stars becomes too small for a statistically significant study. Thus we limited our sample to 12 objects with a low extinction (E(B-V) < 0.25). We also aimed to choose clusters that spanned a wide range in metalicity in order to study the effects of this in separating the populations and on the phenomenon of MSPs as a hole.

Finally, we performed a visual inspection of the images of remaining candidates to discard any possible problems (e.g. a bad filter image, flat or bias problems) and to make sure that they had a sufficient number of stars for a robust statistical assessment. Four clusters passed our selection criteria and the visual quality checks. They are NGC 104 (also known as 47 Tuc), NGC 288, NGC 3201 and NGC 7089 (M2). Table 2 contains general information about each cluster and their individual characteristics are explored in depth in the next sections.

2.2.1 NGC 104

47 Tuc is one of the largest clusters to orbit our Galaxy, both in terms of mass and size. Having a dynamical mass of $7.79 \pm 0.05 \times 10^5\,M_\odot$ (Baumgardt; Hilker, 2018) and a half-light radius of 3.17 arcmin it is a prime target to study multiple populations, specially given its metallicity ([Fe/H] = −0.72). Abundance anomalies in NGC 104 were found as early as 1982. Norris e Freeman (1982) reported a negative correlation between C and N when studying 14 horizontal branch stars. More recently, Milone et al. (2012) did a photometric study of this cluster using HST and ground-based observations. They found splits throughout the MS, subgiant and red giant phases, and using synthetic atmospheric models determined that it can be reproduced by two populations where one is enhanced in N and depleted in CO with a small variation in He. They also found that the second population comprises ∼70% of the cluster and is more centrally concentrated than the first one inside 4 half-light radius.

Carretta et al. (2009) analysed the composition of Na and O in 15 GCs and the relationship between these elements. 47 Tuc shows a clear correlation between them and a double peaked distribution of [Na/Fe]. Nataf et al. (2019) analysed literature and APOGEE data on the abundance of N, Na and Al on 42 GCs, including 47 Tuc. They found that stars with normal [N, Na/Fe], i.e. first population stars, show no variation in the abundance of Al, while stars with enhanced [N, Na/Fe], second population, show a variable [Al/Fe]. This is consistent with other studies, such as di Criscienzo et al. (2010), that suggest a second population composed of two sub-populations in NGC 104.

NGC 104 is also a dynamically interesting cluster as it shows a significant rotation on the tangential component in the plane of the sky and a high V/σ, meaning that rotation is still an important parameter shaping this cluster (Bianchini et al., 2018). Richer et al. (2013) used multi-epoch HST observations to derive the stellar proper motions and photometry to divide the cluster into four populations (from reddest to bluest in the CMD). They report that the bluest population (second population) presents a high anisotropy while the reddest ones have no measurable anisotropy. Another important find is that the 2P is more centrally concentrated than the 1P and it has a larger radial velocity dispersion, hence it is expanding outward via two-body relaxation. Milone et al. (2018) also studied the kinematics of MSPs in NGC 104 using *Gaia* (for the proper motions) and multi-band ground observations. They concur with the results of Richer et al. (2013) that the second population have a high anisotropy. They also show that the 2P has a lower tangential velocity dispersion between ∼2.5 - 3.8 half-light radius when compared to the 1P.

2.2.2 NGC 288

The presence of multiple populations in NGC 288 has been well established by multiple studies. Kayser et al. (2008) used medium-resolution spectra of upper MS, SGB

and RGB stars in 8 GCs to study the CN and CH line indexes. In NGC 288 they found a bimodal distribution in the CN measurements and a negative correlation with the CH. Considering that NGC 288 and NGC 362 form a second-parameter pair (they have very similar overall characteristics, but a very different HB morphology in CMDs) and both present a bimodal CN distribution it is reasonable to eliminate it as the source of the second parameter problem. Piotto et al. (2013) used HST observations to disentangle the populations in this cluster also from the MS, SGB and along the RGB. They estimate that the 1P has $55 \pm 3\%$ of the cluster stars and 2P $45 \pm 3\%$. They also estimate the Helium content of the populations following Milone et al. (2013) and find a difference of $\Delta Y = 0.013 \pm 0.001$. This small helium variation can explain why, as opposite to M 3 and NGC 2808 that have a similar [Fe/H] to NGC 288, this cluster does not have an extended P1 (Lardo et al., 2018).

2.2.3 NGC 3201

NGC 3201 is a cluster with an unusually high orbital velocity of nearly 500 km s^{-1} (Gaia Collaboration et al., 2018a). It also belongs to a small number of MW GCs that have star-to-star Fe abundance variations (Simmerer et al., 2013), which exacerbates the difficulty of modelling its MSPs. One important photometric factor of this cluster is the presence of significant dust clouds in our line-of-sight, resulting in differential reddening that has to be corrected in order to properly study this GC (von Braun; Mateo, 2001). In regards to MSPs, NGC 3201 is part of the sample analysed by Carretta et al. (2009). In the [Na/Fe] vs [O/Fe] plane two populations can be clearly divided into a first population with a primordial composition and a second population with depleted O and enhanced Na. In a further research note they analysed the radial distributions of these populations after separating the 2P into an intermediate and extreme populations (Carretta et al., 2010). They showed that Na-poor stars occupy more the outskirts of the cluster. However, their sample is rather small. Kravtsov et al. (2010) used UBVI to separate the populations in NGC 3201 and found that the 2P is more centrally concentrated.

2.2.4 NGC 7089

With a metallicity of [Fe/H]=-1.65, NGC 7089 (also known as M 2) is the most metal poor cluster in our sample. Milone et al. (2015a) did an extensive study of the MSPs of this cluster and found three distinct populations in NGC 7089 (named A, B and C), which they further divided into seven sub-populations. They used HST and the powerful Chromosome map combined with abundance data from Yong et al. (2014) to characterise the populations. They divided population A, which comprises 96% of the cluster stars, into four sub-populations. It's helium abundance spans a wide range (from Y=0.25 to Y=0.31) and light elements present a variation which is similar to the patterns observed in the

regular MSPs of other clusters. Population B making up ∼3% of the GC stars has a more intermediate metallicity and presents enhanced neutron-capture elements. It is further divided into two components that have light element abundance differences. Population C is ∼1% of the cluster and is highly enhanced in Fe and lower [α, Al/Fe] when compared to populations A and B. This suggests that this population had a very different formation history than the rest of the cluster.

Vanderbeke et al. (2015) studied the HB of this cluster, dividing them into two populations and analysing their radial profiles. They found that no difference is apparent. Lardo et al. (2011) used SDSS photometry to separate the populations in NGC 7089, they reported a large radial variation between them. More specifically, the UV-red (second population) appears more centrally concentrated when compared to the UV-blue. However, Hoogendam e Smolinski (2021) re-analysed the data used in Lardo et al. (2011) and added ground based photometry by Stetson et al. (2019) finding no conclusive evidence of a centrally concentrated population.

2.3 Photometry

The S-PLUS is an automated survey. The observations, the reduction and combining of images, the photometry and the zero point determination are done with minimal human oversight. In the photometry step the normal S-PLUS pipeline uses the SExtractor software which is a great tool for the study of galaxies and sparse fields. It can also be used in moderately crowded fields with enough care. However, a globular cluster is a very crowded environment with stars overlapping each other, especially in the inner regions. Because of this we did not use the standard S-PLUS photometry. Instead we used the package DAOPHOT present in the *Image Reduction and Analyses Facility* (IRAF) software.

DAOPHOT was developed by Stetson (1987) to perform *Point Spread Function* (PSF) photometry. The basic assumption of this method is that the light source can be thought of as a point and that through its interaction with the various optical elements (that include the atmosphere, telescope mirrors, filters, the collecting CCD, etc.) it is distorted once it is observed. The interaction with these objects and the distortions caused by them can be summed up into a single function aptly called the Point Spread Function. By integrating the PSF one can know the brightness of the source object. Since the PSF is different for each image taken, it has to be determined by sampling a number of isolated objects in each observation. One major advantage of this method is that it is capable of estimating the brightness of objects that are so close to each other as to appear blended. Of course there is a limit to the proximity of two objects where it is possible to distinguish them. In our case, the most important thing this limits is how far into the cluster centre DAOPHOT is capable of identifying individual stars.

Table 3 – Number of objects in each step of the selection process. The second column (Gaia) is the initial number of Gaia sources that fit our selection criteria. The third column (S-PLUS) are the objects with magnitudes in the 12 filters. The fourth column (Gaia GC) are the objects classified as GC stars according to our Gaia selection. The fifth column (Gaia GC-RGB) are the objects inside the red polygon. Finally, the two last columns (Gaia—S-PLUS GC and Gaia—S-PLUS RGB) are the matched Gaia and S-PLUS catalogues including only GC stars and the RGB selected stars matched with S-PLUS, respectively.

Name	Gaia	S-PLUS	Gaia GC	Gaia GC-RGB	Gaia—S-PLUS GC	Gaia—SPLUS RGB
NGC 104	1.001.954	11.561	71.569	2.415	6.451	1.865
NGC 288	51.210	2.923	6.466	371	1.268	332
NGC 3201	866.690	27.405	16.733	561	4.589	487
NGC 7089	148.685	9.290	5.608	821	2.210	711

In order to do the photometry in the twelve filters for all clusters in our sample a code was written in python using the PyRAF package. Briefly, first the probable location of stars in the image are located and aperture photometry is performed. A subset of objects is examined and selected by eye in order to determine the PSF for the image. With this, photometry is done on the image and magnitudes, uncertainties and other factors are obtained.

For this study the excellence of the photometry is very important. Consequently, we performed test and quality cuts to obtain the best possible data. Visual inspection were performed by using the SAOImageDS9 software. We plotted on top of the raw image the positions of all objects with measured magnitudes. This is done to evaluate if DAOPHOT is capturing an adequate number of objects, i.e., all bright and visible objects but not the image noise. DAOPHOT also provides other parameters such as Sharpness (SHARP) and Roundness (ROUND) that were used to eliminate unsuitable objects. These measure, respectively, how well the object's profile can be represented by a delta function and if the object is elongated in a particular direction. As a last step we matched the catalogues of all filters for each cluster, thus obtaining a master catalogue containing the positions of all objects, their magnitudes and errors. The full tables are available as extra online materials in the paper. The column titled S-PLUS in Table 3 shows the number of objects with all 12 magnitudes in each cluster field.

2.4 *Gaia* Selection

When using photometry to study a star cluster a number of contaminants are present in the observed field, i.e., foreground and background stars, galaxies and quasars. It is important to eliminate as many contaminants as possible in order to have a clean sample of stars that truly belong to the cluster. There are a myriad number of ways of

doing this, as was demonstrated in Bonatto et al. (2019). Some colour combinations of S-PLUS/J-PLUS can be used for this purpose with some success. Another approach is to use the stars proper motions. This uses the fact that the stars belonging to a GC will all have a very similar motion in the plane of the sky. Thus determining the cluster's locus in proper motion space can separate GC members from contaminants with a high degree of accuracy.

The method used here is based on proper motion data from the *Gaia* Survey (Gaia Collaboration et al., 2018). First we downloaded the available data —position (RA,dec), proper motions, stellar parallax and magnitudes in the three *Gaia* bands as well as their associated errors— for all the objects within the tidal radius of each cluster. We eliminated all objects with at least one unmeasured quantity and with proper motion errors bigger than 1.5 m.a.s yr^{-1}. With this we selected a ring around the centre of the cluster that contained a representative sample of cluster members, this avoids the crowded core region and the outskirts dominated by field objects. With this sample we fitted a 2D Gaussian profile to the proper motion space. This determined the average motion of the cluster. We then classified as cluster members all objects that were within 5 standard deviations from the central peak of the distribution. This process is illustrated in the left and centre panels of Fig. 5.

Furthermore, we created CMDs using the *Gaia* filters and visually defined a polygon around the RGB of each cluster, shown in red in the right most panels of Fig. 5. The purpose is two fold: it is very unlikely that contaminant objects have the same proper motion and similar magnitudes in the three bands as cluster stars. Thus, we obtain a much cleaner sample by selecting only the objects within the red polygon. Second, since we will only examine the phenomenon of MSPs in the RGB of the clusters we use this polygon to determine these objects.

2.5 Differential Calibration

The photometry performed in the S-PLUS yields instrumental magnitudes, therefore a calibration is necessary. To do this we have used a differential calibration process. It is based on the fact that the globular cluster present in the field can be well fitted by an isochrone. First we download archival data from the Hubble Space Telescope for each of the four clusters and use the code `fitCMD` developed by Bonatto et al. (2019). It uses an Initial Mass Function (IMF) to simulate a population of stars and searches for the best set of parameters to represent the observed CMD using PARSEC isochrones (Bressan et al., 2012). With this, it provides important parameters such as age, metallicity, distance modulus and overall reddening as well as other information not relevant to our case.

The next step is to use an isochrone with the structural parameters determined

by the software and corrected by the observational quantities, i.e., distance modulus and reddening. We assumed that this isochrone presents the correct magnitudes for the S-PLUS filters and use a code, named `findZP` to 'fit' the instrumental magnitudes to the isochrone. What this code aims to do is minimise the fitness function, defined as the sum of the distance from each point to the isochrone in a given CMD plane, by guessing zero point values for multiple filters simultaneously. A simple parameters space search is rather slow owing to the fact that thousands of distance calculations have to be performed at each try, to mitigate this we employed the simulated annealing method. The algorithm starts with a given solution (provided by visual inspection) and will search the parameter space for a local optimal (in this case a minimum of the fitness function) with a decreasing chance to accept a worst solution based on the current 'temperature' (the temperature is a linear decreasing function).

It is important to note that the FoV of HST is small compared to the size of the cluster. This implies that a insignificant number of contaminants are present in the catalogue used to derive the basic parameters. However, for the following steps we need to use the clean samples obtained from the *Gaia* proper motions and matched with S-PLUS photometry in order to obtain good zero point estimations. Another point to consider is the Horizontal Branch. This section of the evolutionary track is still a challenge for simulations to properly reproduce. Because of this we have eliminated it from the zero point estimation method. The process is done in steps, the zero points for g, r and i are found first, then u and z followed by the narrow bands. In this sense the code minimises the fitness function in all the possible CMDs that can be constructed with the colours in that step, e.g., for g, r, i we have the colours (g - r), (g - i) and (r - i) forming 9 total CMDs. A flow chart of the procedure can be seen in Figure 6, one caveat is that sometimes the best fit zero points in most CMDs produced a slight deviation in one colour, to fix this a small colour correction was applied.

After obtaining all the zero points, they were applied to all the cluster stars and a final corrected catalogue was produced. Figure 7 shows three CMDs for each cluster, in grey are all the objects with measured magnitudes in all 12 bands of S-PLUS. In black are the GC members according to our Gaia selection. Table 3 shows the number of objects in each step of the process, from the initial Gaia and S-PLUS samples to the final number of RGB stars in each cluster.

2.6 Correction for Differential Reddening

As stated in section 2.2 three of our targets have a relatively low reddening, with NGC 3201 being an outlier with E(B - V)= 0.24. More important for our study, however, is the problem of differential reddening. This arises because clouds of gas and dust are

not distributed homogeneously in the field causing certain regions to be more affected by reddening than others. This can lead to a broadening of the RGB, which is the basis by which we identify MSPs. Thus we need to eliminate differential reddening. Given the large FoV of S-PLUS this problem can be exacerbated and needs to be addressed. To correct for this we used the code described in Bonatto e Chies-Santos (2020) which divides the cluster into cells containing at least 50 stars and constructs the CMDs for each one. The bluest CMD is found and taken as reference and all others are shifted to match, thus obtaining the reddening of each region. For this process to be effective two things have to be taken into account when choosing the appropriate filters: a wide wavelength is covered as to be affected by reddening and that this combination does not show signs of MSPs (as the broadening of the RGB may be attributed to them).

From the literature we know that NGC 104 is not significantly affected by differential reddening and it has the largest number of stars in our sample, thus we have chosen this GC and checked some possible CMDs. We found that colours such as (g - r) and (g - i) served this purpose well and were, consequently, chosen as the basis for correcting the differential reddening. The code was applied to NGC 3201 using the (g - r) colour, we also ran the code using (g - i) and compared the results finding them agreeable. We have also compared the results with literature maps such as the one by von Braun e Mateo (2001) and found them to agree both in shape and values. With the colour excess map shown in Figure 8 we applied the necessary corrections. The top panels of Fig. 8 present the uncorrected (left) and the corrected (right) CMD, we can see a much more defined TO and a tighter RGB sequence after the correction. We have also applied the same code to the other clusters in order to test if our assumption that they are not significantly affected by differential reddening holds true. The generated maps are shown in Fig. 9, they do not exceed ΔE (B - V)$\approx$ 0.06, which is small enough and can be attributed to the spread caused by photometric errors.

2.7 The K-means algorithm

In machine learning the K-means clustering algorithm is a simple unsupervised method of separating the available data into classes (MACQUEEN et al., 1967). Given a number k of centroids the algorithm will attempt o minimise the intra-clusters distance partitioning the data in such a way that each observation belongs to the nearest centroid. In this work this clustering method was used to separate the cluster stars into two populations in each cluster in the six-dimensional space formed by the Δ*colours*. To utilise this method two assumptions have to be made: that two populations are present in each GC and that the populations have a comparable number of objects. The first assumption is supported by the literature in the sense that all the studied clusters have MSPs. However, here we assumed that only two were present. In view of the fact that the T-80s is an 80cm ground

telescope, we are not capable of detecting the more nuanced differences in the populations, a visual inspection of the CMDs produced also does not show clearly more than two populations in each cluster. Thus we have considered only two centroids (populations) in the K-means analyses. The second assumption is also consistent with the literature in the field, where it is well known that the fraction of FG stars varies between ~ 0.4 and 0.8.

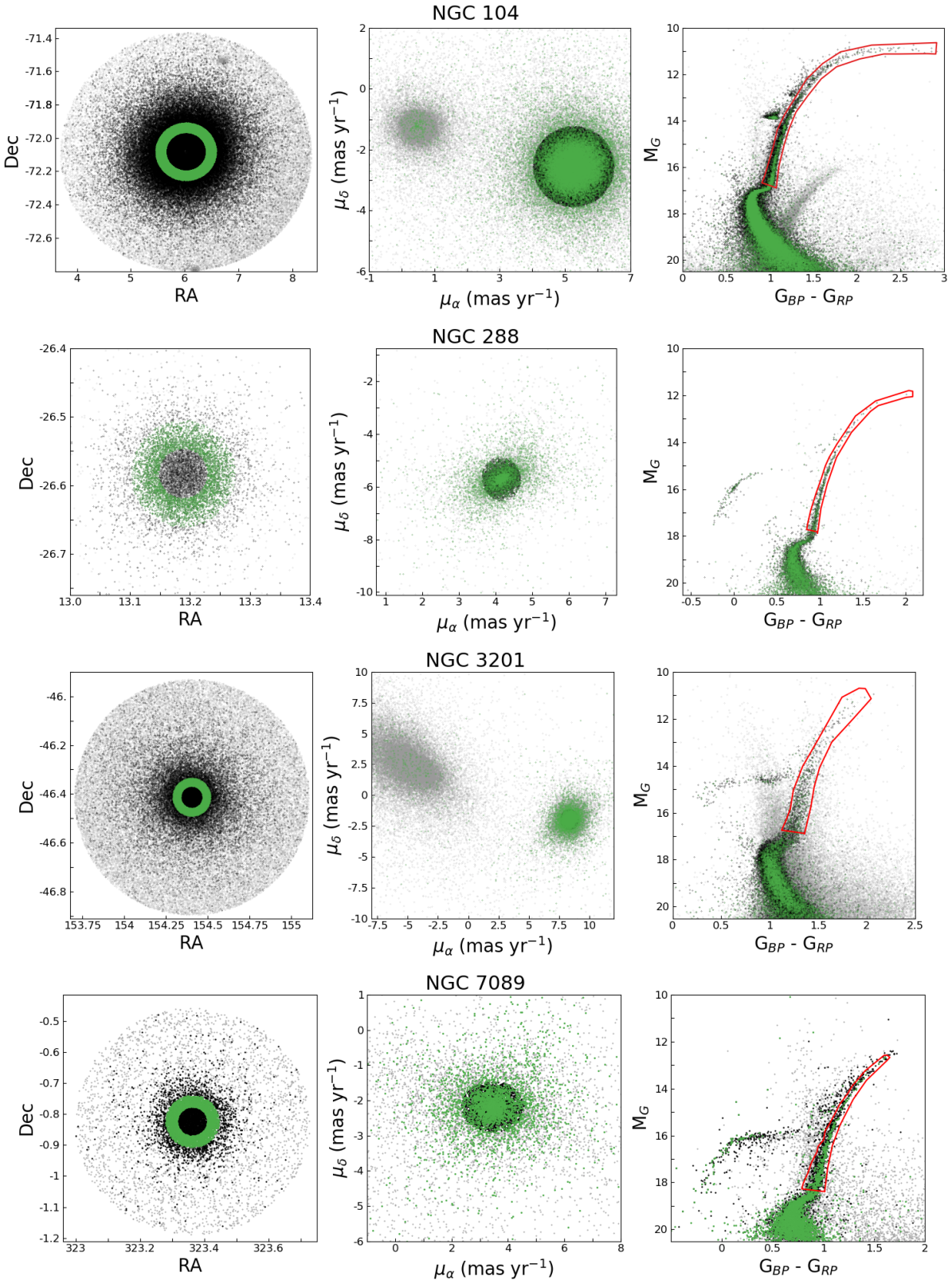

Figure 5 – Cluster members selection using *Gaia*. The left panel is the distribution of Gaia sources on the sky,in green are the ring selected objects and in black are the one classified as GC members. The middle panel shows the proper motion plane. Right panel is a CMD constructed using Gaia colours, the red polygon was hand-made to select the RGB.

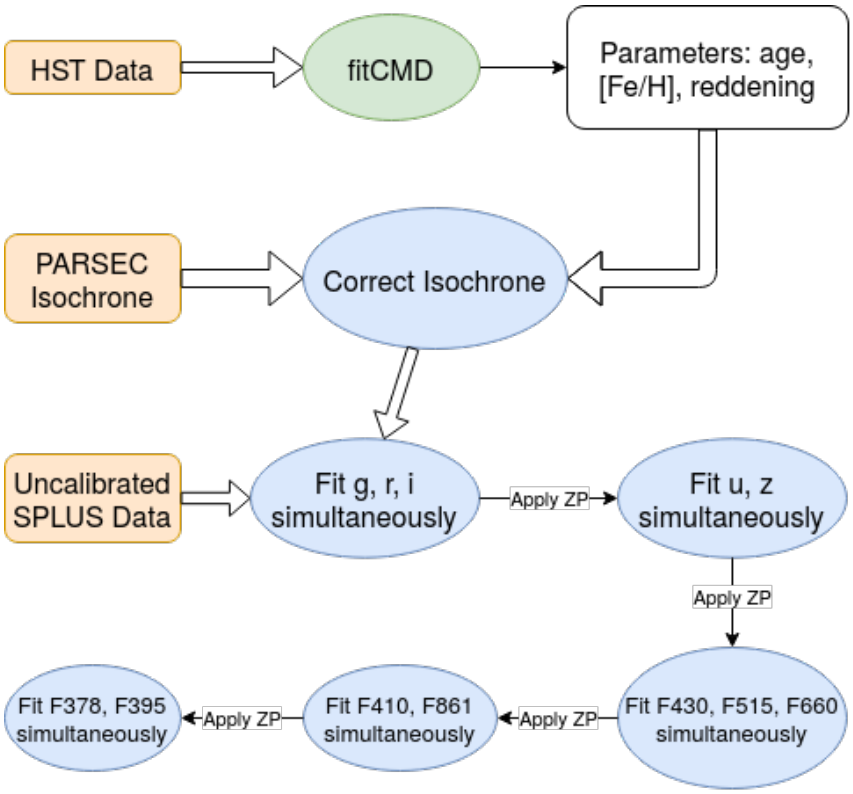

Figure 6 – Flowchart depicting the major steps in obtaining the zero points.

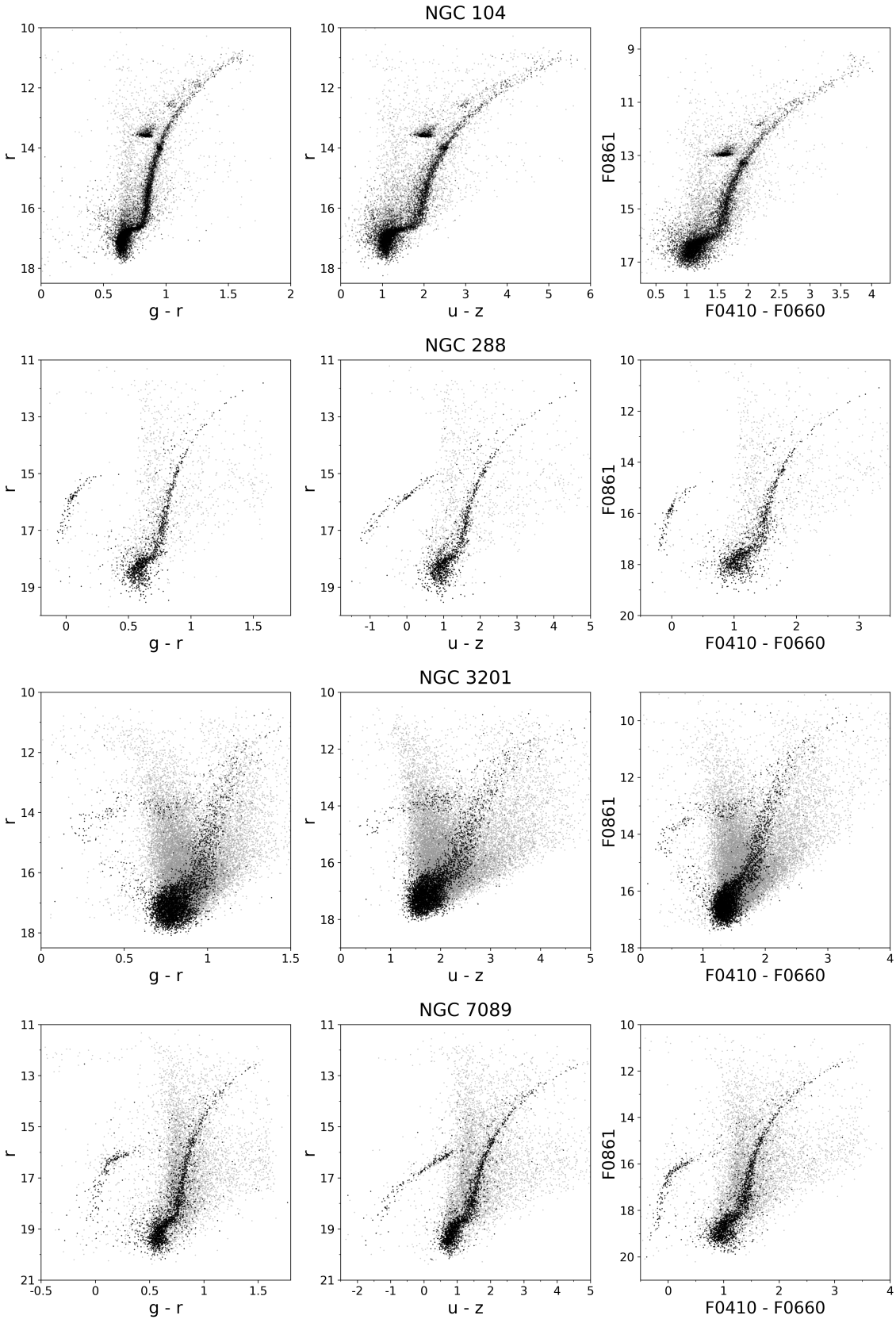

Figure 7 – Three CMDs for each clusters constructed using S-PLUS magnitudes. In grey are all the objects with all 12 magnitudes measured with DAOPHOT. In black are the cluster members selected using Gaia proper motions.

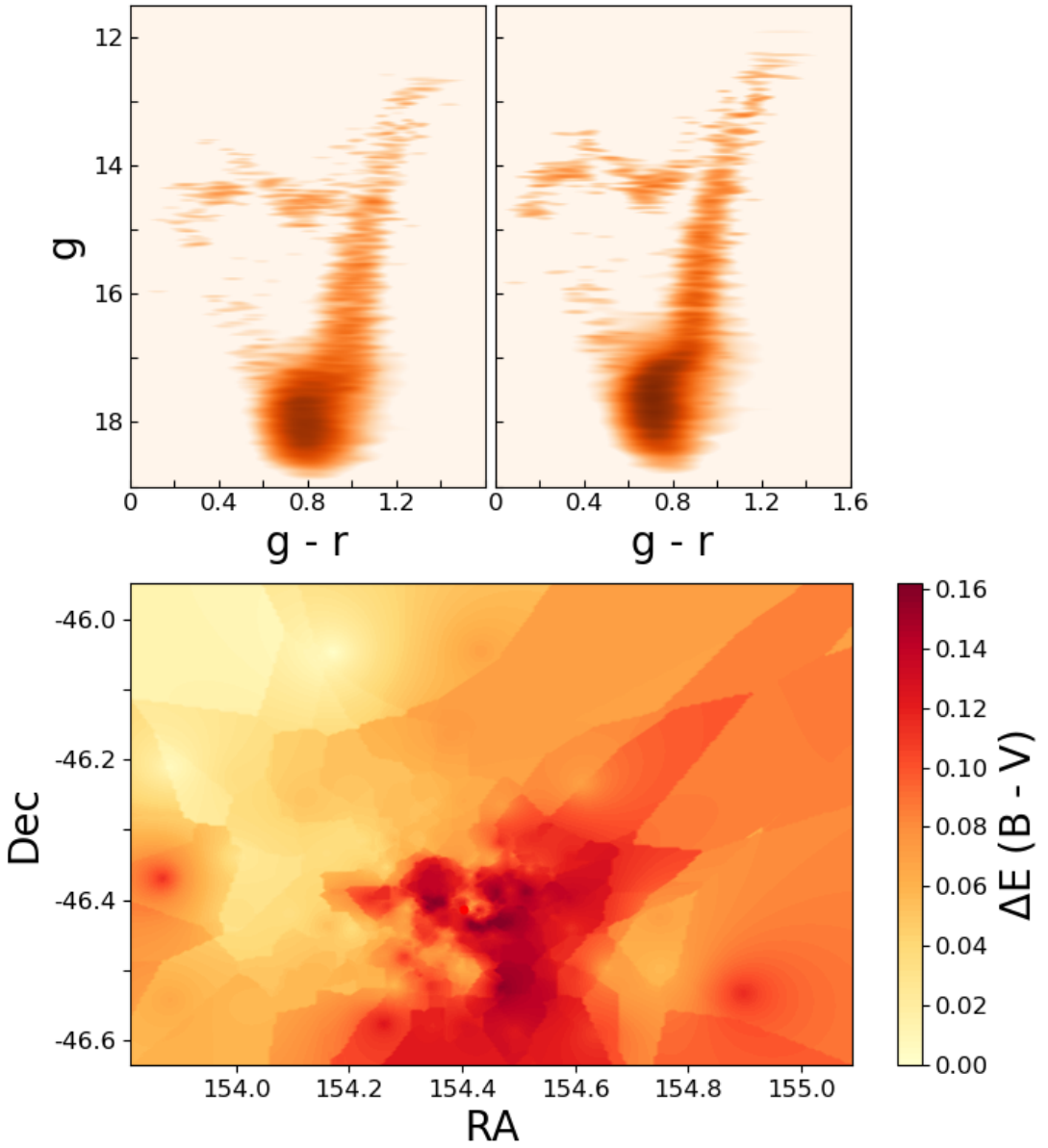

Figure 8 – The top panels show two CMDs of NGC 3201, Hess style. The left one the uncorrected version and the right one after the differential reddening correction. The bottom panel shows a map of the colour excess.

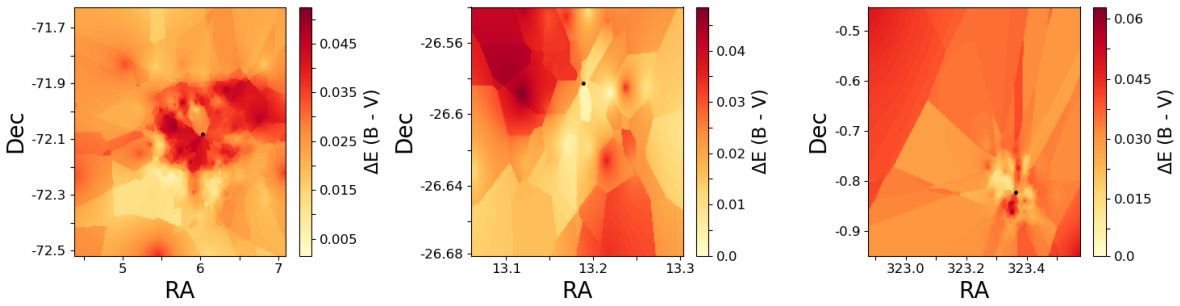

Figure 9 – Colour excess map for the other three GCs, from left to right: NGC 104, NGC 288 and NGC 7089. The black dot marks the centre of each cluster on the field.

3 S-PLUS: exploring wide field properties of multiple populations in galactic globular clusters at different metallicities

Here we present, in its entirety, the published article that contains the analyses of four GCs using S-PLUS and *Gaia* data.

Monthly Notices of the ROYAL ASTRONOMICAL SOCIETY

MNRAS **515,** 4191–4200 (2022) https://doi.org/10.1093/mnras/stac1411
Advance Access publication 2022 May 24

S-PLUS: exploring wide field properties of multiple populations in galactic globular clusters at different metallicities

Eduardo A. Hartmann [1]★ Charles J. Bonatto [1]★ Ana L. Chies-Santos [1,2]★ Javier Alonso-García,[3,4] Nate Bastian,[5,6,7] Roderik Overzier,[8,9] William Schoenell,[10] Paula R. T. Coelho [8] Vinicius Branco,[8] Antonio Kanaan,[11] Claudia Mendes de Oliveira[8] and Tiago Ribeiro[12]

[1]*Departamento de Astronomia, Instituto de Física, UFRGS, Av. Bento Gonçalves, 9500, Porto Alegre, RS, Brazil*
[2]*Shanghai Astronomical Observatory, Chinese Academy of Sciences, 80 Nandan Rd 200030, Shanghai, China*
[3]*Centro de Astronomía (CITEVA), Universidad de Antofagasta, Av. Angamos 601, Antofagasta, Chile*
[4]*Millennium Institute of Astrophysics, Nuncio Monseñor Sotero Sanz 100, Of. 104, Providencia, Santiago, Chile*
[5]*Donostia International Physics Center (DIPC), Paseo Manuel de Lardizabal, 4, E-20018 Donostia-San Sebastián, Guipuzkoa, Spain*
[6]*IKERBASQUE, Basque Foundation for Science, E-48013, Bilbao, Spain*
[7]*Astrophysics Research Institute, Liverpool John Moores University, Liverpool L3 5RF, UK*
[8]*Universidade de São Paulo, São Paulo, Instituto de Astronomia, Geofísica e Ciências Atmosféricas, SP, Brazil*
[9]*Observatório Nacional, Rua General José Cristino, 77, São Cristóvão, 20921-400, Rio de Janeiro, RJ, Brazil*
[10]*GMTO Corporation 465 N. Halstead Street, Suite 250 Pasadena, CA 91107, USA*
[11]*Departamento de Física, Universidade Federal de Santa Catarina, Florianópolis, SC 88040-900, Brazil*
[12]*NOAO, PO Box 26732, Tucson, AZ 85726, USA*

Accepted 2022 May 16. Received 2022 May 16; in original form 2022 February 22

ABSTRACT

Multiple stellar populations (MSPs) are a ubiquitous phenomenon in Galactic globular clusters (GCs). By probing different spectral ranges affected by different absorption lines using the multiband photometric survey S-PLUS, we study four GCs – NGC 104, NGC 288, NGC 3201, and NGC 7089 – that span a wide range of metallicities. With the combination of broad and narrow-band photometry in 12 different filters from 3485A (u) to 9114A (z), we identified MSPs along the rectified red-giant branch in colour–magnitude diagrams and separated them using a K-means clustering algorithm. Additionally, we take advantage of the large Field of View of the S-PLUS detector to investigate radial trends in our sample. We report on six colour combinations that can be used to successfully identify two stellar populations in all studied clusters and show that they can be characterized as Na-rich and Na-poor. For both NGC 288 and NGC 7089, their radial profiles show a clear concentration of 2P population. This directly supports the formation theories that propose an enrichment of the intra-cluster medium and subsequent star formation in the more dense central regions. However, in the case of NGC 3201, the trend is reversed. The 1P is more centrally concentrated, in direct contradiction with previous literature studies. NGC 104 shows a well-mixed population. We also constructed radial profiles up to 1 half-light radius of the clusters with *HST* data to highlight that radial differences are lost in the inner regions of the GCs and that wide-field studies are essential when studying this.

Key words: surveys – globular clusters: individual: (NGC 104) (NGC 288) (NGC 3201) (NGC 7089).

1 INTRODUCTION

The phenomenon of multiple stellar populations (MSPs) in Galactic globular clusters (GCs) has been well observed in almost all GCs older than 2 Gyr, both spectroscopically and photometrically (Piotto et al. 2015). Detailed spectroscopical studies of stars in GCs have shown that there are significant abundance variations in light elements not compatible with a single stellar population (Carretta et al. 2009). Increased abundances of He, N, and Na with a decrease in C and O are the telltale sign of the Second Population (2P) of stars in a cluster. Stars without these characteristics are considered the First Population (1P).

To explain such abundance variations, some formation scenarios propose that the first population of stars enriches the intra-cluster medium forming a second population (or more, e.g. NGC 7089 with seven populations). This scenarios differ primarily on what pollutes the next generation, be that asymptotic giant branch (AGB) stars (D'Ercole, D'Antona & Vesperini 2016), fast-rotating massive stars (FRMS; Decressin et al. 2007; Charbonnel et al. 2014), interacting binary (De Mink et al. 2009), or a supermassive star (Gieles et al. 2018; SMS). One of the big challenges is the mass-budget problem; in short, the observed 2P in clusters is larger (or at least equal to) in number than the 1P. In the popular enrichment scenarios, there would not be enough processed material by the first population for the formation of the second (Prantzos & Charbonnel 2006). Possible

★ E-mail: eduardo.hartmann@ufrgs.br (EAH); charles@if.ufrgs.br (CJB); ana.chies@ufrgs.br (ALCS)

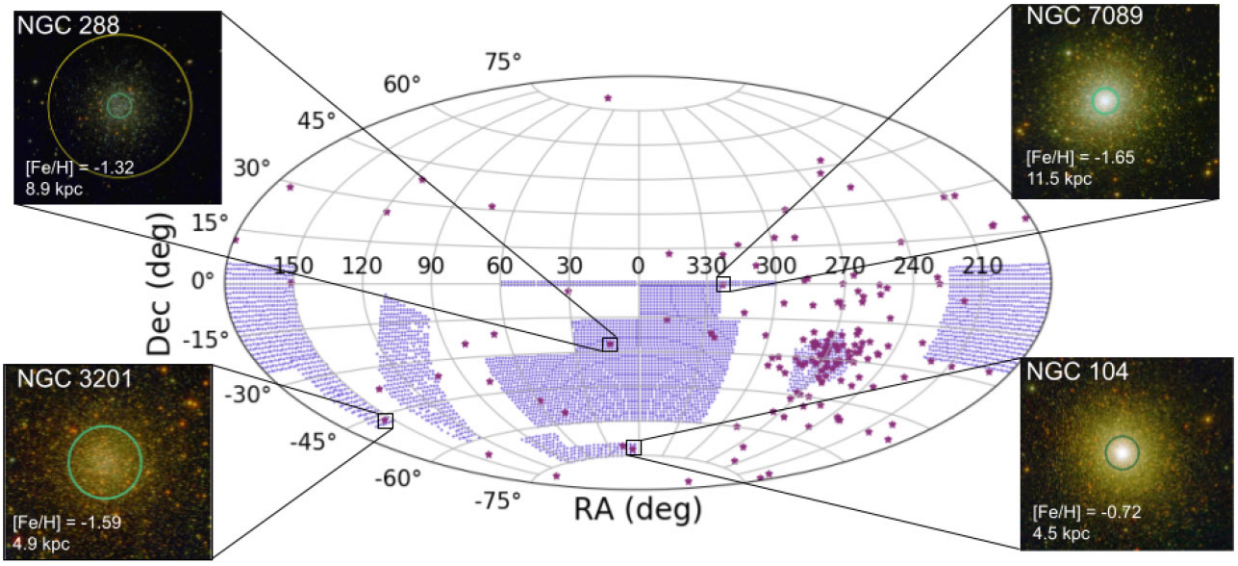

Figure 1. All sky view of the S-PLUS survey footprint in blue. The purple stars are the GCs of our Galaxy from Harris (1996), 2010 version. The insets show the S-PLUS FoV of the four clusters in our sample, as well as their metalicities and heliocentric distances. In these insets, we have highlighted by green circles the core radius and in yellow the tidal radius.

solutions for this include the assumption that clusters were 30–60 times more massive than at present-day and that 90–95 per cent of 1P stars were lost during the evolution of these objects. Wang et al. (2020) developed a scenario based on stellar mergers of binaries when the cluster is very young. This has the advantage of combining previous scenarios such as the FRMS and SMS with merging binaries and introduces the necessary stochasticity observed in GCs. Their results suggest that this may play an important role in forming MSPs, avoiding such pitfalls as the mass-budget problem.

In the most common proposed explanations for MSPs, the 2P is formed in the more dense central region of the cluster. One of the ways to test this is by constructing cumulative radial distributions of both populations. Lardo et al. (2011) looked at the radial profile of nine GCs and concluded that the enriched population is more centrally concentrated in the majority of the clusters. Nevertheless, Hoogendam & Smolinski (2021) reanalysed the data and found that the populations are not as segregated as was thought, recommending caution when doing such studies. Dalessandro et al. (2019) studied 20 GCs of various dynamical ages using the parameter A^+ to quantify the difference between both populations. They showed that the second population is more centrally concentrated in dynamically younger clusters, while no significant difference exists in older GCs. This directly supports the idea that the 2P was formed more centrally concentrated in the cluster.

While spectroscopic studies are limited to small samples of very bright stars in clusters that may contain up to millions of them, high precision multiband photometric studies have been able to identify and characterize the different populations found in GCs with the advantage that they are able to analyse thousands of stars simultaneously (e.g. Lardo et al. 2011; Soto et al. 2017; Larsen et al. 2019). The spread in metallicity manifests itself in colour–magnitude diagrams (CMD) as different evolutionary sequences of stars when appropriate filters are used, especially those that capture conspicuous metallic features. The Hubble UV Legacy Survey has been incredibly successful in using the filters of the *Hubble Space Telescope* (*HST*) to separate populations (Piotto et al. 2015). In addition, pseudo-colours (the difference between two colours) has been a great tool to separate the populations better (Milone et al. 2015)

The Southern Photometric Local Universe Survey (S-PLUS; Mendes de Oliveira et al. 2019) is observing a considerable area of the southern sky in 12 optical filters, including a fraction of the Milky Way GC system, as can be seen in Fig. 1. Bonatto et al. (2019) have studied the Cluster M 15 using observations from the Javalambre Photometric Local Universe Survey (J-PLUS; Cenarro et al. 2019), which uses the same filter system and instrument as S-PLUS. They have shown that the combination of blue and red filters can separate the two sequences of stars in the top of the red giant branch (RGB). It is important to note that this cluster is very metal-poor ([Fe/H] ~ -2.3) and is located at 10.4 kpc from the Sun. In the aforementioned paper, they show two synthetic spectra from Coelho, Percival & Salaris (2011) and Coelho (2014), one with a primordial composition and another with an enhanced metallicity. Although only qualitatively, this helps elucidate the origin of the splits seen in the CMDs. These results are promising, and they suggest studying more metal-rich clusters through the filters of J-PLUS/S-PLUS.

Following this analysis, we have chosen four Galactic GCs in the S-PLUS footprint for this study. They are NGC 104, NGC 288, NGC 3201, and NGC 7089 and encompass one dex in metallicity, from NGC 7089 with [Fe/H] $= -1.65$ to NGC 104 with [Fe/H] $= -0.72$. Moreover, they are relatively close by (see Table 1), which makes them ideal candidates to explore the phenomenon of MSPs in different environments and varied intrinsic properties.

This paper is organized as follows: in Section 2 we detail the extraction and calibration of the S-PLUS photometry in the cluster

Table 1. Characteristics of the studied GCs, heliocentric distance, metallicity, interstellar reddening, half-mass radius, and tidal radius. All information from Harris (1996), 2010 version.

Name	Distance (kpc)	[Fe/H]	$E(B-V)$ (mag)	r_h (arcmin)	r_t (arcmin)
NGC 104	4.5	−0.72	0.04	3.17	42.86
NGC 288	8.9	−1.32	0.03	2.23	12.94
NGC 3201	4.9	−1.59	0.24	3.1	28.45
NGC 7089	11.5	−1.65	0.06	1.06	21.45

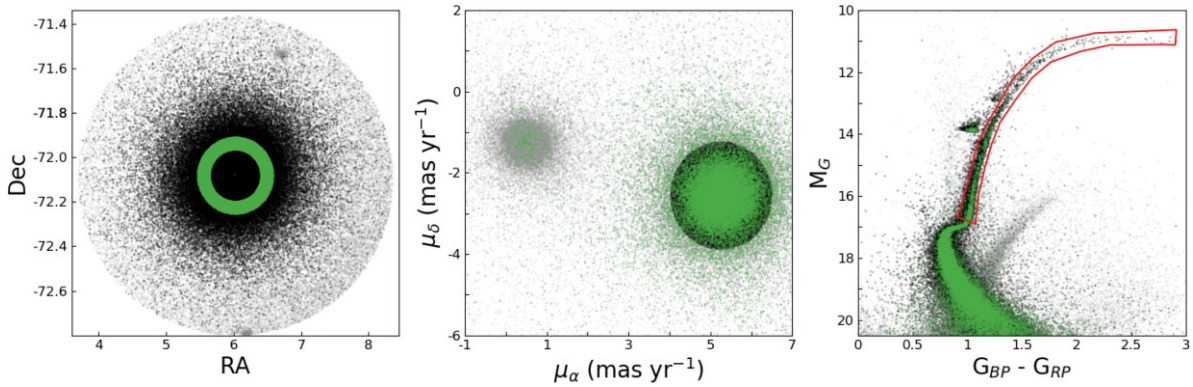

Figure 2. Example of GAIA selection of cluster members for NGC 104. The three panels share the same colour scheme: in grey are all the objects in the field, in green are the selected representative cluster stars, and in black are the GC members. The first panel shows their spatial distribution in right ascension and declination. The second panel is the proper motion space where the cluster locus is very apparent, and the third panel is the CMD using GAIA colours as well as the RGB polygon. This process is applied to all GCs in the sample.

fields and the identification of sources as cluster members. In Section 3 we explore the separation of the populations, and in Section 4 we present the analysis of the clusters and their populations. Finally, in Section 5, we present our conclusions.

2 METHODOLOGY

S-PLUS (Mendes de Oliveira et al. 2019) is a photometric survey that is observing ∼9300 deg^2 of the southern sky in twelve filters: five broad bands (u, g, r, i, z) and seven narrow-bands (F0378, F0395, F0410, F0430, F0515, F0660, F0861). These bands are a subset of the Javalambre filter system and have been chosen for their success in identifying key spectral features in galaxies and stars. It uses the *T80-South*, an 0.8-m telescope in a German equatorial mount located at Cerro Tololo Inter-American Observatory. The detector has a size of 9232 × 9216 pixels with a plate scale of 0.55 arcsec per pixel and a field of view (FoV) of 1.4 × 1.4 deg^2. Data release two (DR2; Almeida-Fernandes et al. 2021) of S-PLUS covers 950 deg^2 with an updated calibration as well as value-added catalogues containing photometric redshift and star-galaxy classification. Since the survey covers the southern part of the sky where the majority of Galactic GCs are, many have been or will be observed by S-PLUS. However, the data reduction pipeline uses SEXTRACTOR, which is not ideal for identifying sources in crowded fields, such as the central regions of GCs. Thus, to study these objects, we performed point spread function photometry using the GAIADAOPHOT (Stetson 1987) package in the IMAGE REDUCTION AND ANALYSIS FACILITY (IRAF; Tody 1993) in all 12 filters for the four GCs in our sample. Fig. 1 shows the area of the sky being observed by S-PLUS and the Milky Way GCs from Harris (1996, 2010 version). In the insets, we highlight the four GCs studied in this work with their colour images constructed using the TRILOGY code (Coe et al. 2012).

2.1 Field-cluster star separation

Given the large FoV (∼2 deg^2) of S-PLUS and our intention of studying the clusters up to their tidal radii, a robust selection process has to be implemented in order to eliminate the maximum number of contaminant objects. For this, the early Data Release 3 of GAIA (Gaia Collaboration 2021) provides us with high precision proper motion information on millions of stars, and we can use them to separate cluster members with a high confidence level. To this end, we first select all objects within the tidal radius (taken from Harris 1996, 2010 version) of each cluster and eliminate the ones with one or more unavailable magnitudes and with proper motion errors larger than 1.5 mas yr^{-1}. We selected a ring around the centre of the cluster to contain a representative population of the cluster. This way, the GC proper motion locus can be easily identified, and we avoid any crowding issues in the cluster centre. We proceed by fitting a 2D Gaussian profile proper motion space to find the average proper motion of the cluster stars within the ring. We define as cluster members all objects that are inside an ellipse of 5σ around the centre of the proper motion distribution. This process is illustrated for NGC 104 in Fig. 2, where we also show a GAIA CMD. In our subsequent analysis, we will concentrate only on the RGB stars. We identify stars in this CMD region through a visually defined polygon, as shown in the right-hand panel in Fig. 2. In Appendix A we show the same figure for the other three GCs.

2.2 Differential calibration

Zero points (ZPs) for our GC fields were not available at the start of this work. Therefore, we employ the following methodology to calibrate our photometry. We use the fact that in the studied regions, there is a GC that can be well represented by an isochrone and use the code FITCMD (Bonatto 2019) with *HST* archival data (Piotto et al. 2015) in order to obtain the best parameters of each cluster, such as age, metallicity, distance modulus, and reddening. The code simulates a population of stars using an initial mass function and searches for the best parameters to represent the real population in the CMD. With this information, we obtain the PARSEC isochrones (Bressan et al. 2012) with S-PLUS magnitudes for each cluster. The next step consists of 'fitting' the instrumental magnitudes to the corrected isochrone. This is done by first guessing by eye the values for the ZPs, then using a PYTHON code that explores the parameter space around the initial guess. It minimizes a fitness function that is defined as the sum of the distance from each point to the isochrone in the CMD plane. This is achieved using the simulated annealing method (Kirkpatrick, Gelatt & Vecchi 1983). This process is performed simultaneously in many CMD planes with different colour combinations [e.g. for filters g, r, and i, the combinations are (g–r), (g–i), and (r–i), resulting in nine CMDs]. We note that first, we attempted to obtain the ZPs by only applying a correction to the magnitude; however, sometimes this is not enough, and a minor correction must be applied to the colours. This process can only yield good results if the stars used are highly likely members of the cluster

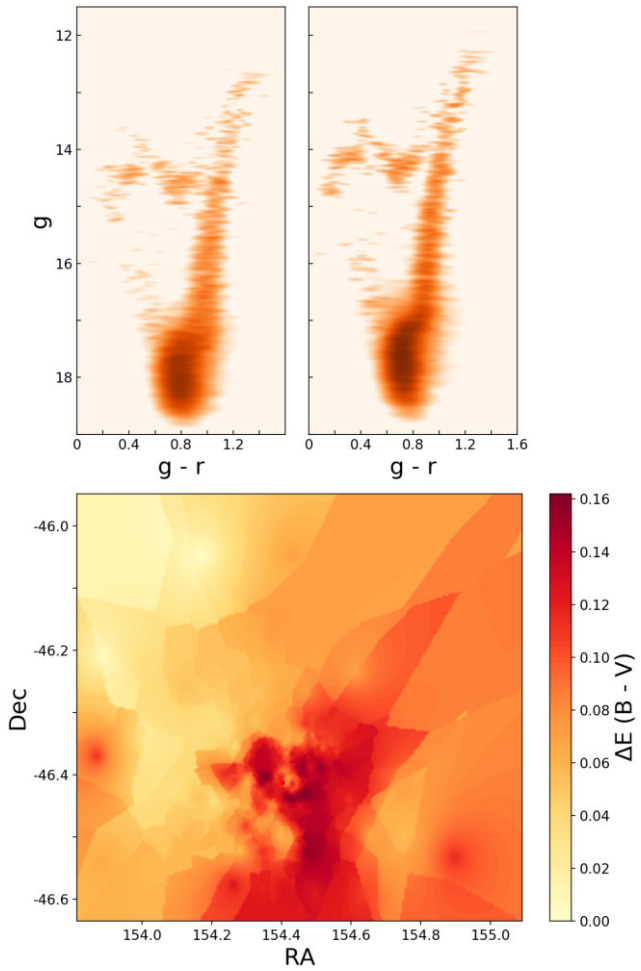

Figure 3. Illustration of differential reddening correction for NGC 3201. On the left are the original values for the cluster members, and on the right, the CMD is corrected by differential reddening following Bonatto & Chies-Santos (2020). We can see a much more defined turn-off point as well as a narrower RGB. The bottom panel shows the differential reddening map.

and can be represented by the isochrone. For this, we utilize the sample selected through GAIA as described in the previous section.

2.3 Differential reddening in NGC 3201

An additional problem in the analysis of NGC 3201 is the presence of significant differential reddening. While this can be safely ignored in the other clusters of our sample given their low reddening (see Table 1) and distance from the Galactic plane, the effects in NGC 3201 are more significant (see left-hand panel of Fig. 3). To correct for this effect, we have used the code described in Bonatto & Chies-Santos (2020). Briefly, the cluster is divided into cells of at least 50 objects, the CMDs for each cell is constructed, and the bluest one is taken as reference. All others are then shifted to match the reference one, and a reddening value for each sub-region is found. It is important for this analysis that the filter combination used is not affected by the presence of MSPs. For this, we have selected (g–r). Fig. 3 shows two CMDs of NGC 3201, before and after the correction and the differential reddening map on the bottom panel. We have also compared the reddening map we obtained with the ones available in the literature, such as Von Braun & Mateo (2001), and found them to be in agreement both in general shape and values. To

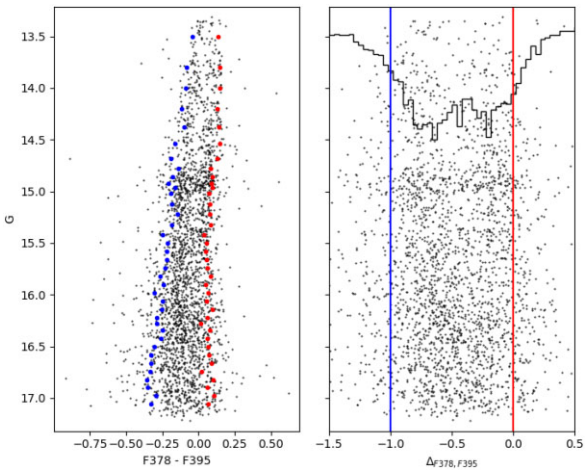

Figure 4. Illustration of the process of making $\Delta_{F378,\,F395}$ for NGC 104. The left-hand panel is a CMD showing only the limited RGB. The red and blue dots show the 10 per cent and 90 per cent percentiles of each horizontal strip. On the right are the straightened lines and the calculated Δ, as well as a histogram of the horizontal axis showing the double-peaked distribution. The same process is done for all other colours in the clusters in the sample.

test our assumption that the other three GCs do not have significant differential reddening we have applied the same code and found that the maximum $\Delta E(B-V)$ does not exceed 0.06.

3 THE SUB-POPULATIONS OF STARS

In order to study the multiple populations, we need to separate them. First, we conduct a visual inspection of all colour combinations in search of a broadening of the RGB, an indication of the presence of MSPs. Six colour combinations are selected, namely: u–F378, u–F395, F378–F395, F378–F430, F378–F515, and F410–F430. With this, we then constructed the Δ*colours* in the same manner as Milone et al. (). To summarize the process illustrated in Fig. 4: the RGB is divided in vertical segments containing a minimum of 50 stars, in each segment the 10 per cent and 90 per cent percentiles horizontally are determined and are used to create two fiducial lines, the red and blue lines shown in the left-hand panel of Fig. 4. Such lines are then used to straighten the RGB and create the Δ's using the same expression from Milone et al. (, section 4) as seen in the right-hand panel of Fig. 4. This process allows the straightening of the RGB and provides a clearer separation of the two populations. This process is repeated for all six colours in all clusters of our sample. One important caveat is that the top of the RGB is ignored in this process because it has a low number of stars, making the process not statistically significant.

To make full use of the six colour combinations selected, we used the K-means clustering algorithm (MacQueen et al. 1967) with two classes to separate the populations present in the clusters. This method requires two main assumptions: first, that two distinct populations are present, as expected for the clusters in our sample, and second that the number of objects is comparable in both populations, as also supported by the literature. The separation was performed in all four clusters, and some Δ combinations for three GCs are shown in Fig. 5. NGC 7089 is a particular case; Milone et al. (2015) identified in this cluster seven distinct populations. In their analyses using *HST* images they identified three main groups (A, B, and C) with very distinct abundance patterns. However, given the low number of objects in population C we do not account for it in our

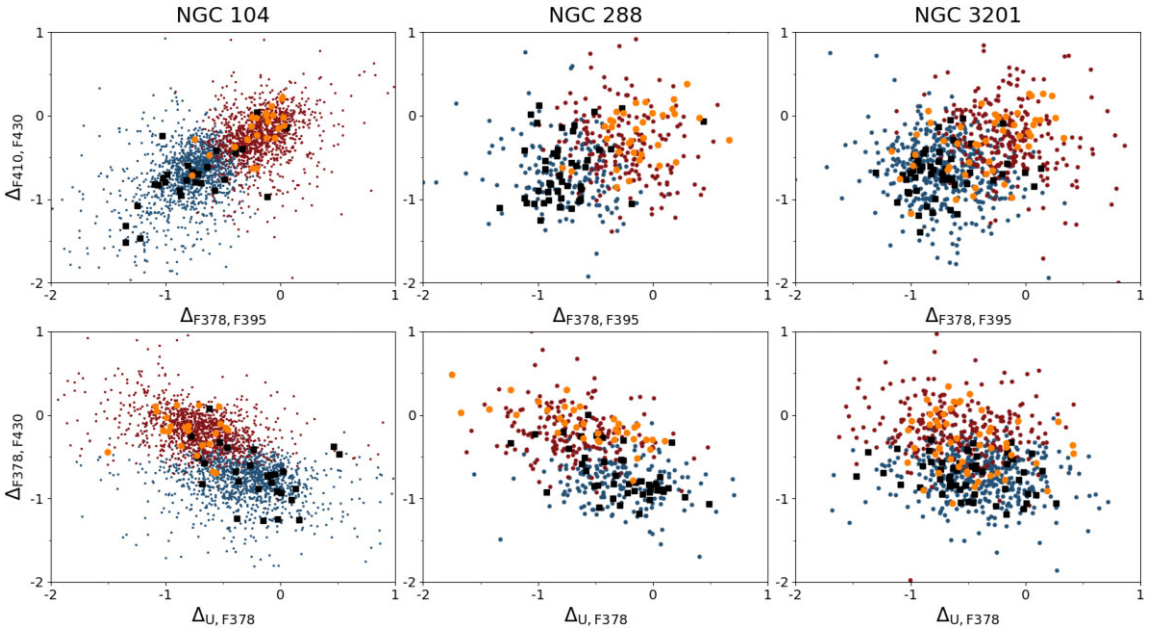

Figure 5. Two Δ combinations for three of the cluster in our sample. The blue and red points are the separation made using the clustering method. The black and orange points are stars with measured Na abundance from Carretta et al. (2009). For NGC 104 and NGC 288, we can see the segregation of Na-poor (orange circles) and Na-rich (black squares) follows our separation. For NGC 3201, the picture is less clear, and the Na-rich stars match very well with the blue population; however, the Na-rich do not occupy a clear locus.

method and do no find it in a visual inspection of the CMDs. Also, we are not capable of separating the more nuanced subpopulations of groups A and B given their relative similarity. This might be one of the reasons why the separation for NGC 7089 is not clear in either the Δ*colours* planes and the CMD shown in Fig. 7.

4 ANALYSIS AND DISCUSSION

4.1 Classifying the populations

The usual understanding of the formation of MSPs states that a primordial population enriches – by different methods depending on the model – the intra-cluster medium forming a secondary population (Decressin et al. 2007; D'Ercole et al. 2008; Charbonnel et al. 2014). One of the elements that can be used to trace the two populations is Na, for which we have abundance measurements from Carretta et al. (2009) for individual stars in three of the GCs in our sample, namely NGC 104, NGC 288, and NGC 3201. We separated the stars in Na-rich and Na-poor by first constructing the histogram of Na abundance is shown in Fig. 6 and determining the central dip in the number of objects (dashed line in Fig. 6). We drew two more lines (orange and black) around this division taking into account the average uncertainty in [Na/Fe] with the intention of avoiding an ambiguous classification. Na-poor stars as those left of the orange line and Na-rich as those right of the black one. Last we matched with our S-PLUS photometry sample in order to evaluate our separation and to classify the populations. Fig. 5 shows two Δ combinations for each cluster with our separation as well as the Na-rich and Na-poor stars.

In general, we see that the objects with blue markers are connected with the Na enhanced stars. We consider this the second population (2P). The objects with a primordial composition (Na-poor) are connected with the objects in red, forming the first population (1P). For NGC 104, this separation is very clear when looking at the top

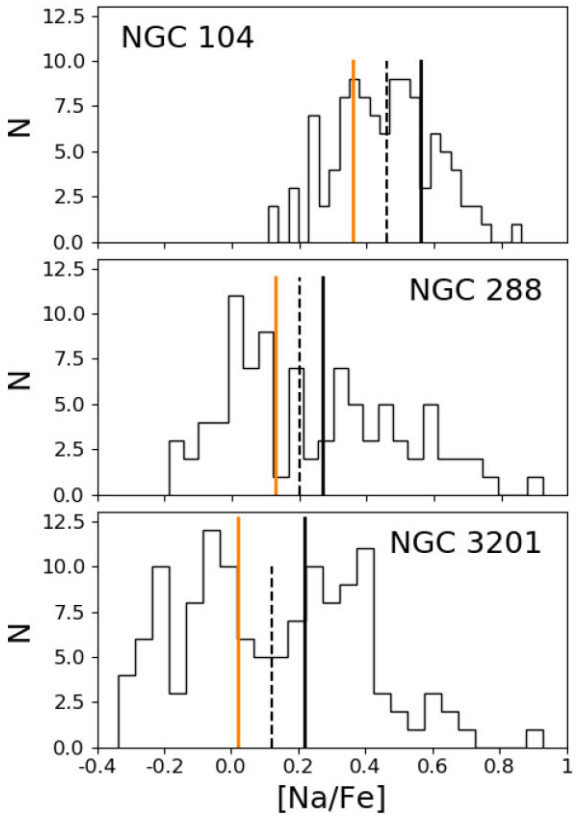

Figure 6. Sodium abundance histograms from Carretta et al. (2009) for three of the clusters. The Na-poor objects are left of the orange line, while the Na-rich is to the right of the black line.

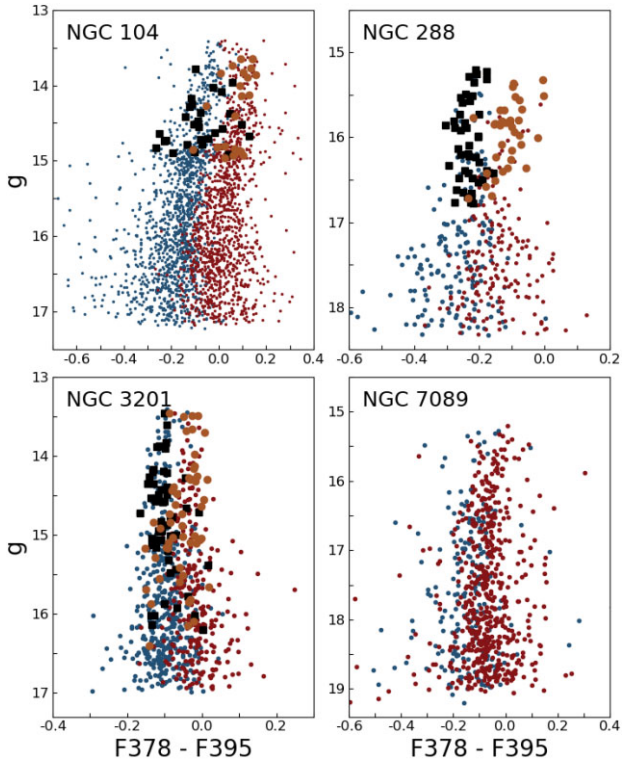

Figure 7. CMDs of only the RGB for the GCs in our sample. In blue and red are the populations separated using the K-means algorithm. The black squares and orange points are the same as in Fig. 5. In the case of NGC 3201, the separation between Na-rich/poor is evident for stars brighter than 15.5 on the g-band below this Na-poor stars seem not to follow the red population.

panel of Fig. 5. NGC 288 also presents a good separation in both Δ spaces. However, for NGC 3201 the separation is fuzzy, with the Na-rich stars occupying a clearer locus matching with the blue population. Meanwhile, the Na-poor are more spread out over the entire distribution. Fig. 7 shows one CMD for each cluster focused in the RGB with the populations separated as described and the Na-poor/rich stars.

The population ratios are shown in Table 2, NGC 104 and NGC 288 have an equal (47 per cent and 51 per cent of 1P, respectively) split between first and second population stars. For NGC 3201, the second population dominates with 63 per cent of the cluster in a number of RGB stars. NGC 7089 stands out as 73 per cent of its stars are in the first population.

4.2 Radial profiles

The present-day distribution of the populations in a GC is a complex interplay between many factors such as the initial conditions (which are strongly dependent on the formation scenario) and the internal dynamical evolution of the cluster (mass-segregation, binaries, core-collapse, etc.; Vesperini et al. 2013, 2021; Calura et al. 2019; Sollima 2021). Looking at the cumulative distribution of the different populations as a function of their distance to the cluster centre is important when evaluating such formation scenarios; however, this must be done with some care. To check the significance of the radial difference between the distributions of the different stellar populations, we submit our radial profiles to a set of statistical tests. The most common one is the Kolmogorov–Smirnov test (KS test) that evaluates whether two distributions differ significantly. However, the KS test has some limitations, and it is less sensitive when the distributions differ in the beginning and end (Feigelson & Babu 2012). Thus the Anderson–Darling test (AD test) was designed to mitigate this (Anderson & Darling 1952). Fig. 8 presents the radial profiles for the four clusters in our sample, and the radial distance is shown in terms of the half-light radius (Harris 1996, 2010 version). Table 2 shows the results for both tests as well as their critical values.

In the following subsections, we discuss the radial distributions of the MSPs of our sampled GCs in light of past literature studies.

4.2.1 NGC 104

One of the most massive clusters in our Galaxy, NGC 104 is an interesting subject for our study. Norris & Freeman (1979) measured the CN abundance in 142 RGB stars and found that the richer population is more centrally concentrated. This result was corroborated by Briley (1997) who studied 300 RGB stars and found that outside of 13 arcmins from the cluster centre, CN-weak stars dominate, while inside, no difference is apparent. Milone et al. (2012) used ground-based and *HST* photometry to study the presence of MSPs along the entire stellar sequence of NGC 104. They found that the second population comprises ∼70 per cent of the cluster and is more centrally concentrated than the first up to 3–4 half-light radius. This result is in agreement with the work of Nataf et al. (2011) that studied the stars in the RGB bump and Horizontal Branch (HB) and found that the He-enhanced population is more centrally concentrated; however, this is a much more tenuous result. Looking at our results for NGC 104, we can see that it is in agreement with the literature up to ∼3 half-light radii (9 arcmin). None the less, beyond this, no significant difference between the populations is apparent.

4.2.2 NGC 288

Vanderbeke et al. (2015) studied the HB of 48 GCs and found that in the case of NGC 288, NGC 362, and NGC 6218 the second population (He-rich) appears less centrally concentrated. However, this is in contradiction with what was found by Piotto et al. (2013). They used *HST* imaging to show that inside the FoV of WFC3/UVIS, the first population makes up more than 50 per cent of the cluster stars. Our results show that the second population (Na-rich) is more centrally concentrated, supported by the KS and AD tests which show that the two distributions are different with a high confidence level, agreeing with Piotto et al.

4.2.3 NGC 3201

NGC 3201 has been extensively studied by Kravtsov et al. (2010), Kravtsov (2017), and Kravtsov & Calderón (2021). Overall they found with a high degree of confidence that the second population is more centrally concentrated. This result was consistent in the SGB and RGB and across different data sets. Carretta et al. (2010) also studied this cluster and corroborated these results, finding that Na-poor RGB stars occupy more the outskirts of the cluster, although their sample size was relatively small. The radial profile shown in Fig. 8 seems to contradict these results, showing a larger fraction of 1P stars towards the centre of the GC. This discrepancy may be due to the fact that the photometric separation provided by our calculated $\Delta colours$ does not provide a consistent separation between 1P (Na-poor) and 2P (Na-rich) as shown in Fig. 5.

Table 2. Population sizes and statistics.

				KS		AD	
ID	N_{blue}	N_{red}	f_1	D	P	A	A_{cr}
NGC 104	1327	1211	0.47	0.08	0.038 per cent	4.57	0.5 per cent
NGC 288	209	221	0.51	0.21	0.026 per cent	9.09	<0.1 per cent
NGC 3201	494	300	0.37	0.16	0.007 per cent	14.53	<0.1 per cent
NGC 7089	199	542	0.73	0.22	0.00019 per cent	16.68	<0.1 per cent

D and P: KS statistic and probability of the two distributions being drawn from the same parent population, A and A_{cr}: AD statistic and critical value.

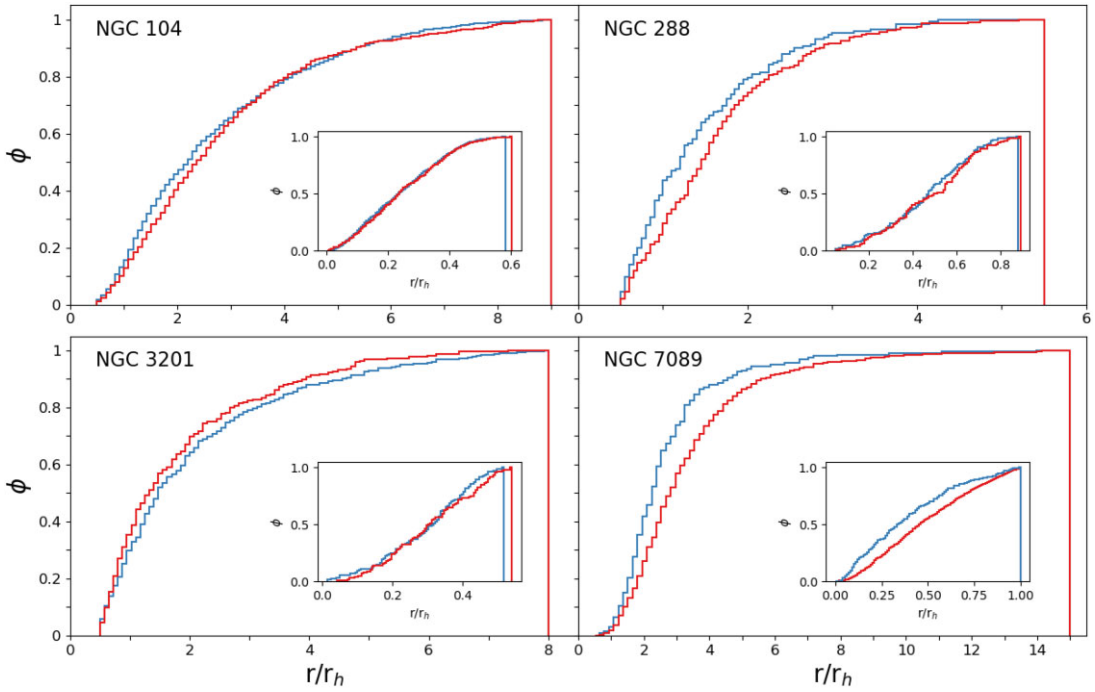

Figure 8. Cumulative radial distributions of the four clusters in our sample. The red and blue lines represent the primordial and enriched populations, respectively. The insets show the radial profiles for the inner region of the clusters constructed with *HST* photometry, highlighting the importance of studying the outer regions.

4.2.4 NGC 7089

Vanderbeke et al. (2015) in the same study of HB stars mentioned earlier found no radial difference when analysing NGC 7089 with a KS probability of 72 per cent. However, Lardo et al. (2011) used SDSS photometry and showed a large radial variation between both populations, finding that the UV-red (2P) population is more centrally concentrated. Hoogendam & Smolinski (2021) have re-analysed the SDSS data and incorporated ground-based photometry by Stetson et al. (2019) and found no conclusive evidence. The SDSS data set suggests a red-concentrated population, while Stetson's data shows the opposite, both to a high significance level in the KS test. According to the KS and AD tests, we find that the 2P of stars is more centrally concentrated with a high probability.

4.3 The importance of looking at the outskirts

Dynamical simulations of MSPs have shown that mixing occurs in a shorter time scale in the inner parts of the cluster due to two-body relaxation being more efficient in denser environments (Vesperini et al. 2013). Some information regarding the concentration of the second population, however, is still preserved for a longer period in the outer regions of the GCs. To test this and highlight the importance of wide-field studies of MSPs, we have taken *HST* archival data from the HUGS project (Piotto et al. 2015; Nardiello et al. 2018), reproduced the chromosome maps as described in Milone et al. (2012), and separated the populations according to Milone et al. (2017). Given the smaller FoV of *HST*, the resulting radial profiles of all clusters extend at most to the half-light radius; they are in the insets in Fig. 8. In three of the clusters – NGC 104, NGC 288, and NGC 3201 – we see that the populations are already mixed, showing no major differences. The exception is NGC 7089, where the populations show no sign of mixing with the second population appearing more centrally concentrated. This follows the trend found in the outer region of the cluster, and simulations by Dalessandro et al. (2019) suggest that in clusters with the dynamical age of NGC 7089, some segregation can still be present inside 2 r_h.

5 SUMMARY AND CONCLUDING REMARKS

When analysing the phenomenon of multiple populations, it is clear that the best tool is spectroscopy. It allows us to get a clear picture of the most significant differences between the populations and provide the best data set to inform possible formation models. However, it is an expensive tool that translates into studies with a relatively small sample size and limited to the outer regions of clusters. This is why photometric studies are so important, capable of providing

information on thousands of objects at once. If we are capable of characterizing the populations, it can provide us with a good picture of what is happening in the GCs. As we have shown here, S-PLUS is a great tool for this purpose. With its wide FoV, it is capable of studying the entirety of the cluster, and its set of 12 filters provides us with a large toolbox to analyse and separate the populations.

In the present study we have used six colour combinations (u–F378, u–F395, F378–F395, F378–F430, F378–F515, and F410–F430) and the K-means algorithm to separate the MSPs present in four GCs. We can see based on the selected filters that the spectral region that provides the best separation tends toward the blue, which is expected as it is in this region where the majority of MSP features appear. When combined with spectroscopic abundances of individual stars from the literature, our photometric separation is well supported in the cases of NGC 104 and NGC 288. However, when considering NGC 3201, the separation does not seem to correspond to a difference in the Na abundance of the cluster stars. One thing to be noted here is that the more metal-rich GCs (NGC 104 − [Fe/H] = −0.72, NGC 288 − [Fe/H] = −1.32) in our sample have a more clear separation in the Δ space. This trend is in agreement with synthetic spectra computed to simulate MSPs (Branco et al., in preparation).

Using the large FoV of S-PLUS, we analysed the cumulative radial distribution (CRDs) of the populations. Using both the KS test and the AD test, we conclude that CRDs of the four clusters differ significantly. In the case of NGC 104, the populations appear well mixed, which, given the age of this GC, could indicate that the populations had enough time to mix. For both NGC 288 and NGC 7089, we can see a clear concentration of 2P population toward the centre of the cluster. This directly supports the formation theories that propose an enrichment of the intra-cluster medium and subsequent star formation in the more dense central regions (see e.g. D'Ercole et al. 2008). However, in the case of NGC 3201, the trend is reversed. The 1P is more centrally concentrated, in direct contradiction with previous literature studies. It is clear that further studies have to be performed in a systematic way to shed light on this subject. Another critical issue is that in order to explain the differences in the clusters, formation scenarios have to be stochastic enough to account for the distinct histories of each GC.

ACKNOWLEDGEMENTS

The authors thank the anonymous referee for the careful reading of the paper and the useful comments that helped improve the manuscript. This paper is based on the research of an undergraduate and masters thesis as part of the requirements for obtaining the title of Bachelor's and MSc in Physics at the Universidade Federal do Rio Grande do Sul. This work was supported by Coordenação de Aperfeiçoamento de Pessoal de Nível Superior (CAPES), *Conselho Nacional de Desenvolvimento Científico e Tecnológico* (CNPq), *Fundação de Amparo à Pesquisa do Estado do RS* (FAPERGS), and *Fundação de Amparo à Pesquisa do Estado de SP* (FAPESP). The authors thank Analía Smith Castelli, Clecio R. Bom, Leandro Beraldo e Silva, Pavel Kroupa, and Emanuele Dalessandro for comments that helped improve the manuscript. CB acknowledges funding from CNPq. ACS acknowledges funding from CNPq and FAPERGS through grants CNPq-403580/2016-1, CNPq-11153/2018-6, PqG/FAPERGS-17/2551-0001, FAPERGS/CAPES 19/2551-0000696-9, L'Oréal UNESCO ABC *Para Mulheres na Ciência*, and the Chinese Academy of Sciences (CAS) President's International Fellowship Initiative (PIFI) through grant E085201009. JA-G acknowledges support from ANID - Millennium Science Initiative Program - ICN12_009 awarded to the Millennium Institute of Astrophysics MAS. This paper has made use of results from the European Space Agency (ESA) space mission Gaia, the data from which were processed by the Gaia Data Processing and Analysis Consortium (DPAC). Funding for the DPAC has been provided by national institutions, in particular the institutions participating in the Gaia Multilateral Agreement. The Gaia mission website is http://www.cosmos.esa.int/gaia. PC acknowledges support from Conselho Nacional de Desenvolvimento Científico e Tecnológico (CNPq) under grant 310041/2018-0.

The S-PLUS project, including the T80-South robotic telescope and the S-PLUS scientific survey, was founded as a partnership between the Fundação de Amparo à Pesquisa do Estado de São Paulo (FAPESP), the Observatório Nacional (ON), the Federal University of Sergipe (UFS), and the Federal University of Santa Catarina (UFSC), with important financial and practical contributions from other collaborating institutes in Brazil, Chile (Universidad de La Serena), and Spain (Centro de Estudios de Física del Cosmos de Aragón, CEFCA). We further acknowledge financial support from the São Paulo Research Foundation (FAPESP), the Brazilian National Research Council (CNPq), the Coordination for the Improvement of Higher Education Personnel (CAPES), the Carlos Chagas Filho Rio de Janeiro State Research Foundation (FAPERJ), and the Brazilian Innovation Agency (FINEP).

The members of the S-PLUS collaboration are grateful for the contributions from CTIO staff in helping in the construction, commissioning and maintenance of the T80-South telescope and camera. We are also indebted to Rene Laporte, INPE, and Keith Taylor for their important contributions to the project. From CEFCA, we thank Antonio Marín-Franch for his invaluable contributions in the early phases of the project, David Cristóbal-Hornillos and his team for their help with the installation of the data reduction package JYPE version 0.9.9, César Íñiguez for providing 2D measurements of the filter transmissions, and all other staff members for their support with various aspects of the project.

DATA AVAILABILITY

The data underlying this article are available in its online supplementary material and at CDS via anonymous ftp to cdsarc.u-strasbg.fr (130.79.128.5) or at https://cdsarc.unistra.fr/viz-bin/cat/J/MNRAS and can be accessed with the volume and page numbers of this article.

REFERENCES

Almeida-Fernandes F. et al., 2022, MNRAS, 511, 4590
Anderson T. W., Darling D. A., 1952, Ann. Math. Stat., 23, 193
Bonatto C. et al., 2019, A&A, 622, A179
Bonatto C., 2019, MNRAS, 483, 2758
Bonatto C., Chies-Santos A. L., 2020, MNRAS, 493, 2688
Bressan A., Marigo P., Girardi L., Salasnich B., Dal Cero C., Rubele S., Nanni A., 2012, MNRAS, 427, 127
Briley M. M., 1997, AJ, 114, 1051
Calura F., D'Ercole A., Vesperini E., Vanzella E., Sollima A., 2019, MNRAS, 489, 3269
Carretta E., Bragaglia A., Gratton R., Lucatello S., 2009, A&A, 505, 139
Carretta E., Bragaglia A., D'Orazi V., Lucatello S., Gratton R. G., 2010, A&A, 519, A71
Cenarro A. J. et al., 2019, A&A, 622, A176
Charbonnel C., Chantereau W., Krause M., Primas F., Wang Y., 2014, A&A, 569, L6
Coe D. et al., 2012, ApJ, 757, 22
Coelho P. R. T., 2014, MNRAS, 440, 1027
Coelho P., Percival S. M., Salaris M., 2011, ApJ, 734, 72
D'Ercole A., D'Antona F., Vesperini E., 2016, MNRAS, 461, 4088
D'Ercole A., Vesperini E., D'Antona F., McMillan S. L. W., Recchi S., 2008, MNRAS, 391, 825

Dalessandro E. et al., 2019, ApJ, 884, L24
De Mink S. E., Pols O. R., Langer N., Izzard R. G., 2009, A&A, 507, L1
Decressin T., Meynet G., Charbonnel C., Prantzos N., Ekström S., 2007, A&A, 464, 1029
Feigelson. E. D., Babu G. J., 2012, in Modern Statistical Methods for Astronomy. Cambridge University Press, UK, p. 476
Gaia Collaboration, 2021, A&A, 649, A1
Gieles M. et al., 2018, MNRAS, 478, 2461
Harris W. E., 1996, AJ, 112, 1487
Hoogendam W. B., Smolinski J. P., 2021, AJ, 161, 249
Kirkpatrick S., Gelatt C. D., Vecchi M. P., 1983, Science, 220, 671
Kravtsov V. V., 2017, AJ, 154, 79
Kravtsov V., Alcaíno G., Marconi G., Alvarado F., 2010, A&A, 512, L6
Kravtsov V., Calderón F. A., 2021, AJ, 161, 7
Lardo C., Bellazzini M., Pancino E., Carretta E., Bragaglia A., Dalessandro E., 2011, A&A, 525, A114
Larsen S. S., Baumgardt H., Bastian N., Hernandez S., Brodie J., 2019, A&A, 624, A25
MacQueen J. et al., 1967, in Le Cam L. M., Neyman J., eds, Proceedings of the Fifth Berkeley Symposium on Mathematical Statistics and Probability: Weather modification. University of California Press, USA, p. 281
Mendes de Oliveira C. et al., 2019, MNRAS, 489, 241
Milone A. P. et al., 2012, ApJ, 744, 58
Milone A. P. et al., 2015, MNRAS, 447, 927
Milone A. P. et al., 2017, MNRAS, 464, 3636
Nardiello D. et al., 2018, MNRAS, 481, 3382
Nataf D. M., Gould A., Pinsonneault M. H., Stetson P. B., 2011, ApJ, 736, 94
Norris J., Freeman K. C., 1979, ApJ, 230, L179
Piotto G. et al., 2015, AJ, 149, 91
Piotto G., Milone A. P., Marino A. F., Bedin L. R., Anderson J., Jerjen H., Bellini A., Cassisi S., 2013, ApJ, 775, 15
Prantzos N., Charbonnel C., 2006, A&A, 458, 135
Sollima A., 2021, MNRAS, 502, 1974
Soto M. et al., 2017, AJ, 153, 19
Stetson P. B., 1987, PASP, 99, 191
Stetson P. B., Pancino E. Zocchi A. Sanna N. Monelli M. 2019, MNRAS, 485, 3042
Tody D., 1993, in Hanisch R. J., Brissenden R. J. V., Barnes J., eds, ASP Conf. Ser. Vol. 52, Astronomical Data Analysis Software and Systems II. Astron. Soc. Pac., San Francisco, p. 173
Vanderbeke J., De Propris R., De Rijcke S., Baes M., West M., Alonso-García J., Kunder A., 2015, MNRAS, 451, 275
Vesperini E., Hong J., Giersz M., Hypki A., 2021, MNRAS, 502, 4290
Vesperini E., McMillan S. L. W., D'Antona F., D'Ercole A., 2013, MNRAS, 429, 1913
Von Braun K., Mateo M., 2001, AJ, 121, 1522
Wang L., Kroupa P., Takahashi K., Jerabkova T., 2020, MNRAS, 491, 440

SUPPORTING INFORMATION

Supplementary data are available at *MNRAS* online.

Catalogs.zip

Please note: Oxford University Press is not responsible for the content or functionality of any supporting materials supplied by the authors. Any queries (other than missing material) should be directed to the corresponding author for the article.

APPENDIX A: FIELD-CLUSTER STAR SEPARATION FOR THE OTHER CLUSTERS

In Figs A1, A2, and A3 we show the process of cluster member selection using GAIA proper motions, as outlined in Section 2.1, for clusters NGC 288, NGC 3201, and NGC 7089, respectively.

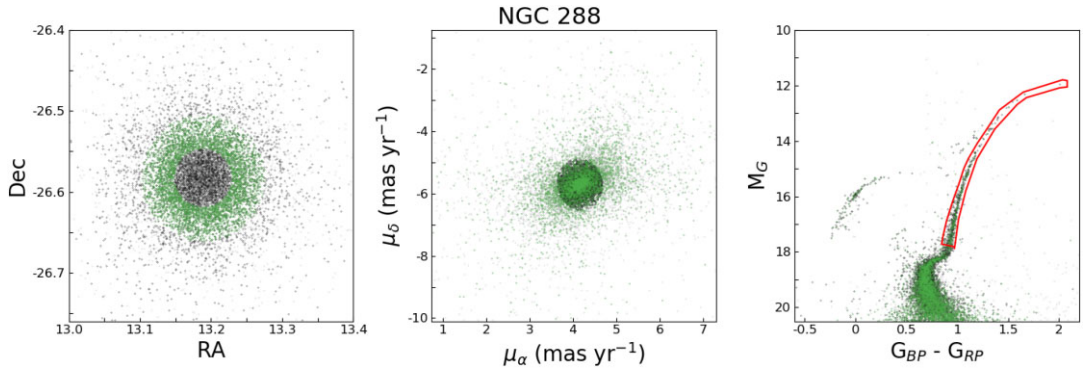

Figure A1. Same as Fig. 2 for NGC 288.

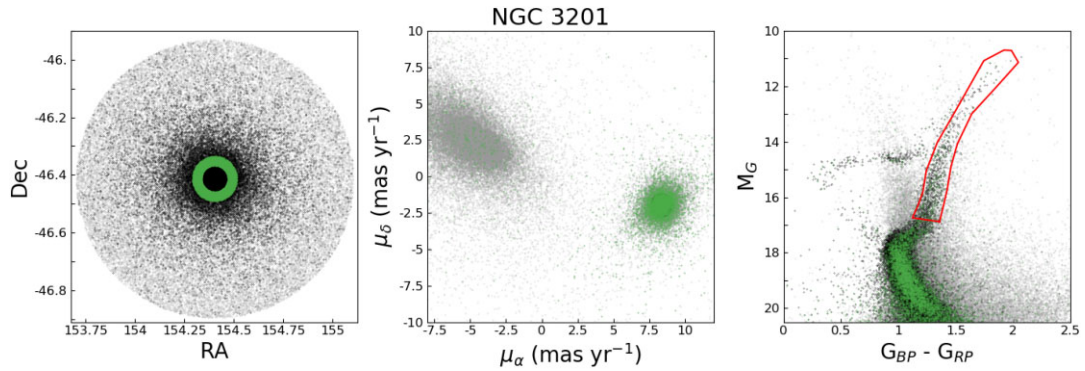

Figure A2. Same as Fig. 2 for NGC 3201.

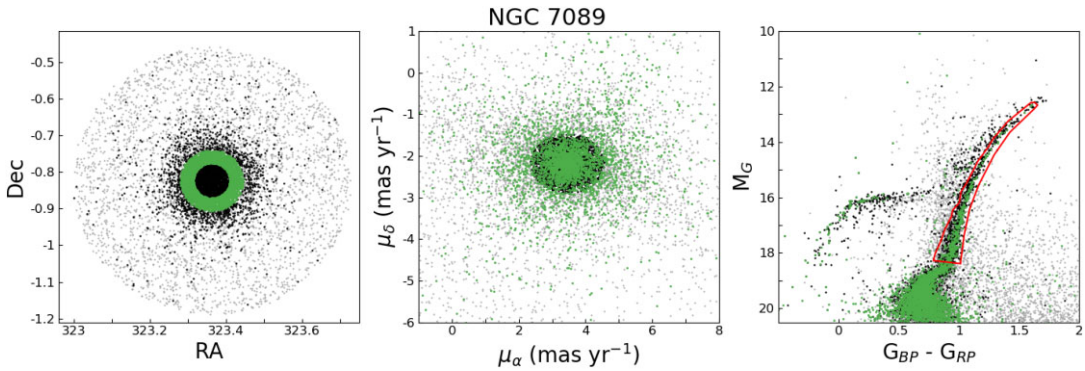

Figure A3. Same as Fig. 2 for NGC 7089.

APPENDIX B: INCOMPLETENESS IN THE GAIA SAMPLE

To analyse the completeness of the GAIA sample we constructed histograms of the number of objects as a function of the M_G magnitude shown in Fig. B1. We also marked the approximate position of the turn-off for each cluster. It is evident that the completeness is essentially unaffected above the TO.

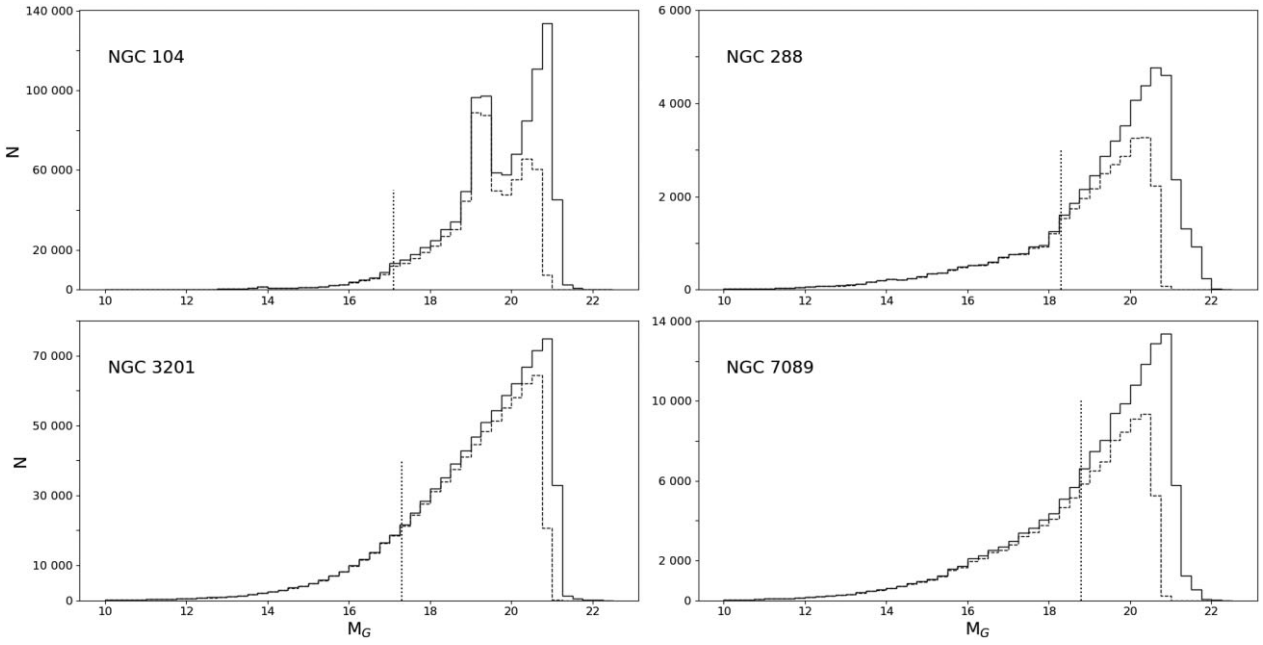

Figure B1. Histograms of the number of objects per magnitude bin. The solid line represent all the objects present within the tidal radius of each cluster, the dashed one are only those that have all three GAIA magnitudes measured and proper motion errors smaller than 1.5 mas yr^{-1}. The dotted line is the approximate position of the turn-off.

This paper has been typeset from a TEX/LATEX file prepared by the author.

4 The kinematics of multiple stellar populations

The study of the distribution of first and second generation stars in GCs is a topic fairly new in the context of MSPs. One early work by Decressin, Baumgardt e Kroupa (2008) explored the Mass Budget problem via N-body simulations showing that two-body relaxation cannot account for the preferential loss of ∼90% of 1P stars. Vesperini et al. (2013) modelled clusters with a 2P initially more centrally concentrated and found that spatial mixing of the populations is only achieved in very evolved clusters. By this point the GCs should have lost the majority (60 — 70%) of their mass due to two-body relaxation, irrespective of the initial concentration of the second generation. A study by Mastrobuono-Battisti e Perets (2013) explored structures within GCs and showed some interesting results. In their simulation a cold disk structure was embedded in a massive GC ($2.5 \times 10^6\,M_\odot$), hints of this initial structure were still present in the simulation even after 12Gyrs, e.g. a small flattening of the cluster due to angular momentum exchanges. More relevant, the disc stars do not reach a completely spherical isotropic distribution. This is relevant in view of Bekki (2010) and Bekki (2011), where they considered the AGB scenario and showed that even a small net angular momentum in the 1P could result in significant initial rotation of the 2P and even a disk-like structure.

Hénault-Brunet et al. (2015) designed a set of simulations to investigate the long term kinematic effects of two MSP scenarios: multiple generations and the accretion. An important factor is that these scenarios imply different initial conditions. The accretion scenarios favour stars that are in radial orbits with low rotation amplitudes. However, the multiple generations scenario implies a larger rotational amplitude of the 2P due to dissipative processes that drove the polluting material to the centre. These differences can survive for long periods of time (importantly, for more than a Hubble time), especially in the outer regions of the cluster. In a recent paper by Tiongco, Vesperini e Varri (2019) they evaluated the time evolution of rotations curves of MSPs considering a more centrally concentrated 2P and with a faster rotational profile. They corroborate the results of previous works in that the redistribution of energy and loss of angular momentum leads to both populations sharing the same rotational curve. This occurred fairly quickly in the dense central regions however, the outer regions are much slower to reach a state of isotropy, as expected (less density means a smaller chance for the encounters that lead to the exchange of angular momentum).

Observational works have also been carried out with the intention of finding (or not) kinematic differences between the populations. Richer et al. (2013) used multi-epoch HST

observations of NGC 104 to derive proper motions and divided the Main Sequence into four populations. They found that the bluest sequence had a large anisotropy (with a larger radial dispersion), while the reddest one presented a negligible one. This, connected with the fact that the bluest population appears more centrally concentrated, could indicate that the blue population is still in the process of moving outwards via two-body relaxation. A more recent look at NGC 104 by Milone et al. (2018) showed similar findings even when considering a larger area of the cluster.

Bianchini et al. (2018) analysed stars within 3 half-light radius (R_h), this is the typical region where the rotation signal is expected to be significant (see Bianchini et al. (2013)), in 51 GCs using Gaia DR2 data. They detected significant rotational signal in 11 clusters, including NGC 104 and NGC 7089. They measured V/σ to assess the importance of internal rotation and correlated it with metallicity, relaxation time and the total mass using a Spearman rank test. The correlation between higher metallicity and V/σ could be an indicative of the early stages of GC formation, implying a higher efficiency of energy dissipation in GCs with high [Fe/H]. However, other studies have not been able to confirm this result (Kimmig et al., 2015; Kamann et al., 2018).

Cordero et al. (2017) used spectra gathered by the WIYN-Hydra spectrograph (6050-6350 Å wavelength coverage) on M13 and existing measurements of Na and O abundance to study the radial velocities of the populations. They found that the O-depleted population rotates faster around the cluster centre than the intermediate population, arguing that this dynamical signature is a remnant of the formation history of the GC. A combination of MUSE spectroscopy (to derive radial velocities) and HST photometry (to separate and characterise the populations) was used by Kamann et al. (2020) to study M80. Using axisymmetric Jeans models and both parametric and non-parametric radial profiles they showed that all three populations have rotational signals, and that the N-rich population has a higher projected rotation velocity in comparison. This is a rather complicated result to explain in view of the fact that M80 seems to be quite dynamically advanced and it has been suggested that the central concentration of the populations has flipped due to mass segregation (Dalessandro et al., 2018). Further N-body simulations are necessary to investigate this.

More recently, Martens et al. (2023) used line-of-sight velocities derived using MUSE spectra to analyse the rotation and dispersion profiles of MSPs in 25 GCs. They separated the populations using the HST photometric observations and the chromosome map. Importantly they found that for NGC 6093 and NGC 7078 the second population rotates faster than the first while NGC2808 presents the opposite result. For 10 other clusters in their sample they found a rotation signal in at least one population (including NGC 104 and NGC 7089), however these results are bellow a 2σ confidence level making affirmations about which formation scenario, single- or multi-epoch, is more likely hard

to make. Libralato et al. (2023) has also analysed the proper motion of MSPs in 56 GCs using multi-epoch observations from HST. They decided to study only bright stars from the RGB, which leads to a smaller sample of objects per population. To mitigate this they combined the stars from all clusters into a single sample, analysing the general velocity dispersion in the populations. One important distinction is that by using HST data the MSPs can be divided into type-I and type-II (see 1.4.2 for the differences between both types), thus type-I GCs were separated into 1G and 2G, while type-II had their red-RGB further separated into 1Gr and 2Gr. They found that 1G stars are kinematically isotropic independent of radius, while the 2G tend to be more anisotropic at the outer regions. This is due to the fact that 2G tend to have a lower tangential velocity dispersion. This is expected in models where the 2G formed more centrally concentrated. They also found a possible link between the perigalactic distance (R_{peri}) of each cluster and the anisotropy of both populations, with system with large R_{peri} preserving a larger radial velocity dispersion.

With all of this in mind we aimed to use proper motion information from the *Gaia* survey to study the kinematics of the populations separated according to Hartmann et al. (2022).

4.1 Changing the reference frame

A star can have its movement in a cluster separated into two components: one is the systematic movement around the Galaxy that the GC follows as a whole. This can be considered the velocity vector of the centre of gravity of the cluster. And the second is the star's movement around that centre of gravity, i.e. its orbit inside the cluster. Our interest is in how the stars move in relation to the cluster centre. Therefore we need to eliminate the movement related to the GC orbit in the Galaxy. To achieve this first we transform the stellar positions from (RA, Dec) into Cartesian coordinates. This is done by projecting the positions onto the plane of the sky along the line-of-sight vector that passes through the cluster centre ((α_0, δ_0) taken from the Harris (1996), 2010 version). A simple transformation ($x = -\Delta\alpha cos\delta$ and $y = \Delta\delta$) is not suitable for our case as it causes distortions due to projections effects in objects with large apparent size and far away from the equatorial plane. Thus we used the equations derived by van de Ven et al. (2006):

$$\begin{aligned} x &= -r_0 \cos\delta \sin\Delta\alpha \\ y &= r_0 \left(\sin\delta \cos\delta_0 - \cos\delta \sin\delta_0 \cos\Delta\alpha\right), \end{aligned} \tag{4.1}$$

where $\Delta\alpha \equiv \alpha - \alpha_0$, $\Delta\delta \equiv \delta - \delta_0$. This gives us coordinates where positive x and positive y values lie West and North, respectively ($r_0 \equiv 10800/\pi$ is a scaling factor putting

(x, y) in units of arcmin). The next step is to transform the proper motions into the same reference frame. To accomplish this we use the expressions

$$\begin{aligned}\mu_x &= \mu_\alpha \cos\Delta\alpha - \mu_\delta \sin\delta \sin\Delta\alpha \\ \mu_y &= \mu_\alpha \sin\delta_0 \sin\Delta\alpha + \mu_\delta \left(\cos\delta \cos\delta_0 + \sin\delta \sin\delta_0 \cos\Delta\alpha\right),\end{aligned} \tag{4.2}$$

from Gaia Collaboration et al. (2018b). Considering that a GC is a spheroidal structure it is natural to study it in spherical coordinates. In our case, we have projected the cluster in 2D and will use a polar coordinate system. However, before we transform the positions and velocities we have to discount the overall movement of the cluster. For this we employ a method described in Bianchini et al. (2018). In summary, we assume that the probability of finding a given star with velocity v_i and uncertainty ϵ_i if the cluster has a mean velocity v and velocity dispersion σ_v is

$$p(v_i, \epsilon_i) = \frac{1}{2\pi\sqrt{\sigma_v^2 + \epsilon_i^2}} \exp - \frac{(v_i - v)^2}{2(\sigma_v^2 + \epsilon_i^2)}. \tag{4.3}$$

We obtain the v and σ_v and estimate the respective 1σ error by sampling the log-likelihood function:

$$-\log\lambda = -\log\prod_{i=1}^{N} p(v_i, \epsilon_i) = -\sum_{i=1}^{N} \log p(v_i, \epsilon_i), \tag{4.4}$$

using the Markov Chain Monte Carlo algorithm from Foreman-Mackey et al. (2013) called `EMCEE`. The values found are presented in Table 4. They were subtracted from the individual stellar proper motions. Fig. 10 is an illustration of the process using NGC 104 as an example. The top panel shows the initial velocity vectors in the plane of the sky of each star in the cluster in grey as well as the estimated systemic velocity of the GC in black. It is clear that this velocity dominates when compared to any movement that the stars have in relation to the cluster centre. The bottom panel shows the same vectors after the subtraction of the GC velocity. In both panels the vectors have been multiplied by the same scale factor for better visualisation. In other words, the direction and relative magnitudes are preserved, but the absolute magnitudes have been increased.

To transform these values into radial and tangential components we use the standard expressions:

$$\mu_r = \frac{x\,\mu_x + y\,\mu_y}{\sqrt{x^2 + y^2}} \quad \text{and} \quad \mu_t = \frac{x\,\mu_y - y\,\mu_x}{x^2 + y^2}, \tag{4.5}$$

where positive values of μ_r are moving away from the cluster centre and positive μ_t are rotating anti-clockwise. Its important to note that in this context radial does not

Table 4 – Systematic proper motion of the clusters in the x and y directions and associated 1σ confidence intervals.

Cluster	μ_x	μ_y
NGC 104 (47 Tuc)	5.261 ± 0.008	-2.548 ± 0.008
NGC 288	4.155 ± 0.005	-5.693 ± 0.007
NGC 3201	8.347 ± 0.007	-1.980 ± 0.006
NGC 7089 (M 2)	3.46 ± 0.01	-2.174 ± 0.007

refer to the line-of-sight velocity as it is commonly used, but to movement to and from the cluster centre in the projected plane of the sky. Although line-of-sight velocities from *Gaia* DR3 are available for some of the stars in our sample, we do not use this information, as the small number of objects (NGC 104 has the largest number of stars with measured line-of-sight velocity, 415; NGC 288 has 13; NGC 3201 has 91 and NGC 7089 has 28) and large uncertainties does not provide a statistically significant sample for our study.

4.2 Modelling radial and tangential velocity dispersion and isotropy

The next step was to trace the velocity dispersion radial profiles of both populations in the radial and tangential directions. The velocity dispersion (σ) of a group of objects is the standard deviation from the mean group velocity. A simple approach to calculate this would be to radially bin the data and calculate the average and 1σ deviation. However, methods such as this can be very dependent on the choice of bin size. To mitigate this we modelled the velocity dispersion using a Heteroscedastic Gaussian Process Regression. A Gaussian Process (GP) is a probability distribution in the function space that fit a set of observations. The Heteroscedasticity comes into play because each data point has a different variance, i.e. errors in the proper motions vary significantly. In our case we use a second order polynomial to model the velocity dispersion as a function of radial distance (r):

$$\begin{aligned} v_{\rm r} &= Normal(\mu, \sigma^2_{v_{\rm r}}), \\ \sigma_{v_{\rm r}} &= \gamma_0 + \gamma_1 r + \gamma_2 r^2, \\ \mu &= \beta_0 + \beta_1 r + \beta_2 r^2. \end{aligned} \tag{4.6}$$

We applied this method using the JAGS (Plummer, 2012) package for R[1]. The results are shown in Figure 11, on the left panels are the radial velocity dispersion for each cluster, while on the right are the tangential ones. The red and blue ribbons represent the primordial and enriched populations, following the separation done in Hartmann et

[1]This method was suggested by our collaborator Rafael da Silva de Souza, with the main code written by him and modified for our case by me.

al. (2022). The stronger and lighter shades of colour refer to the credible intervals for the radial distributions of velocity dispersion, respectively the 50% and 95% intervals.

The tangential velocity dispersion of the second population (in red) in NGC 104 is larger from 1 half-light radius outwards, indicating that this population is more dynamically heated than the first population outside of the central regions of the cluster. The same is true of σ_{V_T} in NGC 288, although the differences in this cluster are smaller. In this cluster, we can see a flattening of the velocity dispersion outside of 1 half-light radius for both populations and in both directions. For NGC 7089, the 1P has a smaller σ_{V_T} between 1 and 5 half-light radius, while in NGC3201, the profiles of both populations are the same. They diverge in the outermost region however, this may be due to the low number of objects.

When considering the radial velocity dispersion shown in the left panels of Figure 11 the populations in each cluster present a more uniform behaviour. In NGC 104 and NGC 3201, the profiles of the first and second populations are very similar, with only a minor deviation in the central region of NGC 104. NGC 7089 presents a flatter profile in the 1P and a steeper one for 2P. In this case, NGC 288 stands out, as it shows an identical profile of both populations in the outer regions, but in the inner half-light radius, the 2P has a much larger value.

Comparing the preliminary results shown here with the ones available in the literature, in the case of NGC 104 we see a disagreement in both the tangential and radial velocity dispersion profiles in relation to Milone et al. (2018), Figure 4. Focusing in the inner $5\,r_h$ ($\sim$16 arcmin, approximately how far from the cluster centre Milone et al. (2018) observations reach), Milone et al. (2018) found that the populations present no difference in the σ_{V_R} and the 2P has a slightly lower σ_{V_T} between 2 and $3\,r_h$. However, Fig. 11 shows a difference in the σ_{V_R} between the populations (and a flip $\sim$1.5 r_h) as well as the opposite behaviour in σ_{V_T}, i.e. the two populations have very similar values near the centre and the 2P has a larger value as we move outwards.

As stated before, Libralato et al. (2023) combined the data from 56 GCs to produce the velocity dispersion profiles. They find that 1G and 2G[2] have very similar profiles when looking at σ_{V_R}. In the outer regions, our results seem to agree with this however, in the inner parts we find that the populations present significant differences, with the 2G in NGC 288 and NGC 7089 having higher values, and the opposite for NGC 104. NGC 3201 is the exception in this case, showing a very similar profile all the cluster. Concerning the 2G, Libralato et al. (2023) shows a tendency of the 2G to have smaller σ_{V_T} in the outer regions of the cluster. Our results appear to show the opposite, when differences are

[2]Here the terms 1P/2P and 1G/2G are used interchangeably, because Libralato et al. (2023) uses the 1G/2G nomenclature. However, this is not our preferred way as it gives the impression that one population came after the other, and this is not established yet in the literature.

present the 1G has smaller $\sigma_{\mathrm{V_T}}$ values.

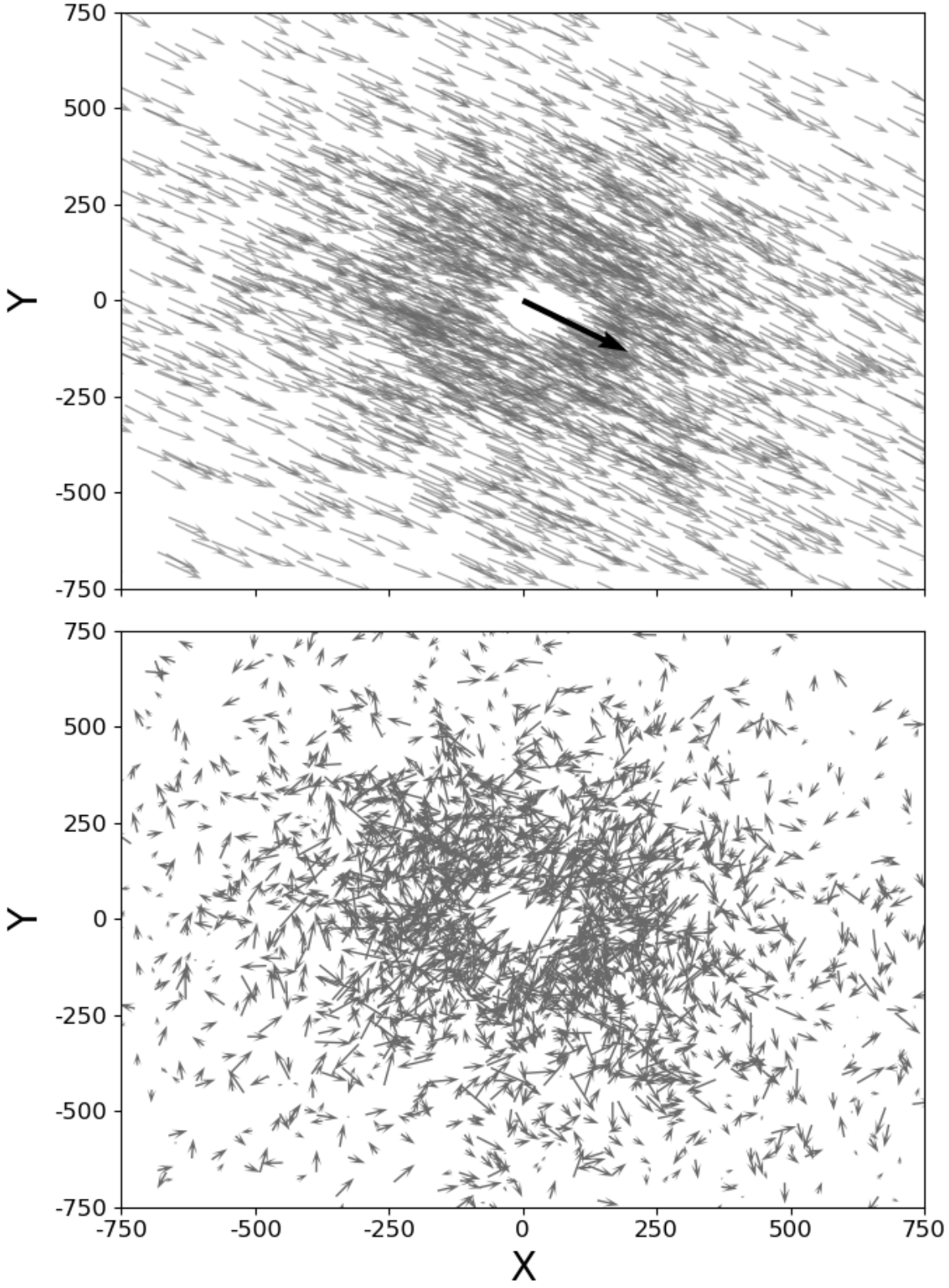

Figure 10 – The process of eliminating the systematic velocity of the cluster on the sky using NGC 104 as an example. In the top panel the grey arrows are the velocity vectors of each star and the black arrow is the systematic velocity of the cluster on the plane of the sky. On the bottom panel this velocity has been subtracted from all stars. The magnitudes of the vectors have been increased by a scale factor for better visualisation. It's very obvious that the cluster movement as a whole dominates in the top panel, while the bottom one we can see the more random motion of the stars in relation to the cluster centre.

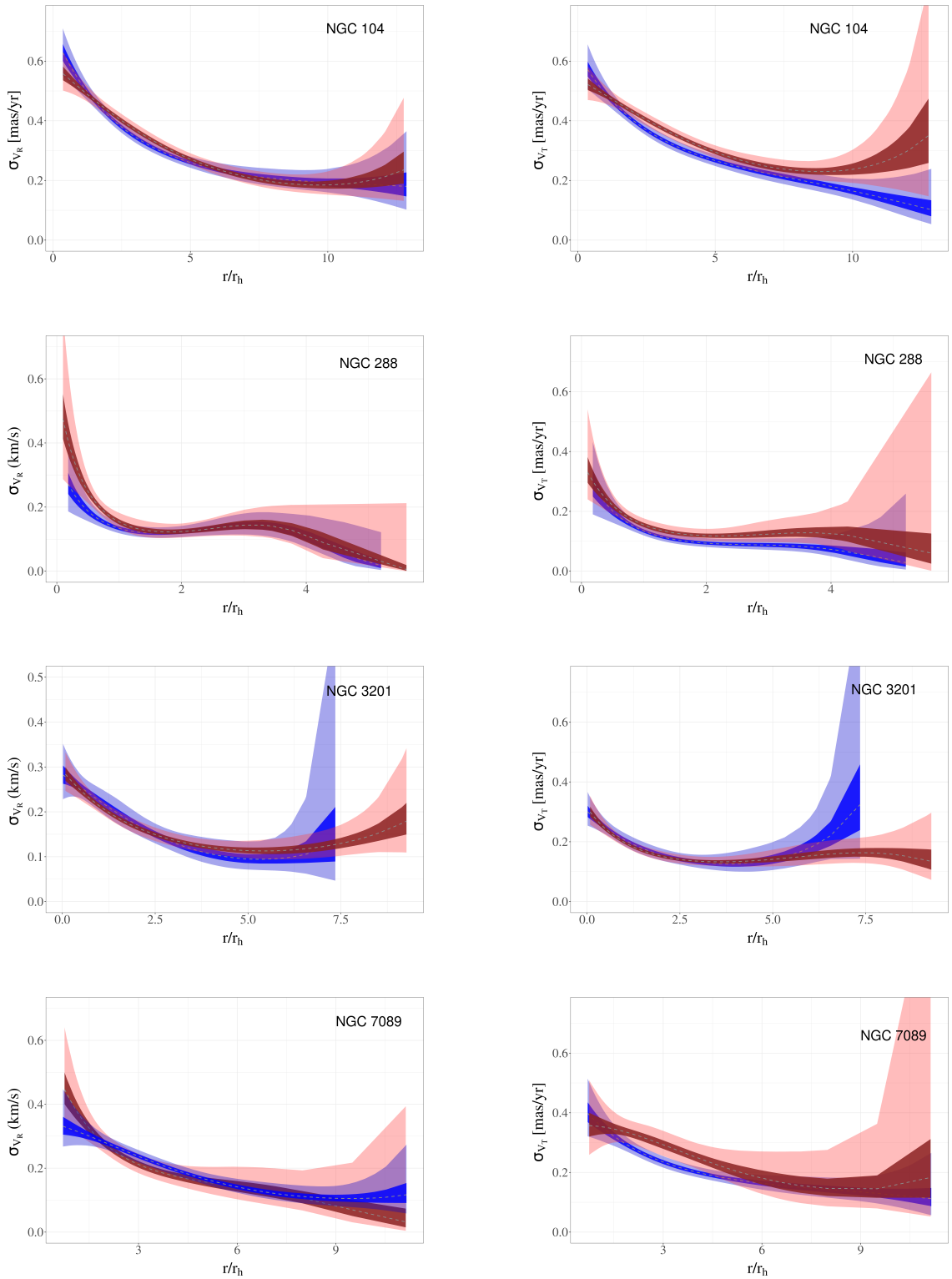

Figure 11 – Radial profiles of the velocity dispersion in the radial and tangential directions for the four clusters in the sample. Red and blue colours refer to the primordial and enriched populations, while the stronger and lighter shades are the credible intervals of 50% and 95%, respectively.

5 Results and Conclusions

In this work we take advantage of the filter system of S-PLUS to study the phenomenon of multiple populations in four Galactic globular clusters. We separated the populations using six filter combinations and the K-means algorithm. Using this separation we traced the cumulative radial distributions of the populations in order to investigate possible differences and infer clues as to their formation. Here we summarise the key points in this process:

- We performed PSF photometry using DAOPHOT, separated the likely cluster members using *Gaia* proper motions, calibrated the photometry using a differential method and corrected NGC 3201 for differential reddening;
- We visually inspected possible filter combinations and found six colours that provided an indication of the presence of MSPs, namely (u - F0378), (u - F0395), (F0378 - F0395), (F0378 - F0430), (F0378 - F0515) and (F0410 - F0430);
- With these colours we created Δs for each of them, essentially a process of rectifying the RGB, and used the K-means clustering algorithm to separate the populations in the six-dimensional space;
- We used literature data from Carretta et al. (2009) on sodium abundance for stars in three of the clusters to corroborate our separation and classify the populations into Na-rich and Na-poor;
- We traced the Cumulative Radial Distribution (CRDs) of each population from $\sim$0.5 up to 15 half-light radius;

Here we discuss the important results and our conclusions:

- The set of filters that presented the best separation of the MSPs are biased towards the bluer part of the spectrum, this is expected as the elements that have different abundances in each population present themselves strongly in the region;
- The sodium abundance data corroborates very well with our photometric separation in the cases of NGC 104 and NGC 288. This is very clear in Figures 5 and 7 of the article where we can see the locus of Na-rich and Na-poor stars correspond very well with the blue and red populations, respectively;
- In the case of NGC 3201 it is more complicated, the Na-rich (black squares in Fig. 5 of the article) seem to correspond to the blue populations, however the Na-poor

(orange circles) are spread out and do not appear to correlate with the red population. It becomes more clear looking at Fig. 7 of the article, we see that the separation is in agreement in the upper section of the RGB and becomes fuzzier as we go down;

- In order to check to probability that the CRDs of the populations in each cluster are different we used two tests: the KS and AD, essentially they indicate the likelihood that both distributions were drawn from a common distribution. Table 2 of the article presents the results of each test, we can see that all of them can be considered different distributions with a high confidence level;

- NGC 288 and NGC 7089 present distributions that would be expected if the second population formed in the central regions of the cluster (see Fig. 8), i.e. the 2P is more centrally concentrated. Literature results are conflicted in both these clusters;

- This is flipped in the case of NGC 3201, where the 1P seems more centrally concentrated. This is in direct contradiction with literature results, this may be due to an inconsistent photometric separation as pointed indicated by the abundance data;

- NGC 104 presents a complex picture, in the inner 3 half-light radius the 2P seems more prevalent, in agreement with the literature. However, outside of this both populations are present in equal numbers. This is unexpected if we consider the scenarios where the 2P formed in the centre, however many aspects of cluster evolution can affect the current distribution of the populations (Dalessandro et al., 2014);

- Dynamical simulations have shown that differences between the distributions of the populations are quickly erased in the inner regions of the cluster, nonetheless they can be preserved for much longer in the sparse region of the outskirts. To highlight the importance of looking at this region we have plotted the CRDs of the populations separated according to (Milone et al., 2012; Milone et al., 2017) using HST data in the insets of Fig. 8. We can see that the only cluster that has a apparent difference in NGC 7089, where the inner region follows the trend observed in the outer parts.

In the second part, we have taken the proper motion data from the *Gaia* survey to analyse if there were kinematic differences between the populations. Using a Heteroscedastic Gaussian Regression we traced the radial profiles of the velocity dispersion for both populations in the radial and tangential directions. Here is a summary of the steps followed and some key preliminary results:

- First we changed the reference frame to the cluster centre using the formulas by van de Ven et al. (2006) and Gaia Collaboration et al. (2018b);

- We obtain the systematic velocity of the cluster using a method described by Bianchini et al. (2018) and subtract the values from each star;
- We transform the velocities into their radial and tangential components on the plane of the sky;
- To avoid the need for binning the data, we used a Heteroscedastic Gaussian Process Regression to construct the radial profiles of the velocity dispersion in each direction;
- In all four clusters both populations show a similar profile in σ_{V_R} outside of the central region, with slight deviations in the cases of NGC 104 and NGC 7089. When looking at the centre, both NGC 288 and NGC 7089 show a smaller value of σ_{V_R} for the 1P, while NGC 104 presents the opposite behaviour;
- When considering the σ_{V_T}, in all clusters except NGC 3201 the 2P show a larger velocity dispersion outside of the central region, where all clusters have a very similar value between the populations;

All of this results put together with the literature on the subject paint a complex picture of Globular Clusters. What were once considered simple objects, surviving remnants of the process of star formation in the early Universe, prove to be a much harder challenge. To explain their formation and evolution large and systematic observational studies are necessary in order to understand all the details of how clusters look today. This is paramount to inform the theoretical and numerical approaches that aim to explain the history of Galactic GCs.

Bibliography

Abazajian, K.; Adelman-McCarthy, J. K.; Agüeros, M. A. e. a. The First Data Release of the Sloan Digital Sky Survey. *ApJ*, v. 126, n. 4, p. 2081–2086, out. 2003. Referenced in page 41.

Archinal, B. A.; Hynes, S. J. *Star Clusters*. [S.l.: s.n.], 2003. Referenced in page 28.

Bastian, N. et al. Early disc accretion as the origin of abundance anomalies in globular clusters. *MNRAS*, v. 436, n. 3, p. 2398–2411, dez. 2013. Referenced in page 37.

Baumgardt, H.; Hilker, M. A catalogue of masses, structural parameters, and velocity dispersion profiles of 112 Milky Way globular clusters. *MNRAS*, v. 478, n. 2, p. 1520–1557, ago. 2018. Referenced in page 44.

Bekki, K. Rotation and Multiple Stellar Population in Globular Clusters. *ApJl*, v. 724, n. 1, p. L99–L103, nov. 2010. Referenced in page 69.

Bekki, K. Secondary star formation within massive star clusters: origin of multiple stellar populations in globular clusters. *MNRAS*, v. 412, n. 4, p. 2241–2259, abr. 2011. Referenced in page 69.

Bianchini, P. et al. The internal rotation of globular clusters revealed by Gaia DR2. *MNRAS*, v. 481, n. 2, p. 2125–2139, dez. 2018. Referenced 4 times in pages 44, 70, 72, and 81.

Bianchini, P. et al. Rotating Globular Clusters. *ApJ*, v. 772, n. 1, p. 67, jul. 2013. Referenced in page 70.

Bonatto, C.; Chies-Santos, A. L. Lifting the dust veil from the globular cluster Palomar 2. *MNRAS*, v. 493, n. 2, p. 2688–2693, abr. 2020. Referenced in page 50.

Bonatto, C. et al. J-PLUS: A wide-field multi-band study of the M 15 globular cluster. Evidence of multiple stellar populations in the RGB. *A&A*, v. 622, p. A179, fev. 2019. Referenced 2 times in pages 42 and 48.

Bressan, A. et al. PARSEC: stellar tracks and isochrones with the PAdova and TRieste Stellar Evolution Code. *MNRAS*, v. 427, n. 1, p. 127–145, nov. 2012. Referenced in page 48.

Cannon, R. D. et al. Carbon and nitrogen abundance variations on the main sequence of 47 Tucanae. *MNRAS*, v. 298, n. 2, p. 601–624, ago. 1998. Referenced 2 times in pages 31 and 34.

Carretta, E. et al. The radial distribution of stars of different stellar generations in the globular cluster NGC 3201. *A&A*, v. 519, p. A71, set. 2010. Referenced in page 45.

Carretta, E. et al. Na-O anticorrelation and HB. VII. The chemical composition of first and second-generation stars in 15 globular clusters from GIRAFFE spectra. *A&A*, v. 505, n. 1, p. 117–138, out. 2009. Referenced 5 times in pages 30, 31, 44, 45, and 79.

Cenarro, A. J.; Moles, M.; Cristóbal-Hornillos, D. e. a. J-PLUS: The Javalambre Photometric Local Universe Survey. *A&A*, v. 622, p. A176, fev. 2019. Referenced in page 42.

Chies-Santos, A. L. et al. The nature of faint fuzzies from the kinematics of NGC 1023. *A&A*, v. 559, p. A67, nov. 2013. Referenced in page 27.

Cordero, M. J. et al. Differences in the rotational properties of multiple stellar populations in M13: a faster rotation for the 'extreme' chemical subpopulation. *MNRAS*, v. 465, n. 3, p. 3515–3535, mar. 2017. Referenced in page 70.

Cottrell, P. L.; Da Costa, G. S. Correlated cyanogen and sodium anomalies in the globular clusters 47 TUC and NGC 6752. *ApJ letters*, v. 245, p. L79–L82, abr. 1981. Referenced in page 35.

Dalessandro, E. et al. The Peculiar Radial Distribution of Multiple Populations in the Massive Globular Cluster M80. *ApJ*, v. 859, n. 1, p. 15, maio 2018. Referenced in page 70.

Dalessandro, E. et al. A Family Picture: Tracing the Dynamical Path of the Structural Properties of Multiple Populations in Globular Clusters. *ApJl*, v. 884, n. 1, p. L24, out. 2019. Referenced in page 39.

Dalessandro, E. et al. First Evidence of Fully Spatially Mixed First and Second Generations in Globular Clusters: The Case of NGC 6362. *ApJl*, v. 791, n. 1, p. L4, ago. 2014. Referenced 2 times in pages 34 and 80.

de Mink, S. E. et al. Massive binaries as the source of abundance anomalies in globular clusters. *A&A*, v. 507, n. 1, p. L1–L4, nov. 2009. Referenced in page 36.

Decressin, T.; Baumgardt, H.; Kroupa, P. The evolution of two stellar populations in globular clusters. I. The dynamical mixing timescale. *A&A*, v. 492, n. 1, p. 101–109, dez. 2008. Referenced in page 69.

Decressin, T.; Charbonnel, C.; Meynet, G. Origin of the abundance patterns in Galactic globular clusters: constraints on dynamical and chemical properties of globular clusters. *A&A*, v. 475, n. 3, p. 859–873, dez. 2007. Referenced in page 36.

Decressin, T. et al. Fast rotating massive stars and the origin of the abundance patterns in galactic globular clusters. *A&A*, v. 464, n. 3, p. 1029–1044, mar. 2007. Referenced in page 36.

Denisenkov, P. A.; Denisenkova, S. N. Correlation Between the Abundances of NA and the CNO Elements in Red Giants in Omega-Centauri. *Soviet Astronomy Letters*, v. 16, p. 275, jul. 1990. Referenced in page 30.

Denissenkov, P. A.; Hartwick, F. D. A. Supermassive stars as a source of abundance anomalies of proton-capture elements in globular clusters. *MNRAS*, v. 437, n. 1, p. L21–L25, jan. 2014. Referenced in page 36.

di Criscienzo, M. et al. The helium spread in the globular cluster 47 Tuc. *MNRAS*, v. 408, n. 2, p. 999–1005, out. 2010. Referenced in page 44.

Doherty, C. L. et al. Super and massive AGB stars - III. Nucleosynthesis in metal-poor and very metal-poor stars - Z = 0.001 and 0.0001. *MNRAS*, v. 441, n. 1, p. 582–598, jun. 2014. Referenced in page 35.

D'Orazi, V. et al. Lithium abundances in globular cluster giants: NGC 1904, NGC 2808, and NGC 362. *MNRAS*, v. 449, n. 4, p. 4038–4047, jun. 2015. Referenced in page 31.

Elmegreen, B. G. Globular Cluster Formation at High Density: A Model for Elemental Enrichment with Fast Recycling of Massive-star Debris. *ApJ*, v. 836, n. 1, p. 80, fev. 2017. Referenced in page 37.

Elmegreen, B. G.; Hunter, D. A. On the Disruption of Star Clusters in a Hierarchical Interstellar Medium. *ApJ*, v. 712, n. 1, p. 604–623, mar. 2010. Referenced in page 29.

Foreman-Mackey, D. et al. emcee: The MCMC Hammer. *PASP*, v. 125, n. 925, p. 306, mar. 2013. Referenced in page 72.

Gaia Collaboration et al. Gaia Data Release 2. Summary of the contents and survey properties. *A&A*, v. 616, p. A1, ago. 2018. Referenced in page 48.

Gaia Collaboration et al. Gaia Early Data Release 3. Summary of the contents and survey properties. *A&A*, v. 649, p. A1, maio 2021. Referenced in page 41.

Gaia Collaboration et al. Gaia Data Release 2. Kinematics of globular clusters and dwarf galaxies around the Milky Way. *A&A*, v. 616, p. A12, ago. 2018. Referenced in page 45.

Gaia Collaboration et al. Gaia Data Release 2. Kinematics of globular clusters and dwarf galaxies around the Milky Way. *A&A*, v. 616, p. A12, ago. 2018. Referenced 2 times in pages 72 and 80.

Gaia Collaboration et al. The Gaia mission. *A&A*, v. 595, p. A1, nov. 2016. Referenced in page 41.

Gieles, M. et al. Concurrent formation of supermassive stars and globular clusters: implications for early self-enrichment. *MNRAS*, v. 478, n. 2, p. 2461–2479, ago. 2018. Referenced in page 36.

Gratton, R.; Sneden, C.; Carretta, E. Abundance Variations Within Globular Clusters. *ARA&A*, v. 42, n. 1, p. 385–440, set. 2004. Referenced 2 times in pages 28 and 31.

Harris, W. E. A Catalog of Parameters for Globular Clusters in the Milky Way. *AJ*, v. 112, p. 1487, out. 1996. Referenced 3 times in pages 17, 43, and 71.

Hartmann, E. A. et al. S-PLUS: exploring wide field properties of multiple populations in galactic globular clusters at different metallicities. *MNRAS*, v. 515, n. 3, p. 4191–4200, set. 2022. Referenced 2 times in pages 71 and 74.

Hénault-Brunet, V. et al. Multiple populations in globular clusters: the distinct kinematic imprints of different formation scenarios. *MNRAS*, v. 450, n. 2, p. 1164–1198, jun. 2015. Referenced 2 times in pages 39 and 69.

Hertzsprung, E. Ueber die Verwendung photographischer effektiver Wellenlaengen zur Bestimmung von Farbenaequivalenten. *Publikationen des Astrophysikalischen Observatoriums zu Potsdam*, v. 63, jan. 1911. Referenced in page 23.

Hesser, J. E. Spectral Inhomogeneities in Faint 47 Tucanae Stars. *ApJl*, v. 223, p. L117, ago. 1978. Referenced in page 34.

Hollyhead, K. et al. Evidence for multiple populations in the intermediate-age cluster Lindsay 1 in the SMC. *MNRAS*, v. 465, n. 1, p. L39–L43, fev. 2017. Referenced in page 34.

Hoogendam, W. B.; Smolinski, J. P. A Careful Reassessment of Globular Cluster Multiple Population Radial Distributions with Sloan Digital Sky Survey and Johnson-Cousins Broadband Photometry. *AJ*, v. 161, n. 5, p. 249, maio 2021. Referenced in page 46.

Johnson, C. I.; Pilachowski, C. A. Chemical Abundances for 855 Giants in the Globular Cluster Omega Centauri (NGC 5139). *ApJ*, v. 722, n. 2, p. 1373–1410, out. 2010. Referenced in page 30.

Kamann, S. et al. The peculiar kinematics of the multiple populations in the globular cluster Messier 80 (NGC 6093). *MNRAS*, v. 492, n. 1, p. 966–977, fev. 2020. Referenced in page 70.

Kamann, S. et al. A stellar census in globular clusters with MUSE: The contribution of rotation to cluster dynamics studied with 200 000 stars. *MNRAS*, v. 473, n. 4, p. 5591–5616, fev. 2018. Referenced in page 70.

Kayser, A. et al. Comparing CN and CH line strengths in a homogeneous spectroscopic sample of 8 Galactic globular clusters. *A&A*, v. 486, n. 2, p. 437–452, ago. 2008. Referenced in page 44.

Kharchenko, N. V. et al. Global survey of star clusters in the Milky Way. II. The catalogue of basic parameters. *A&A*, v. 558, p. A53, out. 2013. Referenced in page 27.

Kimmig, B. et al. Measuring Consistent Masses for 25 Milky Way Globular Clusters. *AJ*, v. 149, n. 2, p. 53, fev. 2015. Referenced in page 70.

Kippenhahn, R.; Weigert, A.; Weiss, A. *Stellar Structure and Evolution*. [S.l.: s.n.], 2013. Referenced in page 23.

Krause, M. G. H. et al. The Physics of Star Cluster Formation and Evolution. *SSRv*, v. 216, n. 4, p. 64, jun. 2020. Referenced in page 28.

Kravtsov, V. et al. Evidence of the inhomogeneity of the stellar population in the differentially reddened globular cluster NGC 3201. *A&A*, v. 512, p. L6, mar. 2010. Referenced in page 45.

Kruijssen, J. M. D.; Dale, J. E.; Longmore, S. N. The dynamical evolution of molecular clouds near the Galactic Centre - I. Orbital structure and evolutionary timeline. *MNRAS*, v. 447, n. 2, p. 1059–1079, fev. 2015. Referenced in page 29.

Krumholz, M. R.; McKee, C. F.; Bland-Hawthorn, J. Star Clusters Across Cosmic Time. *ARA&A*, v. 57, p. 227–303, ago. 2019. Referenced 2 times in pages 27 and 28.

Lada, C. J.; Alves, J.; Lada, E. A. Infrared Extinction and the Structure of the IC 5146 Dark Cloud. *ApJ*, v. 512, n. 1, p. 250–259, fev. 1999. Referenced in page 29.

Lada, C. J.; Lada, E. A. Embedded Clusters in Molecular Clouds. *ARA&A*, v. 41, p. 57–115, jan. 2003. Referenced in page 27.

Lagioia, E. P. et al. The Hubble Space Telescope UV Legacy Survey of Galactic Globular Clusters - XII. The RGB bumps of multiple stellar populations. *MNRAS*, v. 475, n. 3, p. 4088–4103, abr. 2018. Referenced in page 31.

Lardo, C. et al. Mining SDSS in search of multiple populations in globular clusters. *A&A*, v. 525, p. A114, jan. 2011. Referenced 2 times in pages 34 and 46.

Lardo, C. et al. Chemical inhomogeneities amongst first population stars in globular clusters. Evidence for He variations. *A&A*, v. 616, p. A168, set. 2018. Referenced in page 45.

Larsen, S. S. et al. Radial Distributions of Sub-Populations in the Globular Cluster M15: A More Centrally Concentrated Primordial Population. *ApJ*, v. 804, n. 1, p. 71, maio 2015. Referenced in page 34.

Larsen, S. S. et al. Nitrogen Abundances and Multiple Stellar Populations in the Globular Clusters of the Fornax dSph. *ApJ*, v. 797, n. 1, p. 15, dez. 2014. Referenced in page 34.

Libralato, M. et al. The Hubble Space Telescope UV Legacy Survey of Galactic Globular Clusters. XXIV. Differences in internal kinematics of multiple stellar populations. *arXiv e-prints*, p. arXiv:2301.04148, jan. 2023. Referenced 2 times in pages 71 and 74.

MACQUEEN, J. et al. Some methods for classification and analysis of multivariate observations. In: OAKLAND, CA, USA. *Proceedings of the fifth Berkeley symposium on mathematical statistics and probability*. [S.l.], 1967. v. 1, n. 14, p. 281–297. Referenced in page 50.

Marino, A. F. et al. The Hubble Space Telescope UV Legacy Survey of Galactic Globular Clusters - XIX. A chemical tagging of the multiple stellar populations over the chromosome maps. *MNRAS*, v. 487, n. 3, p. 3815–3844, ago. 2019. Referenced in page 31.

Martens, S. et al. Kinematic differences between multiple populations in Galactic globular clusters. *arXiv e-prints*, p. arXiv:2301.08675, jan. 2023. Referenced in page 70.

Martocchia, S. et al. Age as a major factor in the onset of multiple populations in stellar clusters. *MNRAS*, v. 473, n. 2, p. 2688–2700, jan. 2018. Referenced in page 34.

Mastrobuono-Battisti, A.; Perets, H. B. Evolution of Second-generation Stars in Stellar Disks of Globular and Nuclear Clusters: ω Centauri as a Test Case. *ApJ*, v. 779, n. 1, p. 85, dez. 2013. Referenced in page 69.

Mayya, Y. D. et al. On the nature of the brightest globular cluster in M81. *MNRAS*, v. 436, n. 3, p. 2763–2773, dez. 2013. Referenced in page 34.

McKee, C. F.; Ostriker, E. C. Theory of Star Formation. *ARA&A*, v. 45, n. 1, p. 565–687, set. 2007. Referenced 3 times in pages 28, 29, and 30.

Mendes de Oliveira, C. et al. The Southern Photometric Local Universe Survey (S-PLUS): improved SEDs, morphologies, and redshifts with 12 optical filters. *MNRAS*, v. 489, n. 1, p. 241–267, out. 2019. Referenced in page 41.

Milone, A. P. et al. Gaia unveils the kinematics of multiple stellar populations in 47 Tucanae. *MNRAS*, v. 479, n. 4, p. 5005–5011, out. 2018. Referenced 3 times in pages 44, 70, and 74.

Milone, A. P. et al. A WFC3/HST View of the Three Stellar Populations in the Globular Cluster NGC 6752. *ApJ*, v. 767, n. 2, p. 120, abr. 2013. Referenced in page 45.

Milone, A. P. et al. The Hubble Space Telescope UV Legacy Survey of galactic globular clusters - II. The seven stellar populations of NGC 7089 (M2)⋆. *MNRAS*, v. 447, n. 1, p. 927–938, fev. 2015. Referenced 4 times in pages 31, 32, 33, and 45.

Milone, A. P. et al. The Hubble Space Telescope UV Legacy Survey of Galactic Globular Clusters. III. A Quintuple Stellar Population in NGC 2808. *ApJ*, v. 808, n. 1, p. 51, jul. 2015. Referenced in page 31.

Milone, A. P. et al. Multiple Stellar Populations in 47 Tucanae. *ApJ*, v. 744, n. 1, p. 58, jan. 2012. Referenced 2 times in pages 44 and 80.

Milone, A. P. et al. The Hubble Space Telescope UV Legacy Survey of Galactic globular clusters - IX. The Atlas of multiple stellar populations. *MNRAS*, v. 464, n. 3, p. 3636–3656, jan. 2017. Referenced 3 times in pages 33, 34, and 80.

Mucciarelli, A. et al. The Helium Abundance in the Metal-poor Globular Clusters M30 and NGC 6397. *ApJ*, v. 786, n. 1, p. 14, maio 2014. Referenced in page 31.

Mucciarelli, A. et al. Looking Outside the Galaxy: The Discovery of Chemical Anomalies in Three Old Large Magellanic Cloud Clusters. *ApJl*, v. 695, n. 2, p. L134–L139, abr. 2009. Referenced in page 34.

Mucciarelli, A. et al. Lithium abundance in the globular cluster M4: from the turn-off to the red giant branch bump. *MNRAS*, v. 412, n. 1, p. 81–94, mar. 2011. Referenced in page 31.

Nataf, D. M. et al. The Relationship between Globular Cluster Mass, Metallicity, and Light-element Abundance Variations. *AJ*, v. 158, n. 1, p. 14, jul. 2019. Referenced in page 44.

Norris, J.; Freeman, K. C. The anticorrelation of carbon and nitrogen on the horizontal branch of 47 Tuc. *ApJ*, v. 254, p. 143, mar. 1982. Referenced in page 44.

Osborn, W. Two new CN-strong globular cluster stars. *The Observatory*, v. 91, p. 223–224, dez. 1971. Referenced in page 30.

Parmentier, G.; Pasquali, A. Rebounding Cores to Build Star Cluster Multiple Populations. *ApJ*, v. 924, n. 2, p. 81, jan. 2022. Referenced in page 37.

Pasquini, L. et al. Li in NGC 6752 and the formation of globular clusters. *A&A*, v. 441, n. 2, p. 549–553, out. 2005. Referenced in page 31.

Peacock, M. B. et al. Globular clusters in the far-ultraviolet: evidence for He-enriched second populations in extragalactic globular clusters? *MNRAS*, v. 464, n. 1, p. 713–720, jan. 2017. Referenced in page 34.

Peng, E. W. et al. The ACS Virgo Cluster Survey. XI. The Nature of Diffuse Star Clusters in Early-Type Galaxies. *ApJ*, v. 639, n. 2, p. 838–857, mar. 2006. Referenced in page 27.

Piotto, G. et al. The Hubble Space Telescope UV Legacy Survey of Galactic Globular Clusters. I. Overview of the Project and Detection of Multiple Stellar Populations. *AJ*, v. 149, n. 3, p. 91, mar. 2015. Referenced 2 times in pages 23 and 32.

Piotto, G. et al. Multi-wavelength Hubble Space Telescope Photometry of Stellar Populations in NGC 288. *ApJ*, v. 775, n. 1, p. 15, set. 2013. Referenced in page 45.

Plummer, M. *JAGS: Just Another Gibbs Sampler*. 2012. ascl:1209.002 p. Astrophysics Source Code Library, record ascl:1209.002. Referenced in page 73.

Portegies Zwart, S. F.; McMillan, S. L. W.; Gieles, M. Young Massive Star Clusters. *ARA&A*, v. 48, p. 431–493, set. 2010. Referenced in page 27.

Prantzos, N.; Charbonnel, C. On the self-enrichment scenario of galactic globular clusters: constraints on the IMF. *A&A*, v. 458, n. 1, p. 135–149, out. 2006. Referenced in page 37.

Prantzos, N.; Charbonnel, C.; Iliadis, C. Light nuclei in galactic globular clusters: constraints on the self-enrichment scenario from nucleosynthesis. *A&A*, v. 470, n. 1, p. 179–190, jul. 2007. Referenced in page 34.

Richer, H. B. et al. A Dynamical Signature of Multiple Stellar Populations in 47 Tucanae. *ApJl*, v. 771, n. 1, p. L15, jul. 2013. Referenced 3 times in pages 39, 44, and 69.

Russell, H. N. Relations Between the Spectra and Other Characteristics of the Stars. *Popular Astronomy*, v. 22, p. 275–294, maio 1914. Referenced in page 23.

Ryan, S. G.; Norton, A. J. *Stellar Evolution and Nucleosynthesis*. [S.l.: s.n.], 2010. Referenced in page 23.

Simioni, M.; Aparicio, A.; Piotto, G. Statistical analysis of Galactic globular cluster type properties. *MNRAS*, v. 495, n. 4, p. 3981–3989, jul. 2020. Referenced in page 33.

Simioni, M. et al. The Hubble Space Telescope UV Legacy Survey of Galactic globular clusters - X. The radial distribution of stellar populations in NGC 2808. *MNRAS*, v. 463, n. 1, p. 449–458, nov. 2016. Referenced in page 34.

Simmerer, J. et al. Star-to-star Iron Abundance Variations in Red Giant Branch Stars in the Galactic Globular Cluster NGC 3201. *ApJl*, v. 764, n. 1, p. L7, fev. 2013. Referenced in page 45.

Smith, G. H. The chemical inhomegeneity of globular clusters. *PASP*, v. 99, p. 67–90, fev. 1987. Referenced in page 28.

Sneden, C. et al. Oxygen Abundances in Halo Giants. III. Giants in the Mildly Metal-Poor Globular Cluster M5. *AJ*, v. 104, p. 2121, dez. 1992. Referenced in page 30.

Sohn, S. T. et al. Hot Populations in M87 Globular Clusters. *AJ*, v. 131, n. 2, p. 866–888, fev. 2006. Referenced in page 34.

Stetson, P. B. DAOPHOT: A Computer Program for Crowded-Field Stellar Photometry. *PASP*, v. 99, p. 191, mar. 1987. Referenced in page 46.

Stetson, P. B. et al. Homogeneous photometry - VII. Globular clusters in the Gaia era. *MNRAS*, v. 485, n. 3, p. 3042–3063, maio 2019. Referenced in page 46.

Tiongco, M. A.; Vesperini, E.; Varri, A. L. Kinematical evolution of multiple stellar populations in star clusters. *MNRAS*, v. 487, n. 4, p. 5535–5548, ago. 2019. Referenced 2 times in pages 39 and 69.

van de Ven, G. et al. The dynamical distance and intrinsic structure of the globular cluster ω Centauri. *A&A*, v. 445, n. 2, p. 513–543, jan. 2006. Referenced 2 times in pages 71 and 80.

Vanderbeke, J. et al. G2C2 - IV. A novel approach to study the radial distributions of multiple populations in Galactic globular clusters. *MNRAS*, v. 451, n. 1, p. 275–281, jul. 2015. Referenced in page 46.

Vázquez-Semadeni, E. et al. Global hierarchical collapse in molecular clouds. Towards a comprehensive scenario. *MNRAS*, v. 490, n. 3, p. 3061–3097, dez. 2019. Referenced in page 28.

Vesperini, E. Star cluster dynamics. *Philosophical Transactions of the Royal Society of London Series A*, v. 368, n. 1913, p. 829–849, jan. 2010. Referenced in page 28.

Vesperini, E. et al. Dynamical evolution and spatial mixing of multiple population globular clusters. *MNRAS*, v. 429, n. 3, p. 1913–1921, mar. 2013. Referenced in page 69.

von Braun, K.; Mateo, M. NGC 3201 Photometry Results: Differential Extinction Map, Color-Magnitude Diagram, and Variable Star Candidates. In: *American Astronomical Society Meeting Abstracts #198*. [S.l.: s.n.], 2001. (American Astronomical Society Meeting Abstracts, v. 198), p. 42.07. Referenced 2 times in pages 45 and 50.

Wang, L. et al. The possible role of stellar mergers for the formation of multiple stellar populations in globular clusters. *MNRAS*, v. 491, n. 1, p. 440–454, jan. 2020. Referenced in page 36.

Yong, D. et al. Iron and neutron-capture element abundance variations in the globular cluster M2 (NGC 7089)*. *MNRAS*, v. 441, n. 4, p. 3396–3416, jul. 2014. Referenced in page 45.